Functional and Structural Studies of Cytochromes P450 by Resonance Raman Spectroscopy

Yilin Liu
Marquette University

FUNCTIONAL AND STRUCTURAL STUDIES OF CYTOCHROMES P450 BY RESONANCE RAMAN SPECTROSCOPY

By Yilin Liu, B.Sc.

A Dissertation submitted to Faculty of the Graduate School,

Marquette University,

in Partial Fulfillment of the Requirements for the

Degree of Doctor of Philosophy

Milwaukee, Wisconsin

August 2017

ABSTRACT

FUNCTIONAL AND STRUCTURAL STUDIES OF CYTOCHROMES P450 BY RESONANCE RAMAN SPECTROSCOPY

By Yilin Liu, B.Sc.

Marquette University

Cytochrome P450 is a broad class of heme monooxygenase enzymes which catalyze various oxidative transformations. There are two main kinds of mammalian P450s: steroidogenic and drug metabolizing P450s. The first project involves a steroidogenic P450, CYP17A1, occupying a central role in the biosynthesis of steroid hormones. It catalyzes hydroxylation reaction on pregnenolone and progesterone, generating 17OH-pregnenolone and 17OH-progesterone, presumably utilizing a "Compound I" species. However, these hydroxylated products can be further processed in a second oxidative cycle to cleave the C17–C20 bond to form dehydroepiandrosterone or androstenedione, respectively, a crucial step in androgen production. Interestingly, it is well known that cytochrome b_5 is a key regulator of androgen synthesis, by a mechanism that is still not well understood. As the enzymes involved here are both membrane-bound, resonance Raman (rR) studies are performed on unique nanodisc-based dyads to investigate their interaction, including characterization of their ferric state and unstable dioxygen intermediates, the essential results supporting an electron transfer role of cyt b_5. The second project is focused on a fusion enzyme called $P450_{BM3}$, which possesses a covalently linked cytochrome P450 reductase. This fusion enzyme is clearly a good target for biotechnologically application. In the present work, rR studies focus on several biotechnologically important mutants of $P450_{BM3}$, which have altered substrate selectivity, allowing metabolism of the human proton pump inhibitor, omeprazole, producing metabolites that precisely match those generated by human CYP2C19, thereby providing an inexpensive source of these precious materials that are needed for drug metabolism studies. Specifically, it is shown that binding of omeprazole to these BM3 mutants leads to differing degrees of high spin state conversion of the heme iron. Furthermore, the ferrous CO adduct were acquired to interrogate the effect of substrate binding on the distal pocket architecture. The third project involves the biotechnologically important peroxygenases. Specifically, rR studies are applied to CYP152L1 and CYP152L2 enzymes, which are able to convert fatty acids into industrially valuable terminal alkenes without requiring a complex reductase system. Herein, using chemical strategies to trap and isolate key reaction intermediates, rR spectroscopy is being employed to probe their structure and reactivity.

ACKNOWLEGMENT

My deepest appreciation goes first and foremost to my advisor, Dr. James R. Kincaid, for his instructive guidance, constant support and kind encouragement during the past five years of my doctoral studies at Marquette University. His rigorous academic attitude, the enthusiasm to science, inspired my academic pursuits.

My sincere gratitude also goes to my committee members, Professor Christopher Dockendorff, Professor Daniel Sem and Professor Qadir Timerghazin, for their suggestions through my career, writing my thesis and being flexible for my research meeting, annual review meeting and thesis defense. I would also like to thanks Professor Michael M. Ryan, for offering me using the UV-vis instrumental in his lab. I wish to extend my thanks to Drs. Stephen G. Sligar, Andrew W. Munro and Thomas Makris for collaboration and valuable discussions. Special thanks goes to Dr. Piotr Mak, for teaching me using the resonance Raman spectroscopy and I am so grateful for his continued support and advice. I would also like to thanks my past and present group members, Dr Kazik Czarnecki, Qianhong Zhu, Remigio Usai and Ying Wang, for their support and friendship.

Finally, I dedicate this thesis to my parents, Ping Li and Dianli Liu, for their unconditional love and support, no matter where I am and what decisions I made. Thanks my grandparents who believed in me and made me have the happy childhood memory. I would like to express my deepest gratitude to my Uncle, David Liu, who has been with me every step of the way, from editing my graduate school applications to deciding where to go next. I would also like to thank Denan’s accompany during all the time in Milwaukee. It is doubtful that this work could have been finished without them.

TABLE OF CONTENTS

LIST OF TABLES

LIST OF FIGURES

Chapter 1: General Introduction

1.1 Introduction of heme proteins

Heme enzymes are one of the most important classes of proteins that perform a variety of functions throughout the biosphegxre, such as oxygen storage and transfer, electron transfer and catalyzing difficult chemical reactions such as hydroxylation of organic substrates. One or more heme cofactors[1] are recruited into enzyme active sites to accomplish these diverse functions.

Iron-porphyrin complex, known as heme cofactor, plays a key role in biological process and metabolic pathways. So far, several different types of natural heme prosthetic groups are identified, such as heme a, heme b, heme c, heme d, and siroheme.[2] While among these groups, b type heme is the most abundant and widely encountered. The molecular structure is shown in Figure 1.1.1, four methyl groups are located at the 1-, 3-, 5-, and 8- position, two vinly groups are at the 2-, 4- position and two propionate groups are at the 6-, 7- positions. The upper side of porphyrin is hydrophobic which usually interact with the hydrophobic amino acid residues, while the lower side is more polar with the propionate groups attached, preferring to interact with the polar amino acids residues, such as glutamate and aspartate. Thus, heme b is bound in the heme pocket via the non-covalent interactions with amino acid residues as well as by establishing coordination between heme iron and an endogenous axial ligand, such as histidine in myoglobin; relevant to this work, the axial ligand is cysteine in cytochrome P450.[3]

The functions of heme b type proteins are various. Hemoglobin is the most common O_2 transport protein in nature and myoglobin is the O_2 storage sites in muscle cells,[4] cytochrome b_5 is known to be involved in the electron transfer of oxidation reactions in biological tissues,[5] some heme-based sensor proteins such as FixL,[6] CooA,[7] and sGC,[8] are functioned to sense O_2, CO and NO molecules to initiate some chemistry requirement in biological system, and cytochrome P450 and some peroxidases are used to oxidize a wide range of substrates by employing O_2 and H_2O_2, respectively.[9] Thus, study of these enzyme structures and catalytic mechanisms becomes very significant. Resonance Raman spectroscopy is one of the most effective techniques to probe iron electronic structure, heme peripheral environment, ligand binding properties as well as characterization of intermediates in catalytic cycles.[10]

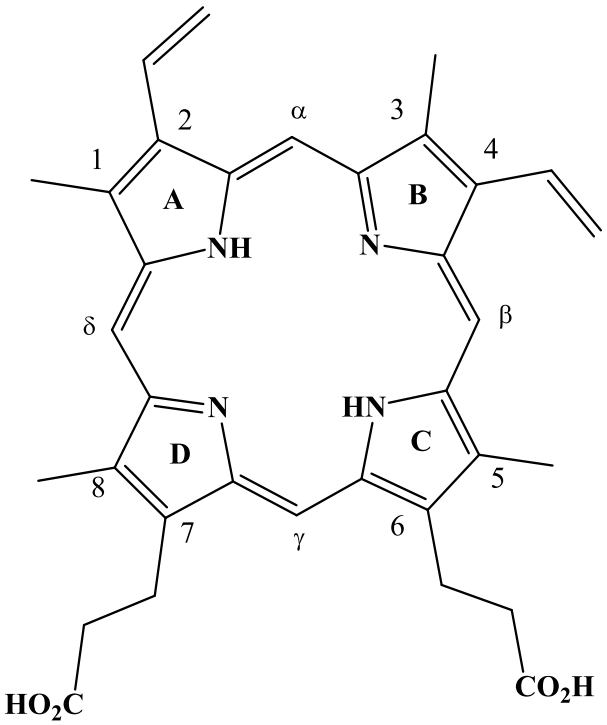

Figure 1.1.1 Molecular structure of heme b.

1.1.1 Globins

The globins are an extensive family of proteins which all have very similar structures, are commonly a three-dimensional folding of a few α helices to form a globin fold which protects the bound heme group and allowing the oxygen binding and transport.[11] Myoglobin and hemoglobin are two main classes which are most well studied. They are the first proteins for which crystal structures were determined by X-ray crystallography.[12] Myoglobin is very abundant in muscles in varieties of organisms, serving as oxygen storage. It is a single peptide chain containing 153 amino acids, which consists of eight α helices connected by turns, with one bound heme (Figure 1.1.2).[13] While hemoglobin carries oxygen from the lungs to peripheral tissues and returns carbon dioxide back to lungs, it is a much larger protein than myoglobin, being a tetramer consisting of two α chains and two β chains. It contains four heme prosthetic groups, each one associated with one polypeptide chain (Figure 1.1.3).[14] Both myoglobin and hemoglobin bind oxygen at the iron atom in heme. In the deoxy form, ferrous heme iron is coordinated by the imidazole part of histidine in proximal side (the fifth ligand), while the sixth ligand is unoccupied, this position serving for binding oxygen. When oxygen binds, the electronic structure of iron ion is rearranged, which gives the bright red color of oxygen-rich blood.

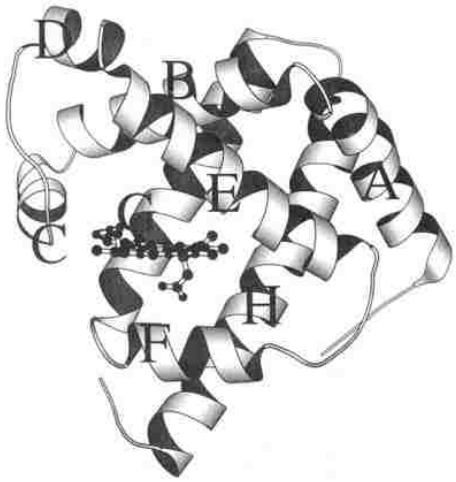

Figure 1.1.2 A ribbon diagram of the sperm whale Myoglobin. Eight α helices are labeled A through H and heme group were shown in ball and sticks.[13]

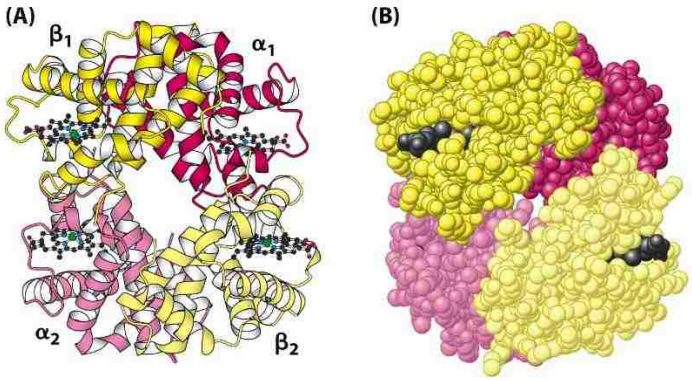

Figure 1.1.3 Quaternary structure of hemoglobin. (A) Ribbon diagram (B) A space filling model.[14]

Though these two proteins adopt nearly identical structure for oxygen binding, hemoglobin obviously has a much higher efficiency. Instead of exhibiting a simple hyperbolic curve like myoglobin, it exhibits a distinct sigmoid curve which means it binds oxygen cooperatively (Figure 1.1.4). This interesting process initiates from the binding of one or two molecules of oxygen, which results in a structural change of the whole protein, enhancing the oxygen affinity in the unligated subunits. Because of this

allosteric effect, hemoglobin is more effective in transporting oxygen concentration in lungs and tissues, loading up with oxygen in the oxygen-rich lungs and more effectively release oxygen in the oxygen-poor tissues, where the reverse allosteric effect to this place after one or two molecules of oxygen were dissociated.[15]

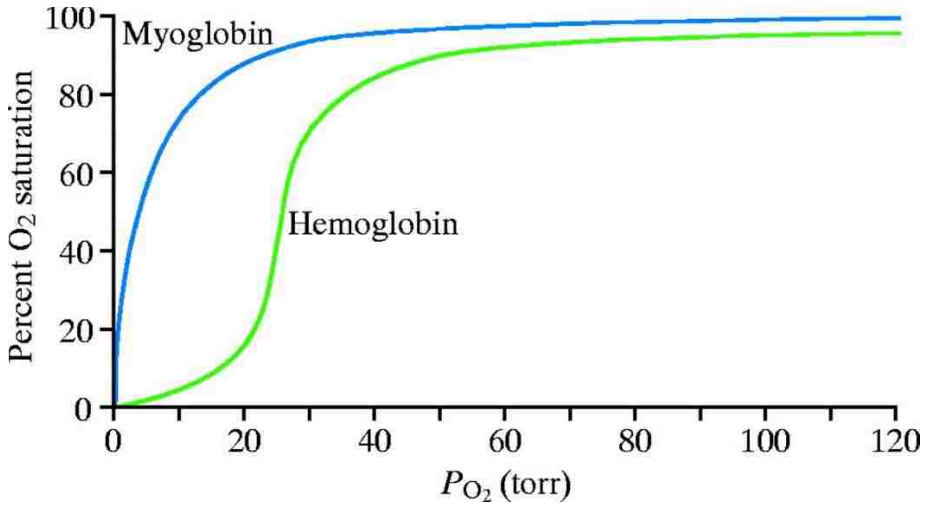

Figure 1.1.4 Oxygen binding by myoglobin (blue curve) and hemoglobin (green "S" shape curve).[15]

1.1.2 Electron transfer hemeproteins

Redox reactions occur in many biological processes, such as photosynthesis and respiration, which are two necessary processes that maintain life. Nature recruited transition metals to overcome the kinetic barrier of these reactions. Cytochrome c and cytochrome b_5 are two representative proteins involved in a large number of biological electron transfer process.[16]

Cytochrome c is an essential component in electron transport chain which is found in inner membrane of mitochondria, where it participates in oxidation and

reduction reactions to produce the energy currency, ATP. It is a small protein containing around 100-120 amino acids with only 12kDa molecular weight.[17] As shown in Figure 1.1.5, there are different types of heme found in cytochromes and cytochrome c contains the c-type heme, with the axial ligands of histidine and methionine to covalently link to the protein peptide chain. Another electron transport hemeprotein, cytochrome b_5, contains a bis-histidine ligated b-type heme and is found in bacteria, plants and animals. They are membrane bound in mitochondria and microsome, while soluble in bacteria. They can exhibit the redox potential span of ~400 mV and interact with their redox partners primarily by electrostatic forces. Of interest in this study, cytochrome b_5 is involved in a fast input of the second electron to P450 monooxygenase enzyme, which is critical for the oxygen activation.[5]

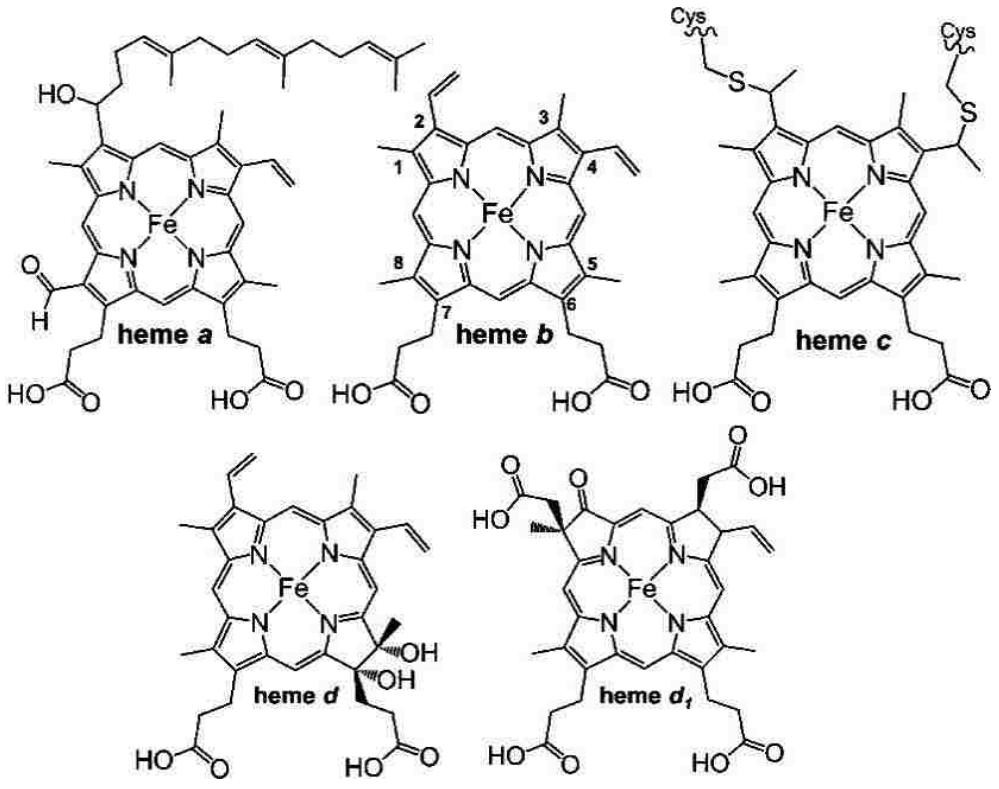

Figure 1.1.5 Schematic of various types of heme.[18]

1.1.3 Signaling hemeproteins

There is a minor class of hemeproteins called sensor proteins, which can sense the presence of small diatomic ligands such as oxygen, carbon monoxide and nitric oxide, thereby responding to fluctuations in the levels, serving to regulate physiological functions, adapting the changes in varieties of organism. All these proteins are composed of a heme-containing domain and a coupled transmitter. Upon the binding of the diatomic small molecules, the conformational of heme binding domain is transmitted to its coupled functional domain (neighbored transmitter region) where it can modulates the signal transduction to fulfil its physiological role.

Some well characterized signaling proteins are the bacterial O_2 sensor, FixL,[19] the CO sensor, CooA[20] and the NO sensors HNOX[21] and soluble guanylate cyclase (sGC). Taking the NO sensor sGC for an example, sGC is a heterodimeric enzyme (one α subunit and one heme-containing β subunit), which contains a five-coordinated b-type heme with the heme proximal coordination being provided by the protein amino acid sidechain of a histidine residue in its nature ferrous form.[22] Resonance Raman studies have shown that this Fe-N_{his} bond is the weakest in all hemeproteins, having a very low frequency of iron histidine stretching mode (204 cm^{-1}).[23] Upon binding of NO molecule in distal pocket, the proximal iron histidine bond cleavage leads to the protein conformational change which further increases the sGC activity in the catalytic domain, converting GTP to intercellular messenger cGMP (Figure 1.1.6). Following Le Chatlier's principle, sGC can spontaneously release NO molecules when NO levels drops to a clinical value, thereby down regulating cGMP.[24]

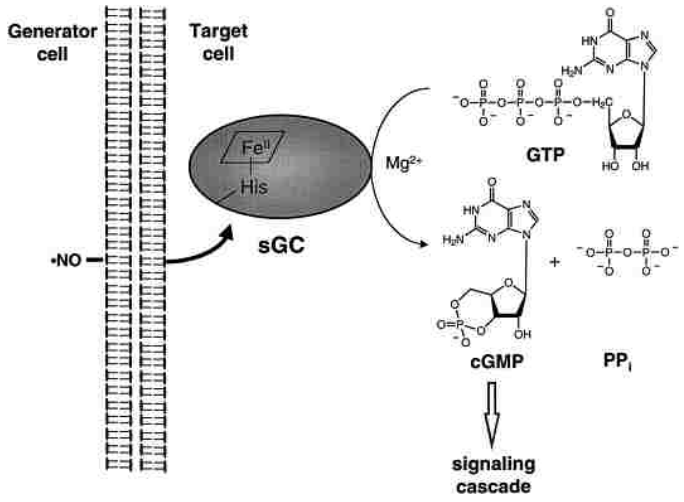

Figure 1.1.6 sGC in the NO signaling pathway.[25]

The discovery of heme sensor proteins has been increasing rapidly, with insights into this class of protein mechanism being developed by using varies of biophysical methods and crystallography, providing a better understanding how these heme binding domain in turn controls the signal transduction domains.

1.1.4 Catalytic hemeproteins (cytochromes and peroxidases)

There are several broad classes of hemeproteins which serve to catalyze oxidation reactions, one of which is the Cytochromes P450, which use O_2 and two electrons and two protons to oxygenate relatively inert substrates, and the other is peroxidases, monooxygnease known using H_2O_2 for substrate oxidation. As shown in Figure 1.1.7, heme oxygenase use NAD(P)H –dependent reductase system and O_2 bound intermediate to produce the active oxidant called compound I. While the peroxidase can directly interact with H_2O_2 to produce compound 0 which then rapidly converts to compound I.

Avoiding any need for partner reductase in the H_2O_2 activation pathway is a big advantage, thus attracting a huge potential interest for biotechnological purpose. Though peroxidases can operate without electron donor protein, H_2O_2 is a major source of reactive oxygen species via Fenton chemistry. Since the release of toxic hydroxyl radicals is highly destructive to the enzyme active site, peroxidases facilitate heterolytic O-O cleavage to avoid radical formation. Since Cytochrome P450s will be discussed later in a much detail in the next sections, emphasis will be placed on the H_2O_2 driven peroxidases.

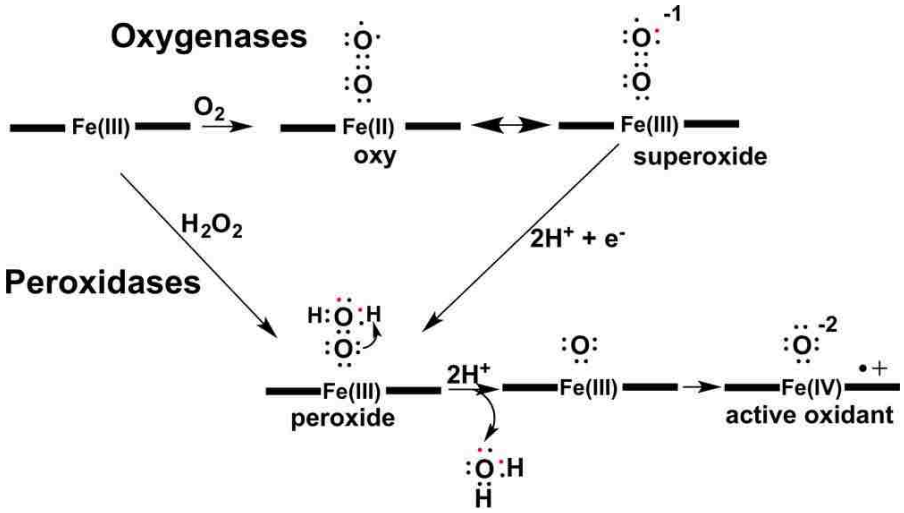

Figure 1.1.7 Oxygen and Hydrogen peroxide activation pathway.[9]

Peroxide enzymes use hydrogen peroxide to oxidize biological molecules including a wide variety of substrates, playing multiple physiological roles, they have been studied extensively owing to their ease of preparation of large amount of purified enzymes. There are two well defined superfamilies of peroxidases: one belongs plant peroxidase superfamily which contains enzymes from plant, fungal and bacteria, while

the other superfamily is mammalian peroxidases such as lactoperoxidase and prostaglandin H synthase. Among all different kinds of peroxidases, horseradish peroxidase (HRP) was first to be thoroughly studied over the past century.

Horseradish peroxidase is an important heme-containing enzyme which exhibits multiple physiological roles, including metabolism of 3-acetic acid, suberin formation and cross-linking of cell wall polymers.[26] It is a single polypeptide chain of 308 amino acid residues, with a heme b cofactor bound via a histidine axial ligand. As shown in Figure 1.1.8, there is a strong hydrogen bonding interaction between proximal histidine 170 and aspartic acid 247 residue, giving the axial ligand more imidazolate character, lowering $Fe^{3+/2+}$ redox potential. The distal pocket remains unoccupied by water and ready for H_2O_2 turnover and substrate oxidation.

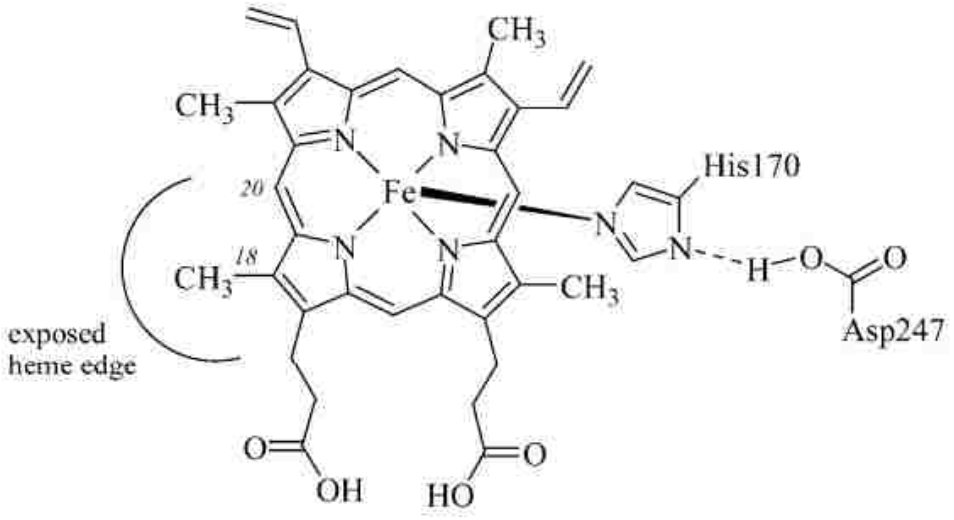

Figure 1.1.8 Horseradish peroxidase heme structure and key amino acids in the proximal site.[27]

Treatment of HRP with hydrogen peroxide yields a relatively stable compound I species (i.e.; a porphyrin pi cation radical) with a distinct green color; then is formed by removal of one electron from iron and a second from the porphyrin ring, with peroxide being reduced to water. Then one electron oxidation of a substrate molecule, reduces the porphyrin pi radical to generate compound II (a ferryl heme). Finally, compound II is reduced to the ferric state by a one electron, one-proton transfer process. This whole catalytic process is shown in Figure 1.1.9.

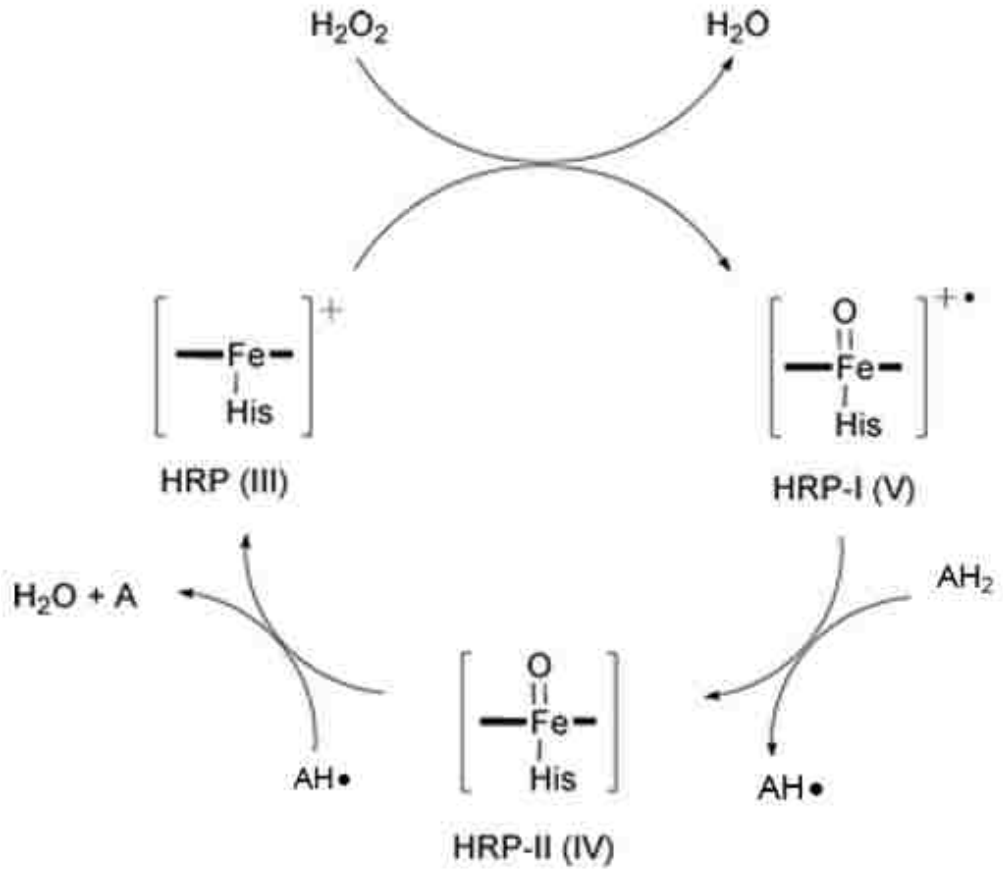

Figure 1.1.9 The reaction cycle of HRP (where AH_2 and AH represent a reducing substrate and its radical product); Roman numerals indicate iron oxidation state.[28]

1.2 Cytochrome P450

1.2.1 General Introduction

Cytochromes P450 is one of the most remarkable enzyme families in the biological kingdom, being found in diverse organisms, such as bacteria, yeast, plants, fungi and mammals. Cytochrome P450 was first identified in liver microsome by Kingenberg[29] and Garfinkel[30] in 1958. The name of P450 was given to it owing to the fact that its carbon monoxide adduct exhibits a maximum Soret band at 450 nm, as shown in Figure 1.2.1.

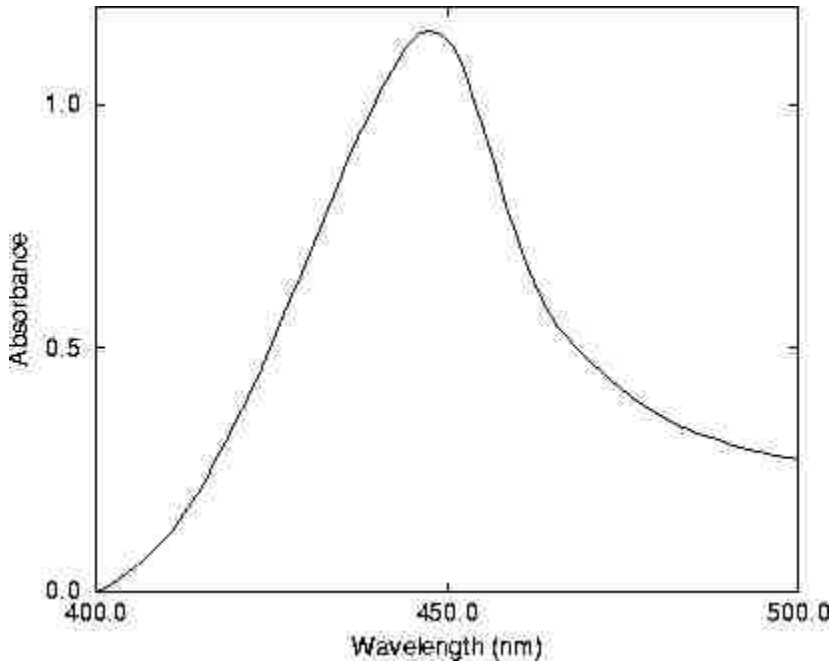

Figure 1.2.1 The absorption spectrum of cytochrome P450-CO complex.[31]

So far over 18,000 P450 sequences have been discovered and this number keeps increasing.[32] The human genome encodes 57 cytochrome P450 proteins, while bacteria possess 153 P450 families. In order to keep a record of this enormous information, a nomenclature system has been derived based on the degree of protein sequencing identity.[33] CYP was abbreviated for cytochrome P450 followed by an Arabic number representing a family in which the proteins have more than 40% sequence identity. Then a letter, indicating the subfamily where proteins share more than 55 % same sequence within the subfamily. Finally, an Arabic number at the end denotes the individual gene, such as CYP2C8 (Figure 1.2.2). However, some cytochrome P450s are also named based on its catalytic function and substrate name; for example, CYP5A1, thromboxane A_2 synthase, was abbreviated to TXAS.[34]

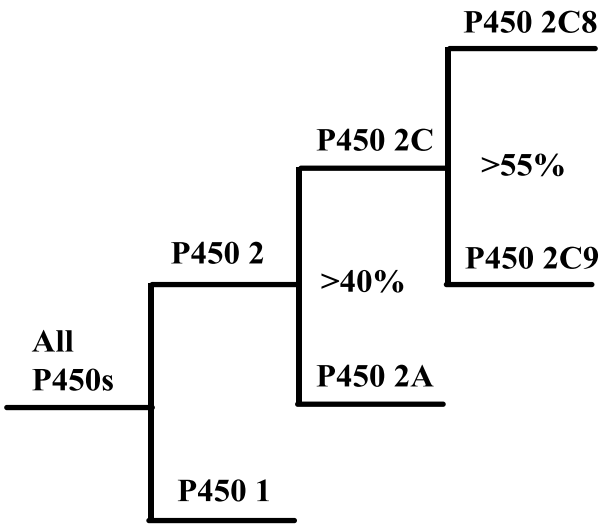

Figure 1.2.2 Nomenclature basis for P450s and classification.

Cytochrome P450s are considered as a significant catalyst in biology, playing a critical role in oxidizing a wide range of substrates.[31] Although the reactions catalyzed by

cytochrome P450 are extremely diverse, most of them can be accommodated to the basic catalytic reaction below.

$$\mathbf{NAD(P)\,H + H^{+} + R\text{-}H + O_2 \longrightarrow NAD(P)^{+} + H_2O + R\text{-}OH}$$

(R-H = substrate, R-OH = product)

P450 can oxidize the organic substrate (RH) by employing the oxygen, to produce a mono-oxygenated metabolite (ROH) and a molecule of water. In this reaction, two electrons provided by redox proteins are required. Based on electron transport chain, three main classes cytochrome P450s are described below. [35, 36.]

Class I type cytochrome P450s usually are found in bacterial and some mitochondrial P450s systems, both systems obtaining electrons from a pyridine nucleotide (i.e. NADH or NADPH) via a FAD-containing reductase (FdR) and a Fe_2S_2 ferredoxin (Fdx). However, there is a main difference between bacteria and eukaryotes systems. In bacteria, the reductase, ferredoxin and P450 are all soluble (Figure 1.2.3 A). In eukaryotes, ferredoxin is alone soluble, while both the reductase and P450 are membrane-associated proteins and can bound to the inner mitochondrial membrane, as shown in Figure 1.2.3 B. Examples of Class I type P450 includes P450cam in bacteria.

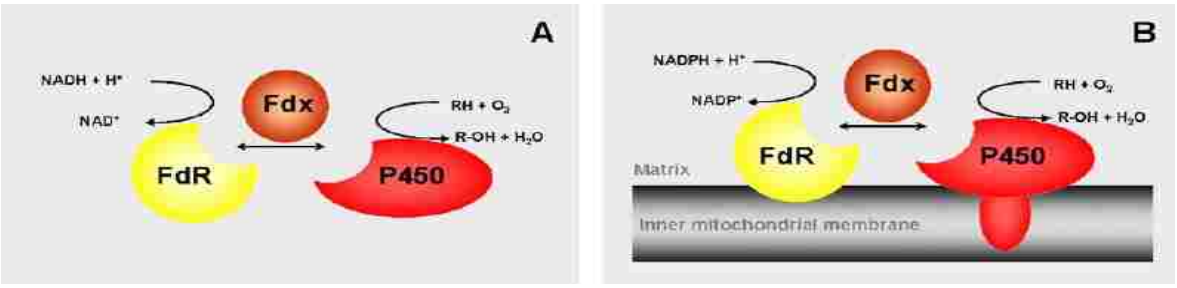

Figure 1.2.3 Schematic organization of electron transfer in (A) Class I bacterial system (B) Class I mitochondrial system.

Class II type cytochrome P450s are involve in mostly microsomal P450 systems. In this system, electrons are transported from NADPH to the heme of P450 via NADPH-Cytochrome P450 reductase (CPR) which contains two prosthetic groups, FAD (Flavin adenine dinucleotide) and FMN (Flavin mononucleotide). Both NADPH-Cytochrome P450 reductase and P450 are anchored in the membrane. The scheme of electron transfer route is shown in Figure 1.2.4**.** In addition, a minor number of microsome P450s also use cytochrome b_5.

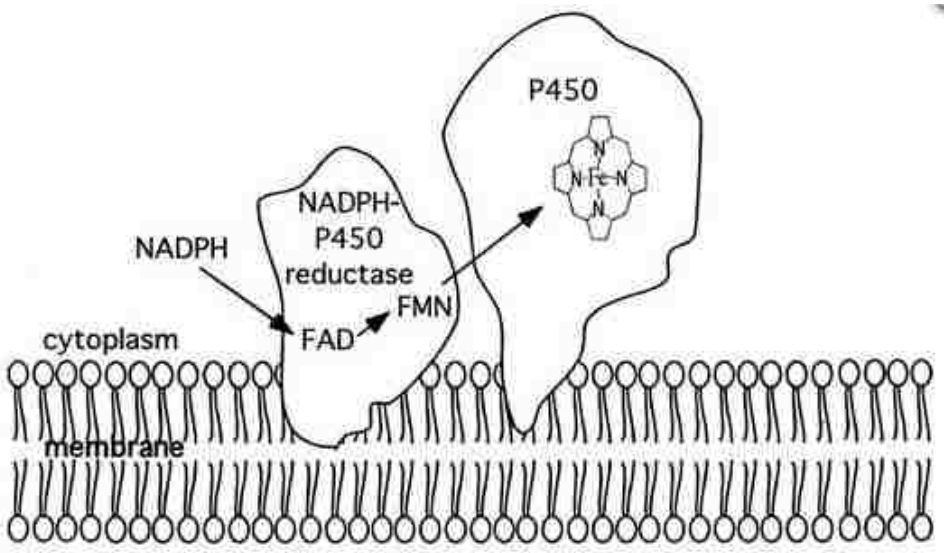

Figure 1.2.4 Schematic electron transfer route in P450s with NADPH-P450 reductase system.[37]

Class III type P450s are self-sufficient and usually do not need any extra source of electrons. Examples of this type includes P450 BM3, it consists of a single polypeptide chain with two different domains, which the heme domain is fused to the reductase domain containing an FAD and FMN. This novel type of fusion is defined as a new class of discovered P450.

1.2.2 Active site structure of Cytochrome P450

P450s are crucial in many biological processes, they are involved in breaking down the xenobiotics in drug metabolism as well as in the biosynthesis of important compounds such as steroids, lipids, and vitamins. In order to better understand the structure-function relationship, very many studies have been undertaken to explore structure function relationships. Owing to the difficulty with purification and recombinant expression of membrane-bound P450s, the soluble P450s such as P450cam, were most heavily studied at earlier time.

The P450 enzymes all are composed of a heme b bound through a thiolate axial ligand to a single polypeptide chain consisting mainly of α-helices and β sheets arranged to form a globular protein, with a size of 40~55 kDa. Even though the complicated P450 enzymes have variable structures, the overall fold and topology are basically same.[38] All enzymes share a highly reserved core which consists of a four-helix bundle, three parallel helices D, L, I and one antiparallel helix E, as shown in Figure 1.2.5**.** The long I helix locates right above the heme prosthetic group and provides important amino acid residues to interact with both substrate and molecular oxygen. While the L helix is located as the proximal side of heme group to provide the cysteine residue to bind to the heme iron as the fifth ligand. Various spectroscopic methods including Resonance Raman spectroscopy was used to detect this iron-sulfur bond.[39]

Cytochrome P450 shows diverse conformation and marked regio- and stereo-selectivity toward different substrates. The non-conserved region, is necessary for this substrate binding and recognition.[40] Six substrate recognition sites were identified by Gotoh which constitute about 16% of the total residues, as shown in Figure 1.2.6. The

SRS1 was assigned to the B' helix region, parts of helices F and G and the F-G loop were identified as SRS2 and SRS3. The center position of helix I was ruled as SRS4 which contributes key role in substrate binding and reaction mechanism. The N-terminus of β4 was SRS5 and β2 connecting region which towards to active site in K helix was SRS6. All these regions are quite flexible which allows the substrates entering and leaving the heme pocket and catalyzing reactions subsequently.[41]

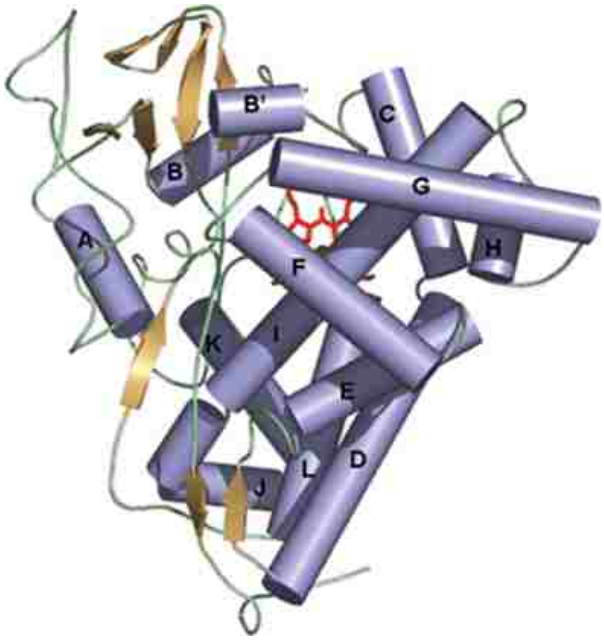

Figure 1.2.5 Schematic representation of P450cam structure.

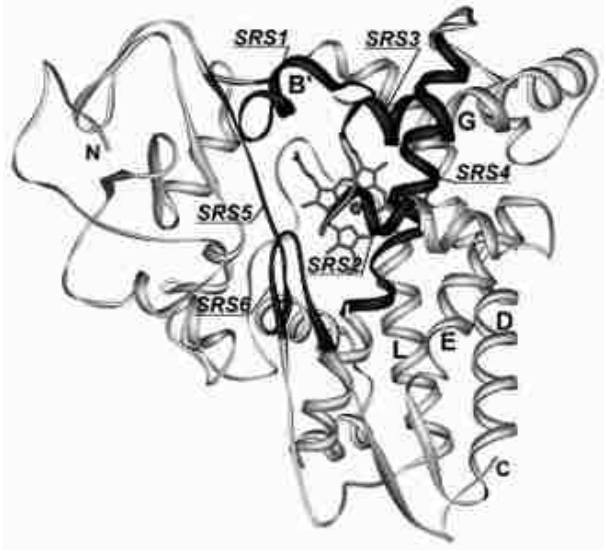

Figure 1.2.6 The substrate recognition sequence (SRS) regions in a ribbon representation.[42]

1.2.3 Catalytic Mechanisms of Cytochrome P450

Owing to the diverse applications of cytochrome P450, there is a wide interest in studying these various enzymes, especially the catalytic mechanism. An overall catalytic cycle proposed is shown in Figure 1.2.7.[43] In the resting state, the heme iron is in the six coordinate, low-spin (6cLS) state, with a water molecule occupying the sixth ligand position. Upon binding a substrate, water molecule was displaced from distal axial position which bring heme iron from low spin state to a five coordinated high spin (5cHS) state. Then an electron is passed from NADPH via a redox partner to the heme iron, the ferric iron being reduced to the ferrous iron while still in high-spin state. Molecular oxygen binds to the heme iron leading to an oxy-P450 species, which is more properly formulated as a ferric superoxide species. Then a second electron is transferred to the Fe-O-O fragment, forming a ferric peroxo species. Generally, this is followed by a

fast protonation from surrounding amino acid residues or water molecule, to become a ferric hydroperoxo species. A second protonation at the distal oxygen atom leads O-O bond cleavage, with a water molecule leaving and formation of highly reactive species compound I. This species hydroxylates the substrate and returns to the resting state after product release.

However, three major abortive reactions can happen in this cycle.[44] The oxy-ferrous enzyme can be auto-oxidized back to its resting state with leaving of a superoxide ion. In addition to this auto-oxidation process, a so-called "peroxide shunt" pathway is possible by producing H_2O_2 from hydroperoxide. The last abortive reaction is "oxidase shunt", the compound I can return to the resting state by leaving two molecules water without going to oxygenate the substrate. These uncoupling processes may happen when the electron or proton delivery is not timely, or the substrate is positioned inappropriately.

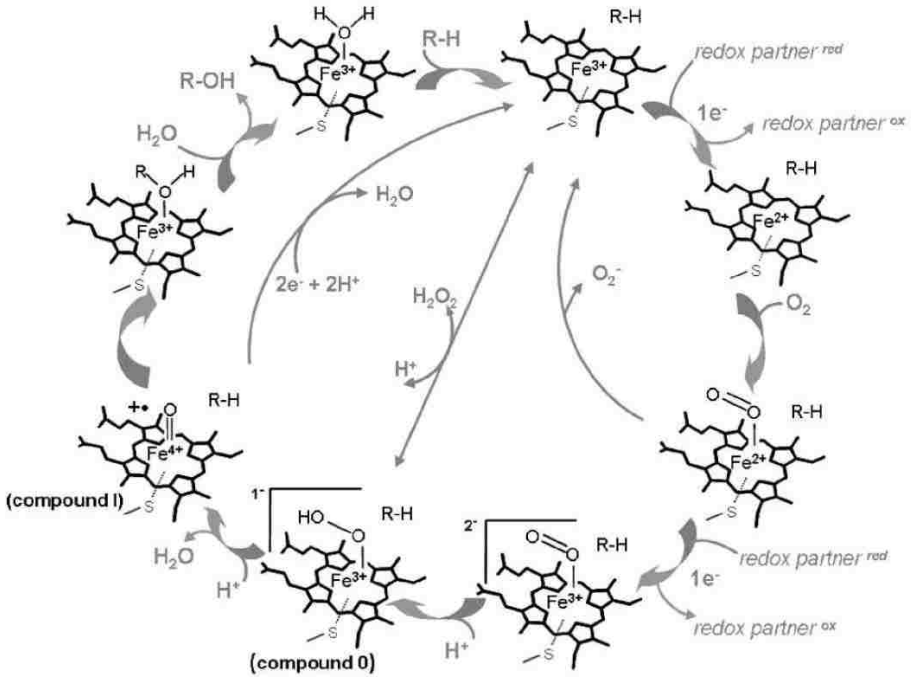

Figure 1.2.7. Catalytic cycle of P450.[45]

1.2.3.1 Substrate binding

The hydrophobic substrate binds in pocket above heme cofactor and the water molecule is displaced. This process not only shifts the heme iron from low spin to high spin state, but also raises the redox potential from -300 mV to a 100mV more positive, such as the case of camphor binding to P450cam.[46] The redox potential shift guarantees electrons are only transferred to the enzyme in substrate-bound form; i.e., since the midpoint potential of reducing equivalent (NADPH) is -320 mV, this balance ensures no waste of NAD(P)H and avoids reducing equivalents formation of toxic species such as superoxide. Moreover, conditions such as temperature, pH and solvent may also affect the low spin and high spin equilibrium as well as the redox potential of heme iron.

Basically, the interactions of substrate with P450s can be seen in the spectral properties of the enzyme. According to the observed UV spectral changes of P450 upon binding substrates, P450s can be classified into three catalogues: type I and type II.[47] Specifically, type I substrate can cause the heme iron change from 6cLS to the 5cHS state, which can be seen from the UV-vis spectra that the decrease of an 420 nm band and an increase at 390 nm depending on the percentage of high-spin state heme iron. Compared with type I substrates, type II substrates usually are inhibitors or certain other substrates which can directly ligate to the heme iron, forming tightly-bound complexes; e.g., N atoms of aromatic and aliphatic amines. The spectrum generally shows a low spin iron.

1.2.3.2 Oxygen complex

Oxygen can readily binds to reduced P450 in substrate bound form, forming the oxy complex which is usually depicted as the ferric superoxide complex, as mentioned above. The gross structure is very similar with the oxygen carrier such as hemoglobin and myoglobin. According to the X-ray crystal structure of P450cam ferrous dioxygen adduct, as shown in Figure 1.2.8, bimolecular oxygen binds to the heme iron in an end-on form with the angle of Fe-O-O 132°, the distance between iron and the nearest O atom is 1.8Å. The iron is slightly out of plane while the heme becomes flatter. The Asp^{251} and Thr^{252} residues play critical roles, serving as H-bond donor and proton transfer agents.[48]

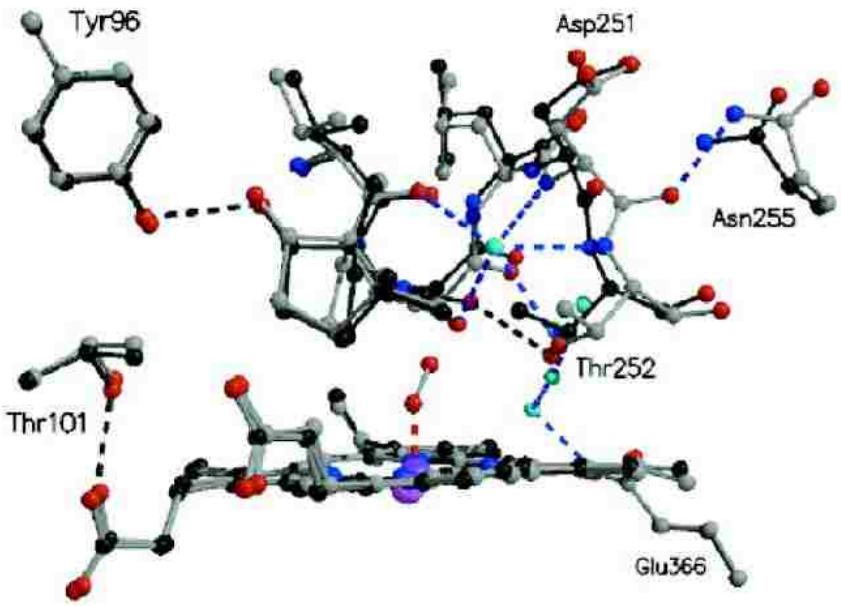

Figure 1.2.8 Stereoview of the camphor complex of ferrous dioxygen-bound P450cam.

1.2.3.3 Peroxo and Hydroperoxo intermediate

With the second electron transferred to the heme iron, the ferric superoxide species is reduced to the ferric peroxide complex in the catalytic cycle. This species is quickly protonated to form a hydroperoxo intermediate. Both of these two intermediates are in low spin state. Owing to rapid delivery of a second proton and facile O-O bond cleavage to generate compound I, isolation and stabilization of these is extremely difficult. As will be seen, cryogenic radiolysis is one of the methods that can be used to trap those intermediates. It was demonstrated that the peroxo species was stable enough to be characterized in the frozen solution at 77K, and thus the hydroperoxo intermediate could be obtained by annealing to elevated temperature.[49] By using this method, both intermediates were identified by spectroscopic methods such as UV-vis, EPR and resonance Raman spectroscopy.[50]

1.2.3.4 Compound I

The protonation of ferric hydroperoxo species and the heterolytic cleavage of the O-O bond lead to the formation of Compound I and release of a molecule of water. Compound I has been characterized as an iron (IV) oxo species, with a π cation radical located on the porphyrin macrocycle. In the presence of substrate, compound I rapidly reacts and is difficult to capture. Over the past decades, different models and methods were tried to characterize compound I with limited success.[51] However, recently compound I was captured and detected in CYP119 by reacting with m-chloroperbenzoic acid, thus enable spectroscopic methods to characterize it. As expected, Mossbauer and

EPR spectra indicated compound I is a Fe (IV) =O species with the ferry iron spin (S=1) antiferromagnetically, porphyrin radical spin equals ½ to yield the total spin state ½.[52]

1.2.3.5 Hydroxylation of substrate

Hydroxylation of substrate is the last step in the catalytic cycle, where Compound I inserts an O atom into the hydrophobic substrate and returns back to the resting state by releasing the product. It is generally accepted that the mechanism for substrate hydroxylation is a radical rebound process.[53] Compound I abstracts a hydrogen atom from the substrate while leaving a carbon radical, and this radical can rebound to the species with a recombination process to give the hydroxylation product.

1.3 Resonance Raman Spectroscopy

1.3.1 The Raman Effect

Resonance Raman spectroscopy is a powerful method to probe the active site structure of heme proteins and other metalloproteins because the vibrational frequencies and intensities are very sensitive to the structure and the protein environment. Although both IR and Raman spectroscopy can be employed to investigate molecular vibration modes, Raman is best to be used in the symmetric and polar molecules. In addition, IR has difficulty working with aqueous solution owing to the intense absorption of H_2O throughout the IR region which make the measurement inconvenient since most proteins are measured in aqueous solution. However, Raman spectroscopy does not suffer this

limitation because water is a poor Raman scatterer.[10] The mechanism for Raman spectroscopy can be explained via the energy level scheme as shown in Figure 1.3.1. When a monochromatic light from a laser source with frequency ν impinges on the sample, it can interact with molecules and lead to the laser energies either unchanged or being shifted up or down. In general, most of light will be scattered as the same energy with the incident light, which is called Rayleigh scattering, giving a very intense peak in the spectrum.

However, some of the incident light is scattered at lower energy if the molecule undergoes a transition from the ground vibrational state (ν_0) to an excited vibrational state (ν_1), which is referred as Stokes Raman Scattering. Occasionally a photon encounters a molecule that is vibrational excited (e.g., in the ν_1 state) and the scattering process leaves the molecule in ν_0, i.e., free photon gains energy from the molecule. This is called anti-Stokes scattering. The intensities of Stokes scattering is stronger than the anti-Stokes region, because few molecules will occupy an excited vibrational state, according to the Maxwell-Bolziman distribution law. The line thickness is roughly proportional to the intensity strength from different scattering in Figure 1.3.1. Thus, the scattering intensities of Strokes line is reported as a function of frequencies in Raman spectroscopy.

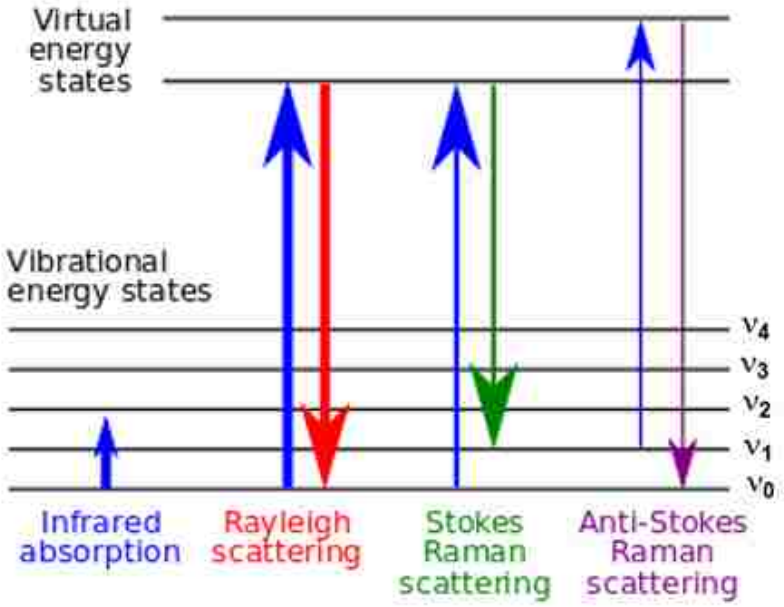

Figure 1.3.1 Energy level scheme of vibrational Raman scattering process.

Resonance Raman spectroscopy can selectively enhance the vibrational modes by using the laser excitation line which is close to the electronic absorption of the chromophoric heme prosthetic group, which is necessary for biological macromolecules which contain thousands of atoms and vibrational frequencies. A detailed illustration of enhanced resonance Raman spectroscopy is shown in Figure 1.3.2, trace A exhibits the structure of a complicated molecule tris-phenanthroline Fe (II) and trace B shows the corresponding absorption spectra with a strong MLCT transition appearing at 514.5 nm. As seen in trace C, different excitation laser lines were employed to characterize the samples which contain a non-enhanced internal standard (SO_4^{2-}). When the 647.1nm excitation line is used (far from the MLCT maximum), the Raman spectra is dominated by the sulfate ion with ν(S-O) occurring at 981 cm^{-1}. However, as the excitation line approaches to the MLCT maximum bands, the vibrational modes for tris-phenanthroline

Fe (II) are greatly enhanced, even though its concentration is 1000 times less than the internal standard sulfate ion.[54]

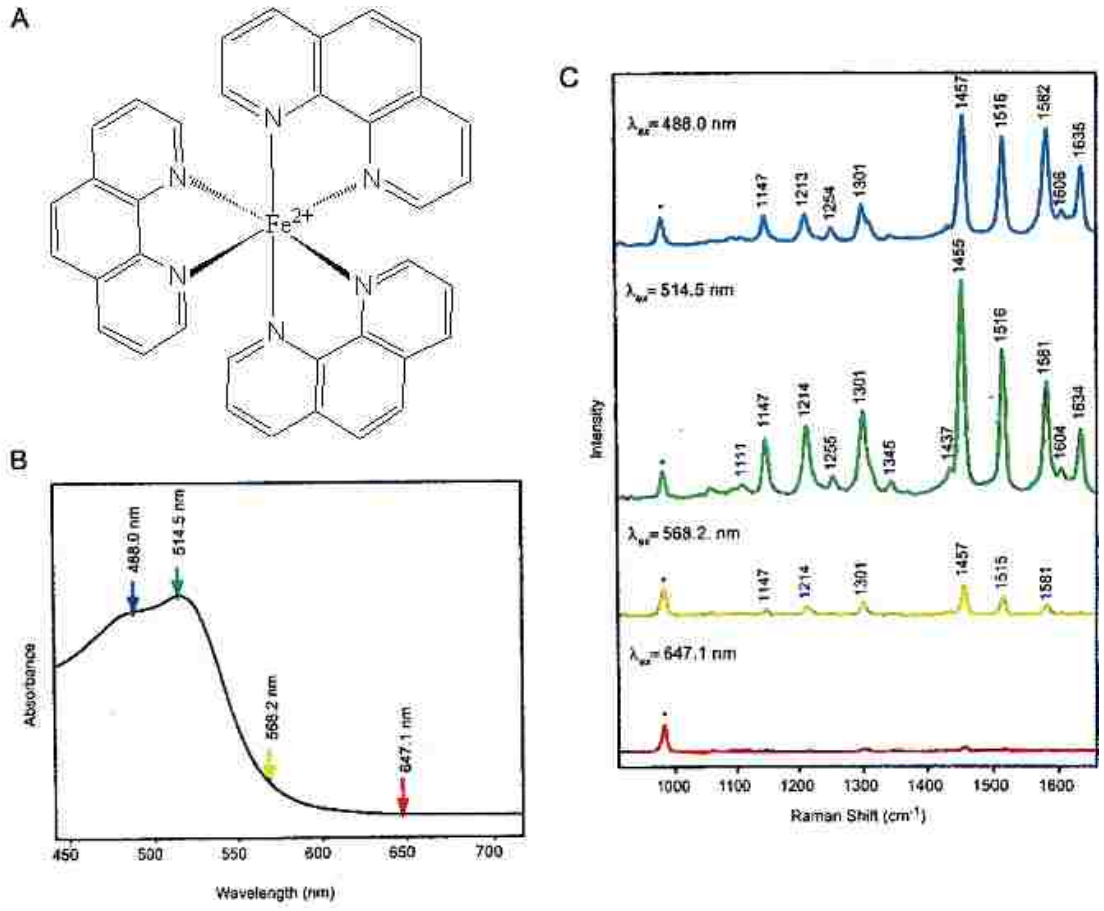

Figure 1.3.2 (A) Structure of tris-phenanthroline Fe(II); (B) Absorption spectroscopy of tris-phenanthroline Fe(II); (C) Resonance Raman spectroscopy with different excitation laser lines.

1.3.2 Resonance Raman Spectroscopy applied in heme proteins

Resonance Raman spectroscopy is a powerful method to study the structure and function of metalloproteins especially heme enzymes. By adjusting the wavelength of the exciting laser line close to that of allowed electronic transition in a molecule, certain vibrational modes can be selectively enhanced. Such an advantage provides the

possibility to collect good quality data even though using a small amount of sample. For example, hemoglobin is a large molecule with a molecular weight of 64 kDa, and its visible spectra is shown in Figure 1.3.3.[55] Generally, the vibrational modes of the peptide chain gains much weaker scattering and are not detectable, however, if a deep UV laser is applied, at 280 nm, it will selectively enhance vibrational modes from the surrounding amino acid residues in hemoglobin such as tyrosine, histidine, tryptophan and phenylalanine, which have electronic absorption in this region.[56] Alternatively, if the laser line is near the Soret band (most intense π-π* transition), only the heme bands can be seen. Thus resonance Raman spectroscopy allows us to observe the vibrational modes only in the active site.

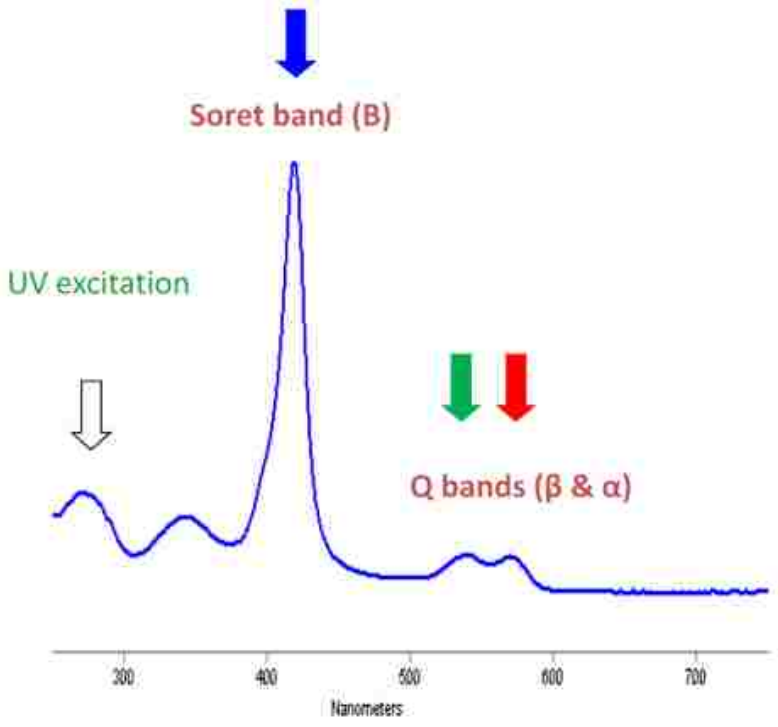

Figure 1.3.3 Electronic absorption spectroscopy of human hemoglobin.

1.4 Resonance Raman studies of Iron-axial ligated P450 Adducts

1.4.1 Metal-ligand interactions in Hemeproteins

The heme prosthetic group in heme enzymes is capable of binding the exogenouos diatomic ligands XY, such as CO, NO and O_2. The Fe-XY adduct can interact with the surrounding amino acid residues, affecting the bond strength of the Fe-X and X-Y linkage, as reflected in changes of the vibrational modes by resonance Raman spectroscopy. Binding the exogenous ligands can activate or inhibit key biological processes. For example, hemoglobin can transport O_2 by ligation of molecular oxygen with heme iron, whereas binding with CO can prevent O_2 binding. The general geometry of Fe-X-Y can be linear or bent depending on the electronic configurations and bond properties of XY ligands. As shown in Table 1.4.1, The CO ligand has an empty π^* orbitals and thus form a linear adduct which d_π- π^* overlaps in a perpendicular directions. However, NO and O_2 have one and two electrons on π^* orbitals, respectively, and thus form the bent geometry, owing to a π antibonding interactions. However, the geometry can be disturbed by the steric hindrance in the protein environment.[57]

Table 1.4.1. Electronic configuration and bond properties of diatomic ligands.

Ligand (A-B)	CO	NO	O_2
σ*	◯	◯	◯
π*	◯◯	↿◯	↿↿
σ	↿⇂		
π	↿⇂↿⇂	↿⇂↿⇂	↿⇂↿⇂ π
		↿⇂	↿⇂ σ
	$[\sigma(1s)]^2$	$[\sigma(2s)]^2$	$[\sigma^*(2s)]^2$
Bond length (re. Å)	1.128	1.15	1.207
Force const. (k. mdyne /Å)	18.6	15.5	11.4
Bond energy (kcal/mol)	258	162	118
υ(A-B)(cm^{-1})	2.145	1.877	1.555
Badger'd rule	$r_e=0.68 + 1.23\ k^{-1/3}$		

The binding interactions between iron and the ligand can be classified into two kinds; σ-bonding and π-bonding, as shown in Figure 1.4.1. σ-bonding is formed by the interaction between the metal d_z^2 with either the ligand lone pair electrons or the π* orbital of ligand. Because the energies of the d_z^2 and π* orbitals are very close, the strength of bond is relatively strong. In the case of CO, NO and O_2, the energy of π* orbitals decrease from CO to NO to O_2, leading to increased bond strength.

The π-bonding is formed between the metal d_π (d_{xz} and d_{yz} orbitals) and the ligand π* orbital. This interaction involves the electron shift from iron to the ligand in the d_π- π* system and a back donation to the iron in the σ system, thus leading to a strengthened M-X bond and a weakened X-Y bond. In addition, the axial ligand of heme protein, usually histidine or cysteine, can also affect these bond strengths. A σ competition between the trans axial ligand and the exogenous ligand can weaken the Fe-X bond.

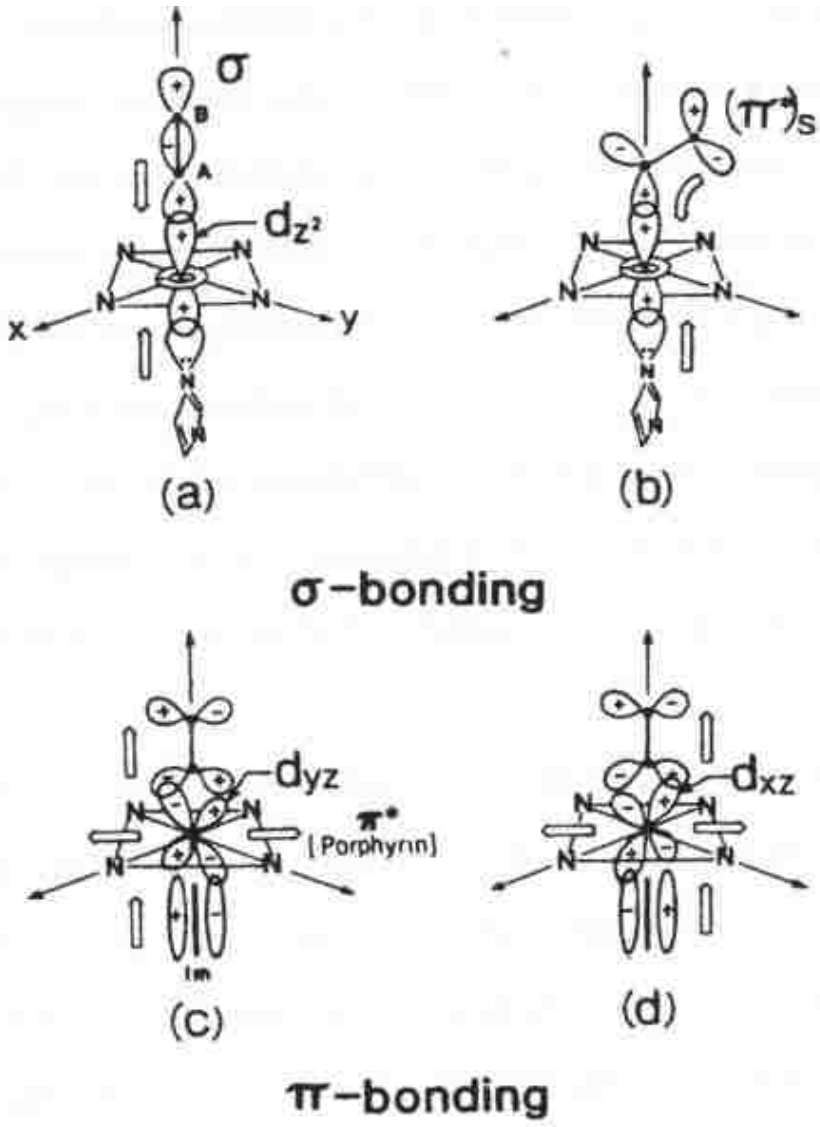

Figure 1.4.1 Representation of σ- and π-bonding interactions between metal ion and diatomic ligand.[58]

1.4.2 Resonance Raman spectroscopy to probe CO, NO and O_2 P450 complex and unstable fleeting intermediates in the catalytic cycle.

1.4.2.1 Ferrous CO P450 complex

CO can bind to the high spin ferrous heme iron to produce a low spin heme in P450s, giving a maximal absorption band around 450 nm. As mentioned earlier, the Fe-CO fragment is expected to be linear. However, in some cases, it can cause a slight bent geometry due to the steric constriction in the protein environment.

Since resonance Raman is an effective method to detect the subtle environmental alternations, vibrational modes of Fe-CO fragment have been identified by isotopic substitution of the bound CO. Both the modes of Fe-C and C-O can be enhanced in resonance with the heme Soret absorption band, i.e, using the 441.6 nm excitation line.

In Figure 1.4.2, it can be seen that a band occurs at 481 cm^{-1} shifted to 478 cm^{-1} upon the isotope substitution from $^{12}C^{18}O$ to $^{13}C^{16}O$ in substrate-free P450cam, and upon substitution by $^{13}C^{16}O$, it shifted to 473 cm^{-1}. Thus this feature occurs at 481 cm^{-1} was first assigned as ν(Fe-CO) stretching mode.[59]

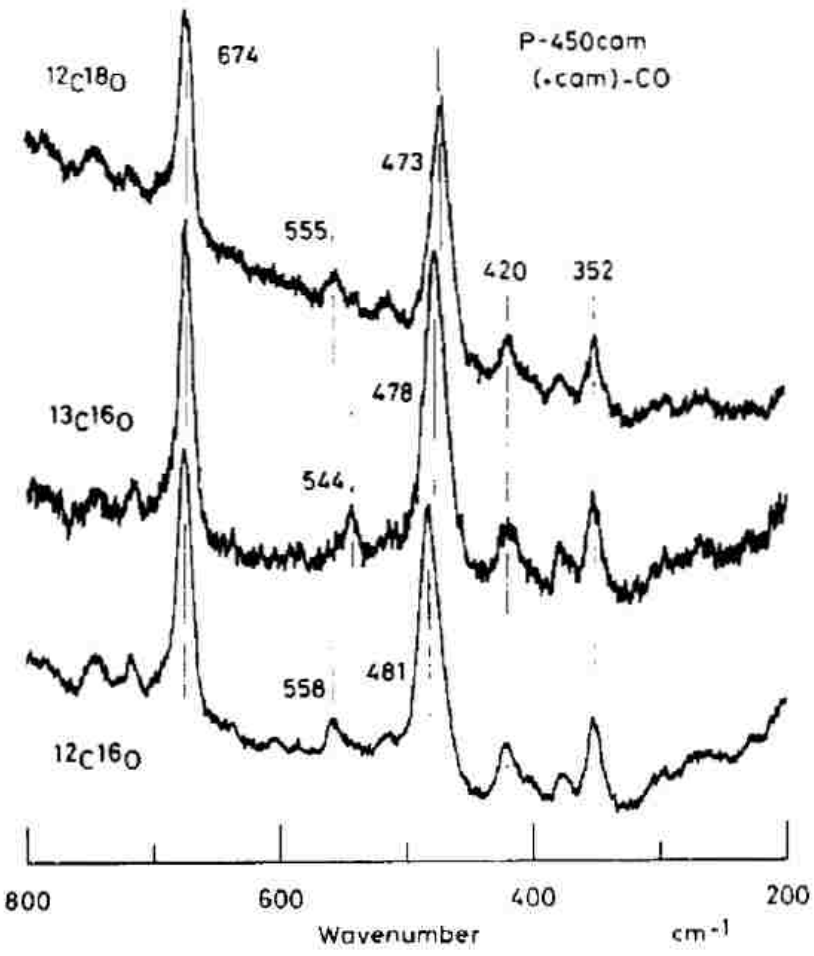

Figure 1.4.2. Effect of the substitution by isotope-labeled CO on the substrate-free form of P450cam.

The Fe-C-O bending vibration was assigned at 558 cm^{-1} owing to the significant shift (14 cm^{-1}) upon $^{13}C^{16}O$ substitution, giving only a -3 cm^{-1} on $^{12}C^{18}O$ substitution. The substrate binding on the P450cam caused a shift of Fe-CO stretching mode from 481cm^{-1} to 464 cm^{-1}, which indicates the bound substrate can interact with Fe-CO fragment, distorting the active site structure.

1.4.2.2 NO P450 complex

Nitric Oxide is able to bind with heme iron both in ferric and ferrous states. The geometry of Fe (III)NO is expected to be linear for compounds without distal steric effects, whereas it can become slight bent in the presence of substrates, in a manner similar to Fe (II)CO since they are isoelectronic. However, one main difference between these two adducts is that the electron in the NO π^* orbital is delocalized over the Fe d_π and NO π^* orbitals which lead to a strengthened NO bond owing to an increased bond order. This can also be detected in the high frequency region of rR spectra, where a feature occuring at 1877 cm^{-1} assigned as ν (NO) was observed.[60] Limited studies have been conducted on Fe(III)NO, owing to laser-induced photo reactivity and O_2 sensitivity.

Resonance Raman spectra of the nitric oxide adducts of ferrous cytochrome P450cam in substrate-free form and different substrate-bound forms were reported by Hu et.al.[61] By using isotopic substations of ^{15}N and ^{18}O, the axial vibrations were assigned. The ν (Fe-NO) stretching mode and δ(Fe-NO) bending mode are assigned at 522 and 546 cm^{-1}, respectively. The geometry of Fe(II)NO fragment is expected to be inherently bent, but can also be sensitive to the presence of different substrates. Thus, it is interesting to investigate the bending modes of Fe-N-O for various substrates. It is shown that the size of substrate can affect these modes, the larger substrate binding can lead to an enhancement of the Fe-N-O bending mode.

1.4.2.3 Fe-dioxygen complex

The study of P450-O_2 adducts is a way to get direct information about the catalytic mechanism. However, there are lots of challenges to acquire the vibrational data

for the dioxygen adduct, owing to its instability; it can be easily autoxidized back to Fe (III) OH rapidly. In addition, for some heme proteins, it is difficult to detect the stretching mode of O-O bond since it is only weak enhanced in the rR spectroscopy. However, in the case of P450cam and selected proteins, it is found that the ν (O-O) mode can be enhanced owing to the fact that axial ligand is thiolate, the enhancement is presumably attributable to altered electronic coupling involving the S-Fe-(O_2^-) fragment.[62]

The rR assignment of P450 dioxygen adducts was done by employing isotopic labelling.[62-63] In the case of camphor bound P450cam, the ν (O-O) and ν (Fe-O_2) stretching modes were assigned at 1140 cm^{-1} and 540 cm^{-1} by using ^{18}O substitution, respectively. Both of these two modes are sensitive to the substrate size; when the camphor is replaced with the larger sized substrate, adamantanone, two ν (O-O) modes can be seen at 1139 and 1147 cm^{-1}, indicating that in the presence of adamantanone, two structural conformer exist.[64]

1.4.2.4 Cryoradiolysis studies on intermediates in hemeprotein catalytic cycle

Resonance Raman spectroscopy is not only used to characterize the oxy complex, but also can be applied to following fleeting intermediates in the catalytic cycle including peroxo-, hydroperoxo- ferric forms. Radiolytic reduction in frozen solutions is an effective method for trapping and studying the unstable catalytic intermediates in P450s. Usually, radiolysis of a protein solution can produce lot of radicals which can lead to diverse products depending on the solvent condition; however, using a frozen solution, one can avoid such obstacles because the diffusion in solid matrix is limited.[65] Thus, the cryoradiolysis studies on frozen samples made accumulating the active intermediates

possible. The irradiation on hemeprotein frozen solution can be conducted at 77K and irradiated by γ ray which is usually a ^{60}Co source to generate the free electrons in presence of some organic solvent such as glycerol and ethylene glycol. This method was first pioneered by Martyn Symons in 1980s,[66] and more recently defined and used extensively by Hoffman and Sligar and coworkers.[67]

The general process of cryoradiolysis of hemeproteins is shown in Figure 1.4.3. The hemeprotein is prepared in H_2O or D_2O buffer which both containing around 30% glycerol which is a good electron source during irradiation. By adding the chemical reductant such as sodium dithionite in anaerobic environment, the ferric iron can be reduced to ferrous state, then the dioxygen gas is bubbled into the protein solution at low temperature and quickly frozen in liquid nitrogen. Such trapped dioxygen adduct (Figure 1.4.3 a) can be characterized by resonance Raman spectroscopy. Upon the γ-ray irradiation on the frozen solution, the electrons and free radicals were produced and the electrons can migrate to the Fe-O-O fragment, at this temperature, only electrons can move but the proton and other species are restricted. At this point, the ferric peroxo species (Figure 1.4.3 b) can be generated and characterized. For the next stage, to allow the proton transfer to generate the hydroperoxo form (Figure 1.4.3 c), the samples need to be carefully annealed at higher temperature, the precise temperature could be detected by EPR. Ideally, subsequent annealing further allows the transfer of another proton to facilitate O-O bound cleavage to yield compound I (Figure 1.4.3 d) or eventually neutral compound II species (Figure 1.4.3 e), but usually they are too reactive to trap.

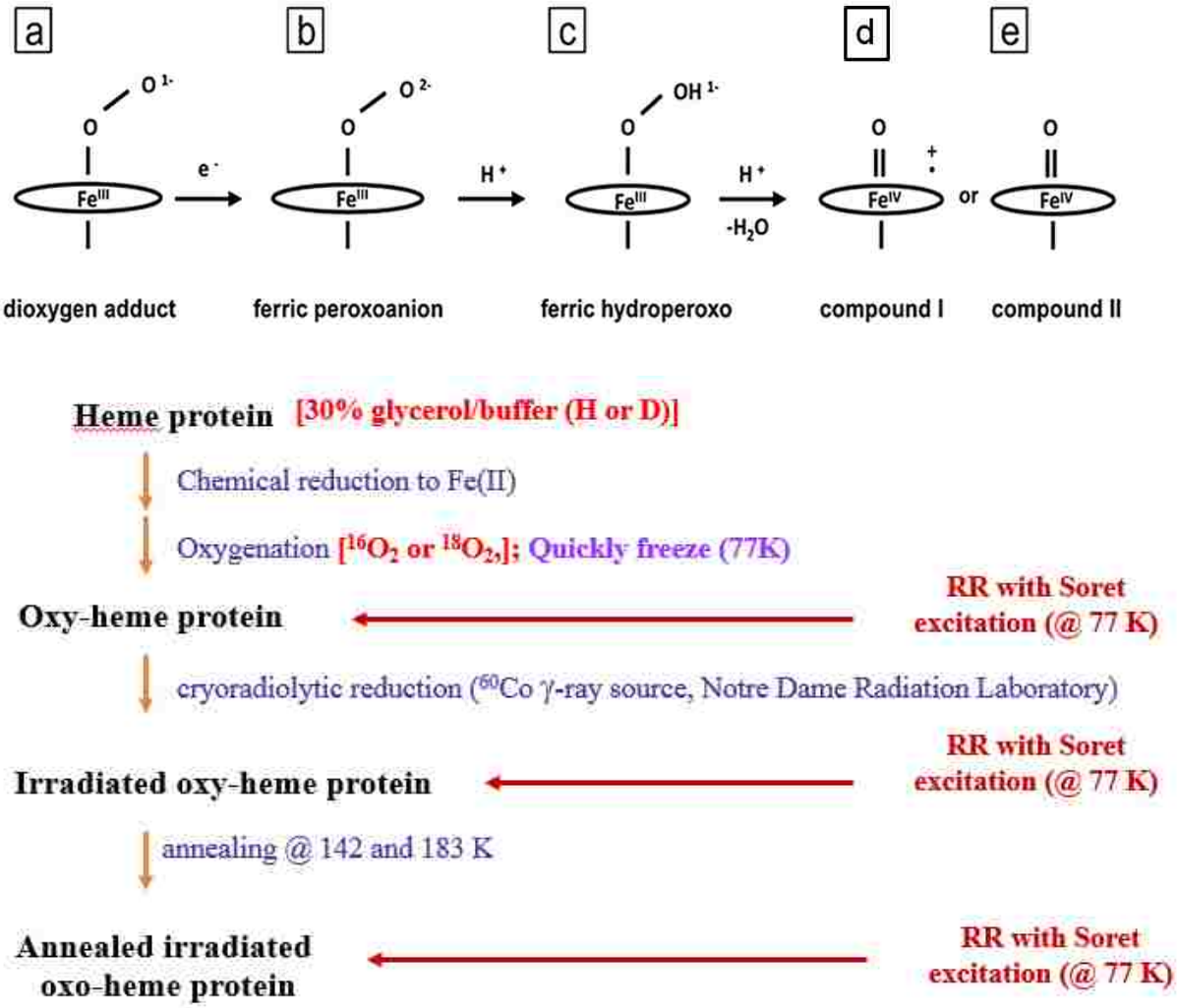

Figure 1.4.3 Process of cryoreduction of heme proteins.

1.5 Nanodiscs Technology application in Cytochrome P450

The self-assembled Nanodisc system is considered as a versatile tool to study structure and function of membrane proteins by rendering them soluble in aqueous solution while still providing them a native like bilayer environment to keep function active.[68] This system provides possibilities for measuring membrane-bound cytochrome P450s which previously suffered limitation on using soluble P450s only. Moreover,

assembly of membrane proteins is achieved by using this technique. It allows detailed analysis from spectroscopic and kinetic methods which is extremely helpful to understand the mechanism of P450's catalytic cycle. So far, numerous membrane bound P450s have been incorporated in nanodisc and characterized by rR spectroscopy. For example, nanodisc incorporated CYP3A4 shows a fully spin-state conversion upon type-I substrate binding.[69] In addition, the nanodisc system is useful to isolate the unstable catalytic intermediates in cryogenic methods.

Nanodiscs consist of an engineered scaffold protein that surrounding the lipid domains which plays a key role in keeping protein homogenous and soluble, Figure 1.5.1 shows a schematic view of a nanodiscs. To approach this, the target membrane protein is solubilized in detergent with phospholipids and scaffold protein. By adding hydrophobic Bio Beads, the target protein self-assembles into a lipid bilayer discoid, the size being dependent on the length of scaffold protein. The advantage of nanodisc, such as small size, less light scattering and faster diffusion, allows careful characterizations of P450 enzymes in a native like environment.

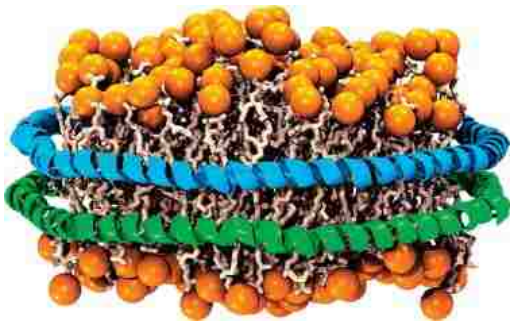

Figure 1.5.1 Schematic view of a nanodisc.

It is also possible to incorporate the target P450 with a reductase in one nanodisc, which better mimic the interaction in membrane environment.[70] One successful case is the generation of cytochrome P450 reductase (CPR) and CYP3A4 in the same nanodiscs (Figure 1.5.2). Thus, starting with solubilizing both proteins in detergent, once the Bio Beads are removed, nanodiscs can be assembled in different ways. There are several possibilities that different types of nanodiscs are generated; it could be the empty nanodiscs, nanodiscs with single protein incorporated (either CPR or CYP3A4), or both properly incorporated. Desired products can be separated by using several different columns, e.g., firstly, a size exclusion column is applied to the mixture to obtain the nanodiscs with right size (some get proteins incorporated and some are empty), then the fractions are applied on a Nickel affinity column, which can selectively bind the CYP3A4 incorporated nanodiscs, then the eluted fractions are loaded into a 2' 5' ADP column which allows binding of CPR incorporated nanodics, finally, both CYP3A4 and CPR incorporated nanodicscs products can be washed out from this column. This is amazing because it is able to study a protein with the reductase partner in isolated membrane. You can never study those in aqueous solution because different kinds of aggregate.

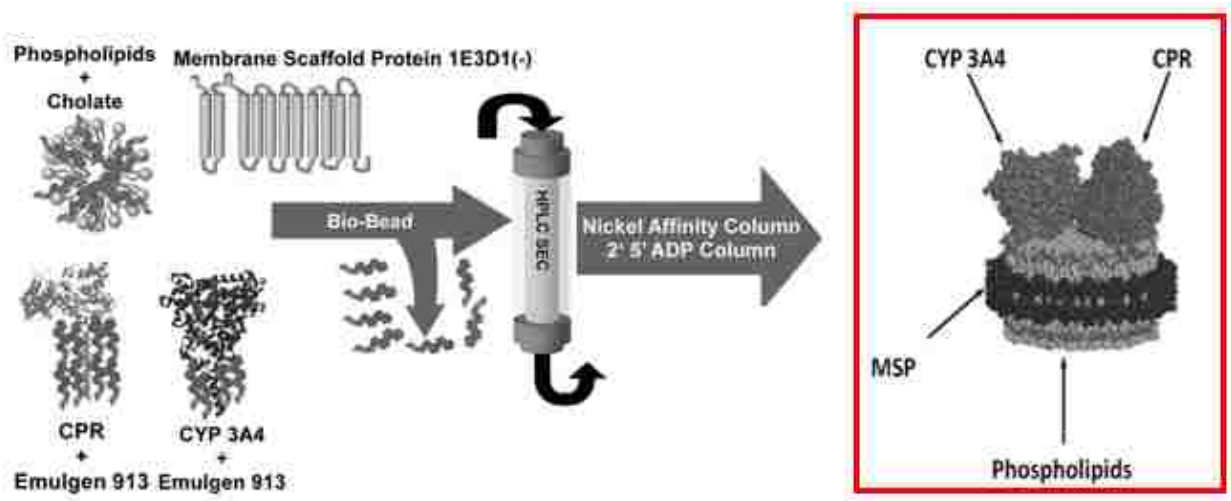

Figure 1.5.2 Process of the self-assembly of CYP3A4 and CPR into Nanodiscs.[70]

However, this approach requires generating a large excess of proteins incorporated in nanodiscs, with low overall yield. So recently, a new alternative approach was described by Dr. Sligar's group, by directly incorporating of CPR into a performed population of CYP3A4 nanodiscs, a stable and fully functional complex could formed within several minutes at 37 Celsius degree.[71] The optimized ratio between CPR: CYP3A4 is found to be 2:1, when the ratio is 1:1, only 40% of 3A4 nanodisc was incorporated with reductase, but when at 2:1 ratio, most of CYP3A4 is involved in the 1:1 complex. If the ratio increase further, a larger complexes with an increasing amount of CPR per CYP3A4 are formed. A highly active nanodiscs form with both target protein and reductase can be formed with high yield. Once formed, rR spectroscopy was used to investigate different P450 enzyme either expressed from bacteria or the Nanodiscs incorporated mammalian P450. In our studies, to better understand the interaction between different proteins and heme environment, individual proteins such as CYP17A1 is investigated using rR spectroscopy.

1.6 Overview of my research

Generally, the main goal of my research is to use resonance Raman spectroscopy to study the structure and function of cytochromes P450. In our paper, the interaction between CYP17A1 and its redox partner cytochrome b_5 was undertaken, including characterization of their ferric state and unstable intermediates, CYP17A1 ferrous dioxygen adduct in presence of cyt b_5. The second project is focused on the enzymes which are good targets of exploration for biotechnologically useful purposes. There is high interest in study of the enzyme called P450 BM3 with the fact that it is covalently linked with its cytochrome P450 reductase, showing remarkably high monooxygenase catalytic activity, can functional convert fatty acid to short chain hydrocarbons or other commercial products. These rR studies are focus on several gatekeeper mutants of P450 BM3 which can alter substrates binding to allow the PPI drug, omeprazole, to be processed. Specifically, the ferrous CO adduct are being analyzed to interrogate the effect of substrate binding on the distal pocket architecture. In another project, trapping and characterization of crucial intermediates in peroxygenases (CYP152L1 and CYP152L2) by rR is performed, providing information about Compound I and Compound II intermediates that can directly react with substrate. Aside from those important studies, it is also of great interest to document any differences in the key Fe-O-O fragment of the "precursor" to the Compound I intermediate. In addition, a small project dealing with the enzyme, DGCR8, included as an appendix, the results having been recently published in the ACS Journal of *Biochemistry*.[72]

Chapter 2: Methods and material

2.1 Expression and purification of P450cam

The procedure for expression and purification of P450cam is summarized in this section, just for practice and to get familiar with the purification process, making preparation for collecting good quality rR data in later research work.

2.1.1 Agents and buffer

Trizma-HCl, Trizma base, potassium chloride, (R)-(+) camphor, potassium monophosphate, potassium phosphate dibasic, ammonia sulfate, sodium chloride, bacto tryptone, bacto yeast, LB broth, ampicillin, and antipain were purchased from Sigma-Aldrich**.** Pepstatin, DNase, RNase, lysozyme, Phenylmethylsulfonylflouride (PMSF) and Isopropyl β-D-1-thiogalactopyranoside (IPTG) were obtained from Amresco. Leupeptin, antipain, and δ –amino levulinic acid (δ-ALA) were purchased from Alfa Aesar. The DEAE-52 (pre-swollen) anion exchange was purchased from Whatman, Phenyl Sepharose hydrophobic gel was obtained from GE Healthcare.

All buffers were made with highly deionized water (>16.5 MΩ/ cm) which is generated by a deionizing system from Barnstead. The running buffer for DEAE column contained 50 mM Tris-Cl, 25 mM KCl and 1 mM camphor, pH was adjusted to 7.5. While the elution buffer for DEAE column was same as the running buffer except increasing the KCl concentration to 300 mM. For phenyl sepharose column, the running buffer contained 50mM Tris-Cl, 50 mM KCl, 25% $(NH_4)_2SO_4$ and 1 mM camphor, pH

was adjusted to 7.5. While the elution buffer was same as the running buffer but without adding ammonia sulfate. Potassium phosphate buffer were made by adding K_2HPO_4 solution to KH_2PO_4 solution to bring up pH to 7.5. All buffers finally used contained 1mM camphor. To avoid the formation of inactive form P420, all the procedures were done at 4°C environment.

2.1.2 The enzyme assay and purity index

The concentration of P450cam was determined by using the reported extinction coefficients of their character absorption band. In this case, the camphor-bounded P450cam has a 102 Mm^{-1} cm^{-1} coefficient at λ= 391 nm.[73] According to beer's law, concentration would be easily obtained.

The UV absorbance ratio (A_{392}/A_{280}) was adopted to check the purity of the P450 protein. In the substrate-bound P450cam, an Rz (A_{392}/A_{280}) value of an enzyme greater than 1.5 was shown as electrophoretically homogeneous.

2.1.3 Expression of P450cam

2.1.3.1 Preparation of LB agar Plates

1.75g LB agar was dissolved in 50ml distilled water in a plastic conical flask, solution was heated in a microwave oven for 2 mints but pause every 15 seconds, gently shaking to avoid formation of bubbles. Allow the solution to cool down to room temperature, 50ul of 100mg/mL ampicillin was added. In a sterile environment, the solution was poured into plates continuously until the solution cover the plates, cool

down for 30mins. Transfer the transformed cells to the plates and spread the cell using autoclaved glass beads. Incubate the cells at 37° for overnight to allow cell growth.

2.1.3.2 Preparation of 2YT media

24g bacto tryptone, 15g bacto yeast and 7.5g NaCl were dissolved in 1.5L highly polished water in a 2L plastic bottle, water is added first to prevent micro-fog, four of such kind of 2L bottles were prepared. To anther 250ml plastic Erlenmeyer flask, 2.5g LB broth was dissolved in 80ml distilled water. All these five flasks were covered with aluminum foil and autoclaved for 20 minutes. Cool it to room temperature. 1.5ml of ampicillin was added into each four 2L plastic bottle, and solutions are stored in the cold room overnight.

100uL of 100mg/mL ampicillin was added to the small flask, 1 colony of P450cam culture in plates grown previously was transferred into this flask. Incubate this culture solution at 37°C in the shaker with speed of 250 rpm for overnight.

2.1.3.3 Bacterial growth

15ml of culture solution grown overnight was transferred to each large plastic bottle, then incubate for 45 minutes at 37°C with rate of 250 rpm. The growth of the cells were checked by measuring optical density (OD_{600}) values using UV-Vis, spectra were taken to monitor until OD600 was 0.6~0.8. Results obtained are shown in the table below.

Table 2.1.1 Changes of OD_{600} values with time of cell growth.

Time (mins)	0	40	80	120	150	170	180
Abs at 600nm	0.0082	0.0142	0.0609	0.155	0.268	0.5048	0.7977

1M Isopropyl β-D-1-thiogalactopyranoside (IPTG) was prepared by dissolving 2.38g of IPTG in 10 mL water in a large tube. IPTG was stored in cold room with aluminum foil covered to avoid photo degradation.

1.5mL of 1M IPTG and 167uL of 45 mg/mL aminolevulinic acid were added into each flask to induce protein expression. The addition of IPTG to cultures causes lacl repressor displacement from DNA, simultaneously inducing expression of T7 RNA polymerase from the chromosome. The best time to add IPTG was when the cell shows logarithmic growth phase, then IPTG can perform better to induce transcription. Aminolevulinic acid (ALA) worked as a precursor for heme synthesis, which is added to enhance the production of P450. Then these solutions were incubate at 24°C at the speed of 190 rpm for 21hrs.

0.2g camphor was added into each flask one hour before harvest and incubated for another hour. Cells were harvested by centrifuging at 7000rpm for 10 minutes. Cells were collected in a plastic tube and stored in the freezer at -80°C. Mass of wet cells is 53.65g.

2.1.3.4 Cell lysis

Cell lysis was done in a lysis buffer by using sonication. To make lysis buffer, 1 mM Phenylmethylsulfonylflouride (PMSF), 1 μg/mL Leupeptin, 1 μg/mL Antipain, 1 μg/mL Pepstatin, 32 units/mL DNAase, 3 units/mL RNAse, 1 μg/mL Lysozyme were added into running buffer (50 mM Tris buffer, pH=7.4, 25 mM KCl, 1 mM camphor) to

dissolve the cell wall to release the protein. Assume the density of cell is 1 g/mL, the final lysis volume would be 3 times of cell volume, equals to 150 mL in this case. Note this volume included both the wet cells and lysis buffer.

The cells were physically cracked into small pieces and transferred to a 50ml plastic beaker, and then cells were sonicated for 5 times for each time 1 minute to allow cooling down, using the power 3, 60% duty and timer on hold. In all this process, the cells were kept on ice to avoid frothing. The crude P450 were obtained by centrifugation for 90 minutes at speed of 7000 rpm, using rotor of code 03. The solution was concentrated to 20ml by using concentration cell. Buffer exchange was done on protein by adding DEAE running buffer before loading onto the DEAE anion exchange column.

2.1.4 Purification of crude P450cam

2.1.4.1 DEAE-52 Column

According to manufacturer's recommendation, the size of column should be about twice of cell lysis solution. Specifically, 100 g of pre-swollen DEAE-52 resin were suspended in 0.5M Tris acid, pH was adjusted to 7.4 by adding Tris base. The supernatant fine particles were decanted after settle down for 30 minutes, this step was repeated for 3 times to remove all the fine particles in order to slow down the flow rate of column. Then the gel was degassed in a suction flask with gentle mixing for 45 minutes, decant the top layer with fine particles, and a 4×25 cm column was packed. The column was washed with 1L of running buffer to ensure the equilibration. The crude P450 was loaded onto the column and washed 4 column volumes of the running buffer. The protein was eluted by using a salt gradient of 25 mM to 300 mM KCl with a flow rate of 2-3

mL/min. Fractions was collected every 2.5 mL and UV-Vis spectroscopy was used to check purity. The factions with Rz values >0.5 were combined and concentrated for 10 mL for further purification.

2.1.4.2 Phenyl Sepharose (Hi-Res) Column

Phenyl Sepharose is a hydrophobic interaction column, the fraction of hydrophobic amino acid in the protein will bind to the resin in the presence of moderate to high concentration of salt. According to manufacturer's recommendation, a 2×20 cm column for phenyl sepharose gel was prepared, and this column was equilibrated with 4 columns volumes of running buffer (50 mM Tris buffer, pH=7.5, 25% $(NH_4)_2SO_4$, 50 mM KCl, 1 mM camphor). Ammonia sulfate was added slowly to the protein obtained from the DEAE column to make it saturate, ensure the solution is clear without protein precipitation, diluted with running buffer if precipitation happened. Then this ammonia sulfate saturated P450cam is loaded onto the phenyl sepharose column at the rate of 1 mL/min. The column was washed with several column volumes of running buffer to obtain purer protein. Elute protein with elution buffer using a salt gradient of 25% ~0%. Fractions were collected every 3 mL and checked by UV-Vis spectroscopy. Fractions 2-11 with Rz value > 1.4 were pooled, shown in Table 2.1.2 below, potassium phosphate buffer was used to exchange buffer to remove ammonia sulfate, and the protein was eventually concentrated to 200 μL**,** stored in -80°C freezer.

Table 2.1.2 Rz values > 1.4 fractions collected from phenyl Sepharos column.

Fractions	A_{280}	A_{392}	Rz
2	1.1134	1.6259	1.461
5	1.4157	2.3335	1.648
8	1.7204	2.7559	1.601
11	1.5567	2.534	1.627

2.2 Purification of Glycerol for cryogenic studies

Cryogenic radiolysis reduction is an effective method to trap the peroxo-ferric and hydroperoxo-ferric intermediates, which is very helpful for mechanistic studies of Cytochrome P450. In order to stabilize these intermediates, data needs to be collected at cryogenic temperature in aqueous glycerol glasses. On the other hand, to prevent samples freezing at low temperature, glycerol is also necessary when making oxy samples, as preparation of this intermediate requires efficient mixing with oxygen. However, the commercial glycerol exhibits strong fluorescence background in rR spectrum due to the impurity, thus purification of glycerol is an absolute necessary for rR studies, the procedure is summarized in following sections.

A low temperature apparatus used in our lab is shown in Figure 2.2.1. A double wall glass cell was used to keep the low temperature by continuously adding liquid nitrogen. Spectra were acquired using 415 nm from Kr^+ laser (Coherent Innova Model 100-K3) with a 180 back-scattering geometry, laser power is maintained at 20mW. Glycerol is used as solvent to form transparent glasses at 77K, in order to remove the

fluorescence impurities that may obscure the Raman bands, glycerol was purified by treating with charcoal[74] and later vacuum distillation.

2.2.1 Treatment of glycerol with active carbon

99.5% Spectrophotometric grade glycerol and activated charcoal were purchased from Sigma-Aldrich. 27mL of glycerol was mixed with 0.34g activated charcoal and heated under a nitrogen atmosphere at 70℃ for 4 hours.

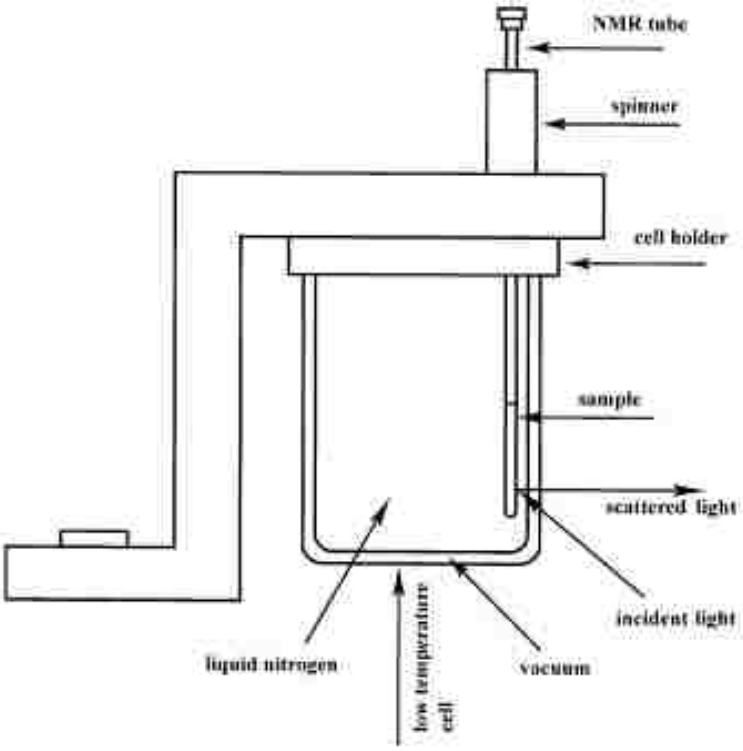

Figure 2.2.1 Set up for low temperature rR measurement.[75]

2.2.2 Vacuum distillation of glycerol

In order to remove charcoal and further purification, vacuum distillation was applied. The mixture obtained above was placed in a round bottom flask and then

connected to vacuum line. The mixture was degassed first and then the temperature was increased by heating very slowly in an oil bath. The glycerol starts to distill off at about 155 °C. The first 1ml glycerol was discarded; the middle part (around 20ml) was collected in a 25ml flask. Figure 2.2.2 shows the set up for vacuum distillation of glycerol.

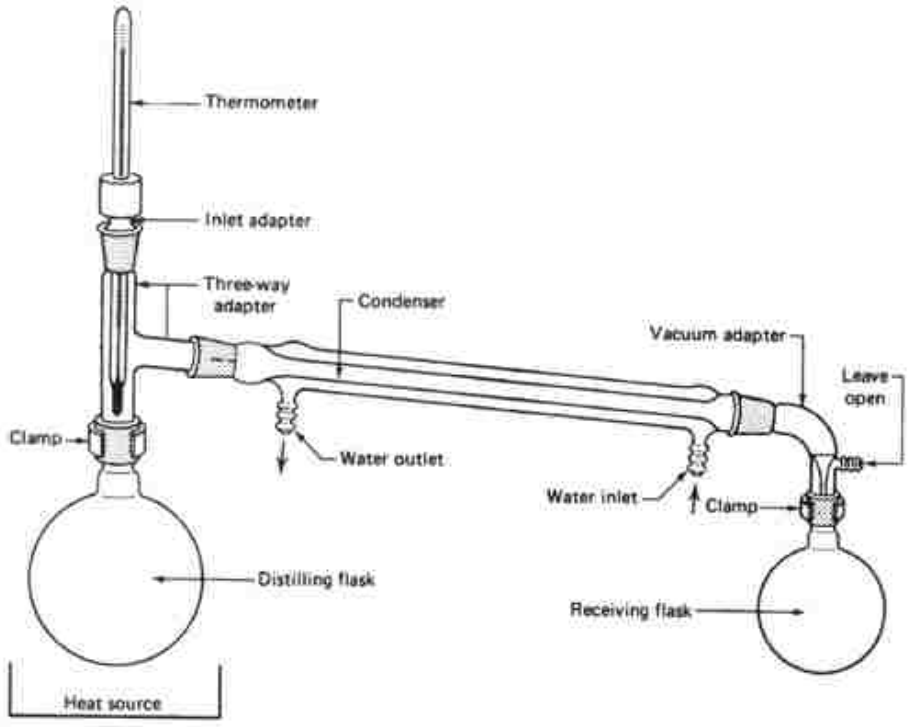

Figure 2.2.2 Set up used for vacuum distillation of glycerol

Another method was tried to remove the charcoal in glycerol. After glycerol reacted with charcoal for 4 hrs, the mixture was cooled down; 0.2mM syringe filter was then used to remove charcoal instead of vacuum distillation. Transparent glycerol was collected. Resonance Raman spectroscopy was used to check the fluorescence background of each sample, as shown in Figure 2.2.3, it was noticed that the vacuum distillation is the best method to get purer glycerol.

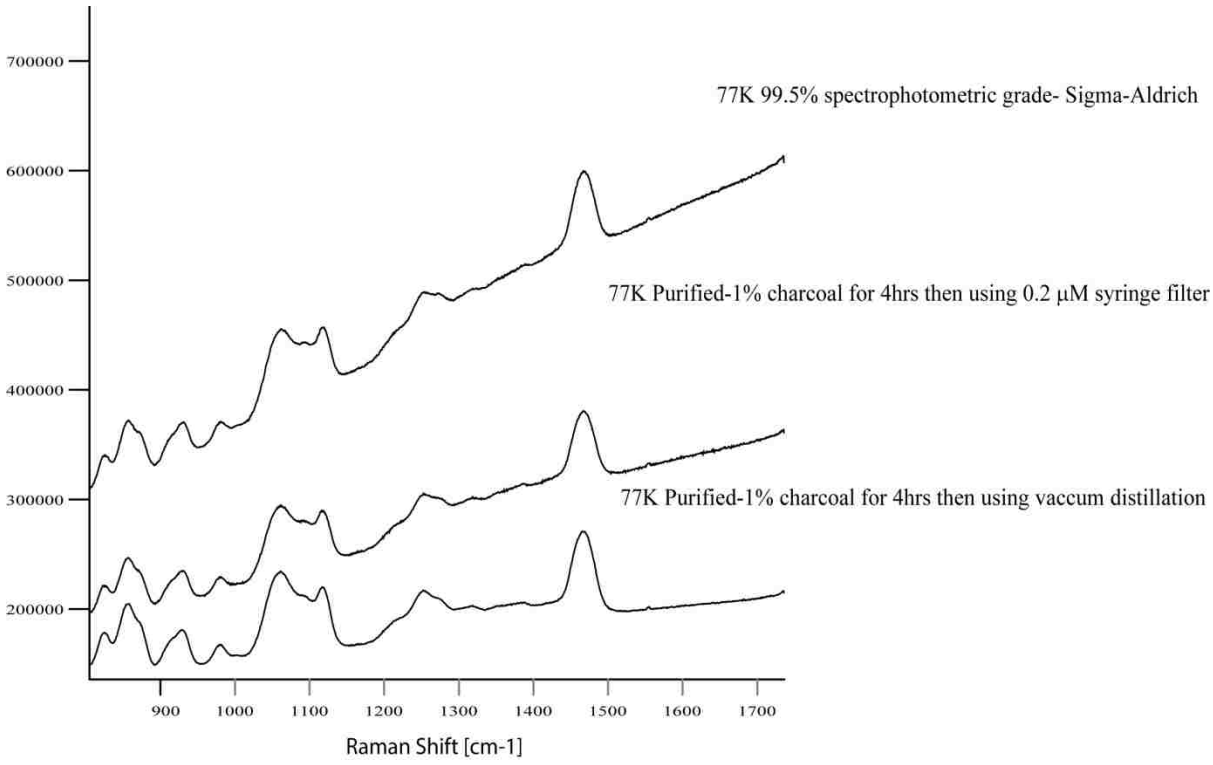

Figure 2.2.3 High-frequency resonance Raman spectra of glycerol from manufacturer and the purified glycerol according to the procedure above. (Measured with 415nm excitation line, 20mw power)

2.3 Resonance Raman Measurement

The Resonance Raman spectra were acquired using a Spex 1269 spectrometer equipped with a Spec-10 LN liquid nitrogen-cooled detector (Princeton Instruments, NJ). The 406.7 nm and 413.1nm excitation lines from a Kr^+ laser (Coherent Innova Sabre Ion Laser) were used to measure the ferric P450 and oxy samples. While the 441.6nm excitation line from a He-Cd laser (IK Series He−Cd laser, Kimmon Koha CO., Ltd.) was used to probe the P450 ferrous-CO form. The laser power incident on ferric samples was ~10 mW, while the power used for ferrous-CO or ferrous-O_2 samples are adjusted to ~1

mW. Rayleigh scattering was removed from the Raman signal by using an appropriate notch filter (Kaiser Optical). Owing to thermal effects arising from photon absorption and local heating by the laser beam, the possibility of decomposition of the samples can be enhanced. To overcome this problem, the samples were placed in a N_2–driven spinning NMR tube and the spectra were collected by using a 180° backscattering geometry with a cylindrical lens.[76] All spectra were calibrated with fenchone and data were processed with Gram/32 AI Software. The accumulation time for the RR spectra depended on the quality of protein. The basic set-up for resonance Raman instrument is shown in Figure 2.2.4**.**

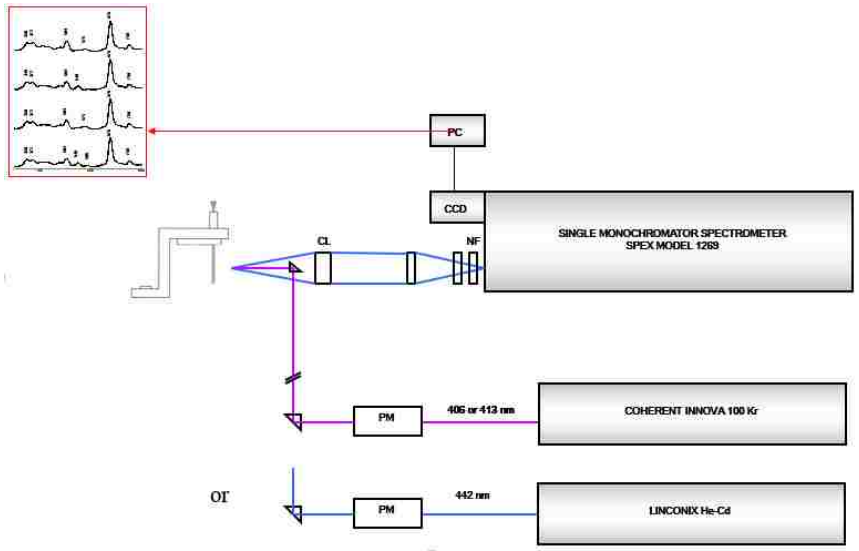

Figure 2.2.4 Basic Resonance Raman instrument set-up.

Chapter 3. Studies of the interaction between CYP17 with reductase partner

Portions of this chapter have appeared in the paper:
Duggal, R,; **Liu, Y**,; Michael, C. G.; Ilia, G, D.; Kincaid, J. R.; Stephen, S. G.; ., "Evidence that cytochrome b5 acts as a redox donor in CYP17A1 mediated androgen synthesis" *Biochemical and Biophysical Research Communications*, **2016**, *477*, 202-208

3.1 Introduction

Cytochrome P450 17A1 (CYP17A1) is an important drug target for castration resistant prostate cancer. It is a bi-functional enzyme, catalyzing production of glucocorticoid precursors by hydroxylation of pregnene-nucleus, and androgen biosynthesis by a second C-C lyase step, at the expense of glucocorticoid production. It is also known that Cytochrome b_5 (cyt b_5) is a key regulator of CYP17 reactivity and androgen synthesis in vivo, but the mechanism for this effect has been the subject of intense debate for decades. Although its essential role of cyt b_5 in the fatty acid biosynthetic pathways is well appreciated,[77] early work with hepatic drug metabolizing enzymes often yielded conflicting results. For instance, Sato and coworkers suggested that the binding of cytochrome b_5 (cyt b_5) to cytochrome P450 elicited a structural change in the enzyme which activated product turnover, either by increasing the inherent catalytic rate or by inhibiting non-productive auto-oxidative shunt processes (As shown in Figure 3.1.1).[78] Alternatively, as cyt b_5 contains a bisimidazole coordinated heme, direct transfer of electrons from cyt b_5 to P450 has been proposed.[79] In this latter role, the relatively high redox potential of cyt b_5 (~0 mV versus Normal Hydrogen Electrode)[80] suggests that electron transfer to ferric P450 (redox potential ~ 300 mV vs. NHE) is

unfavorable. Hence it was suggested that the redox function of cyt b_5 involved electron transfer to the ferrous dioxygen intermediate which has a redox potential near 0 mV thus providing the "second electron" in the normal monooxygenase stoichiometry.[81] In an attempt to differentiate between these two roles, Coon and co-workers reconstituted apo-cyt b_5 with manganese protoporphyrin IX.[82] They observed no reduced Mn-b_5 in the presence of cytochrome P450 reductase (CPR) and NADPH, whereas iron cyt b_5 was rapidly reduced. Hence Mn-b_5 is incapable of any electron transfer to the P450. From their experiments on various P450 reactions they concluded that cyt b_5 effects depend on the specific P450 in question, the substrate being examined, and molar ratio of CPR to P450. This suggested that their observations could not be explained solely by a simple electron transfer role and some effects may also be caused by possible conformational changes caused by cyt b_5 binding. While the role of cyt b_5 in drug metabolism continues to be explored, a more interesting and potentially critical function of cyt b_5, is in human steroid biosynthesis.

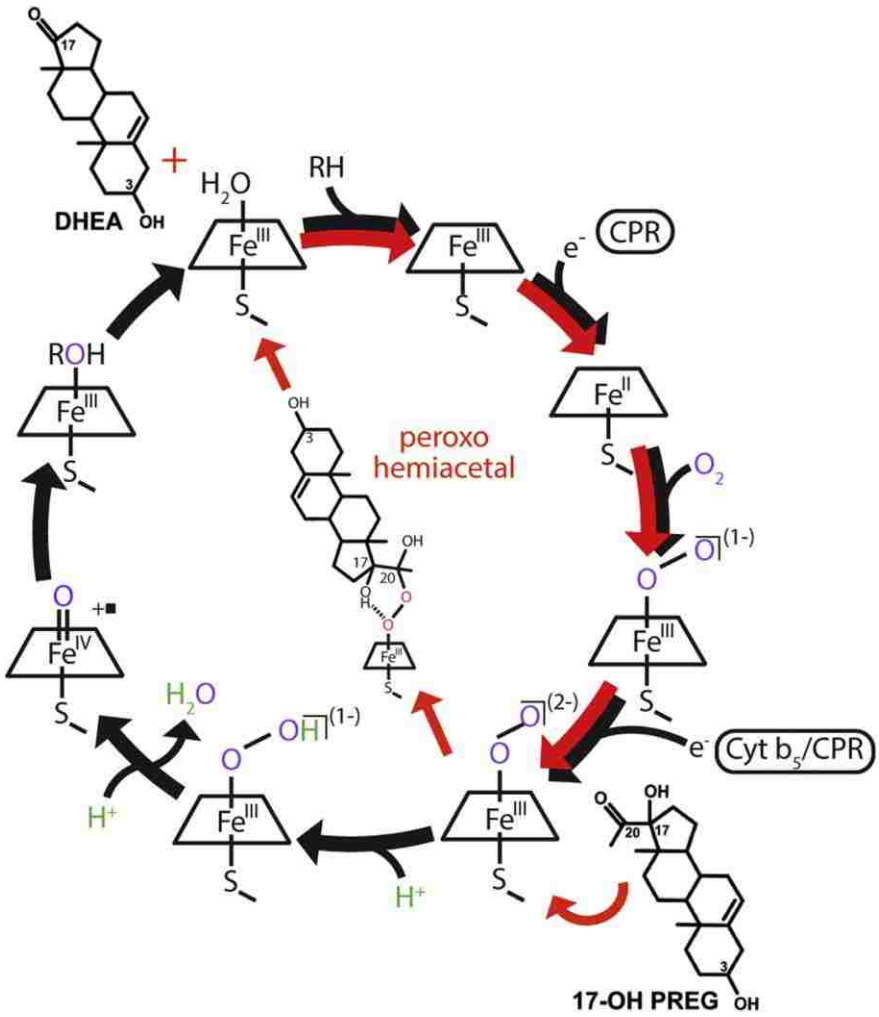

Figure 3.1.1 Cytochrome P450 reaction cycle. Black arrows represent the path followed for CYP17A1 mediated hydroxylation chemistry, while red arrows represent the CYP17A1 mediated carbon-carbon scission reaction, the lyase chemistry. The first reduction is indicated as being carried out by CPR, while the second electron can be donated by either CPR or cytochrome b_5.[105]

The synthesis of androgens, estrogens and corticosteroids involves multiple P450 catalyzed reactions. Cytochrome P450 17A1 (CYP17A1) is a key player in these reactions, being responsible for catalyzing 17α-hydroxylation of pregnenolone and progesterone followed by C17-C20 bond scission in a separate lyase reaction to form dehydroepiandrosterone (DHEA) and androstenedione (AD) respectively (shown in Figure 3.2.2). The hydroxylation reactions occur throughout a person's lifetime, and

when a person approaches adrenarche, the hydroxylated products can be shunted towards the subsequent step of formation of androgenic precursors by CYP17A1 in addition to the production of glucocorticoids.[83] The presence of membrane bound form of cyt b_5 has been known to selectively and significantly enhance the rate of the lyase reaction.[84] Mutations of CYP17A1 surface residues: R347, R358 and K89 which are known to interact with cyt b_5, have been shown to cause impairment of lyase activity. In a recent report, significant lyase impairment was shown in mice testicular Leydig cells lacking cyt b_5.[85] Additionally, male patients with mutations causing a lack of cyt b_5 present with pseudo hermaphroditism, while high cyt b_5 expression in adrenocortical adenomas in Cushing's syndrome patients has been associated with increased androgen synthesis.[86] Clearly, cyt b_5 has a physiological significance in maintaining normal levels of androgen synthesis. The nature of this role has been long debated,[84 87 88 89] with Auchus and coworkers studying lyase activity in recombinant yeast using apo b_5 which stimulated the lyase reaction, leading these workers to conclude that there is no redox role.[90] A similar report from Akhtar and coworkers mentions unpublished results demonstrating lyase enhancement in a reconstituted system utilizing Mn-b_5. On the contrary, Estabrook and others demonstrated in an in vitro reconstituted system in the presence of lipids that a zinc substituted derivative of b_5 did not stimulate the lyase activity of CYP17A1, and that the previous reports of rate enhancement by apo b_5 are the result of transfer of the heme group from the P450 to apo b_5 forming the holoenzyme.[91] Another property of cyt b5 that complicates all previous reports is the need for an intact membrane to influence the P450 activity.[92] Given the key importance of cyt b_5 in the regulation of androgen synthesis, it is imperative that this disparity about the role of cyt b_5 be solved in a reproducible system

representative of the membrane environment of these proteins. To this end, we employ the Nanodisc system to reconstitute CYP17A1, CPR and cyt b_5 in controlled stoichiometric ratios. We reconstituted cyt b_5 with manganese protoporphyrin IX and investigated the rate of lyase reaction by CYP17A1 in Nanodiscs, with iron containing cyt b_5, or with Mn-protoporphyrin IX substituted form of cyt b_5 (Mn-b_5) and compared each case versus the rate in the absence of cyt b_5. In humans, androgens are primarily derived from the 17α-hydroxypregnenolone substrate, therefore we decided to investigate this reaction to determine whether cyt b_5 is a redox donor in CYP17A1 mediated lyase reaction for androgen synthesis. Additionally, we probed the ferric resting state of CYP17A1 in the presence of native substrates to indicate formation of the b_5-CYP17A1 complex.

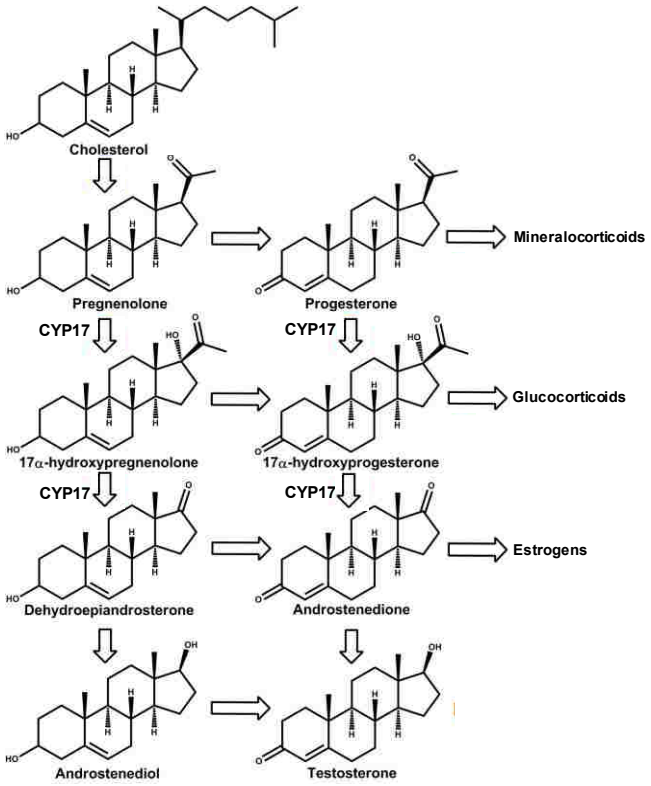

Figure 3.1.2 CYP17A1 catalyzed reactions in steroidogenesis.

3.2 Experimental

3.2.1 Assemble CYP17 in nanodisc

The expression and purification of CYP17A1 was performed as described.[93] The expression and purification of membrane scaffold protein and cyt b_5 were performed as described.[94 71] Both samples were prepared by our collaborator, Dr. Stephen Sligar's group. To assemble CYP17 in nanodiscs, materials such as membrane scaffold proteins, phospholipids and bio beads need to be prepared ahead. Among which, membrane scaffold proteins can be expressed and purified followed by a previous published protocol.[95] And Bio beads we used here is called amberlite XAD-2 which can be purchased from Sigma Aldrich (catalog number is 21646-1). These polystyrene beads need to be washed with ethanol in advance and thoroughly rinsed with water.

Phospholipid stock solutions are prepared in chloroform (50-100 mM, of precisely known concentration). As shown in Figure 3.2.1, to prepare a thin film of the proper amount of lipid, the desired precise amount of the chloroform solution of lipid was dispensed into a glass tube. The chloroform was removed by using a gentle stream of nitrogen gas to evaporate the chloroform; this was continued for ~ 4 hours in a fume hood. To further remove the residual solvent, the tube was placed in a vacuum desiccator under high vacuum overnight. Then a thin film should be seen on the wall of tube. Dried lipid has an opaque, white appearance. Then adding triton 100 contained buffer and vortex the tube, sonicate the solution in an ultrasonic bath until the solution is clear, and no lipid remains on the walls of the tube. The working lipid stock for the assembly mixture is ready. All these procedures result in a heterogeneous population of unilamellar

vesicles whose final size distribution is very sensitive to slightly changes in experimental conditions.

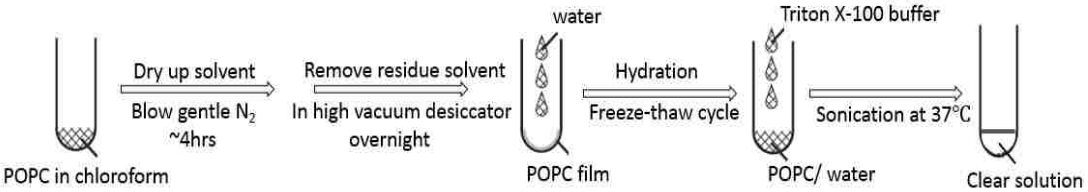

Figure 3.2.1 Preparation of working lipid stock.

To generate homogenous nanodiscs structure, the most key factor to success is having the phospholipids, scaffold protein and target protein in correct stoichiometry. If the stoichiometry ratio is not controlled strictly, then various other aggregates will form. According to previous studies, the optimized ratio between POPC and MSP1 is 65:1 at 4 degree,[96] as shown in the Table 3.2.1. To get the exact stoichiometry ratio, the concentration of lipids and MSP needs to be determined carefully. MSP concentration is determined spectrophotometrically using beer's law using molar extinction coefficient 18200 @ 280nm. To successfully assemble CYP17 in Nanodiscs, Final reconstitution molar ratio of mixture is 0.1:65:1 of CYP17A1/POPC/MSP1.

Table 3.2.1 Idea stoichiometry of membrane scaffold protein (MSP) and target protein at different incubation temperature.

Optimal ratios for MSP1		Optimal ratios for MSP1E3	Incubation temperature
DPPC	90:1	170:1	37 °C
DMPC	80:1	150:1	25 °C
POPC	65:1	130:1	4 °C

The concentration of lipid solution is determined by phosphate analysis.[97] By developing a calibration curve (Figure 3.2.2) of phosphate standard (Table 3.2.2), we can easily calculate the concentration of stock solution, here is 98.5mM. In details, the

solution was first heated in acidic medium to liberate the inorganic phosphate, reacting with ammonium molybdate to form phosphomolybdic acid, this acid can form highly colored molybdenum blue after reduction by ascorbic acid, which has strong absorption at 820 nm.

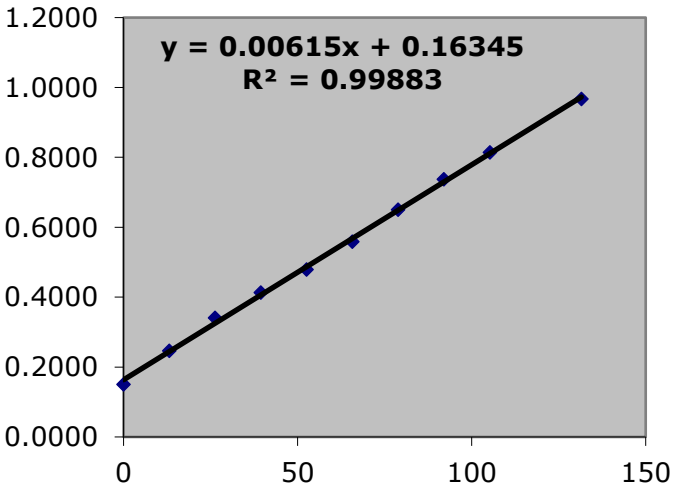

Figure 3.2.2 Calibration curve of a series of standards of phospholipids.

Table 3.2.2 Concentration of phospholipid standard prepared for calibration curve.

nmol P	uL standard
0	0
16.2	25
32.5	50
48.8	75
65	100
81.2	125
97.5	150
113.8	175
130	200
162.5	250

Once we set up the reconstitution mixture in an ideal stoichiometry, the Bio Beads are removed to assemble the nanodiscs. As shown in Figure 3.2.3, firstly, by using a nickel affinity column, the empty nanodiscs was separated from the P450 Nanodiscs due to a histidine tag attached on the target protein. Then the further separation was done by loading fractions on a size exclusion chromatograph to get a correct size of CYP17 nanadiscs monomers. The ideal size is around 10nm. The SDS-PAGE gel shows the target protein CYP17 was successfully incorporated into nansodics.

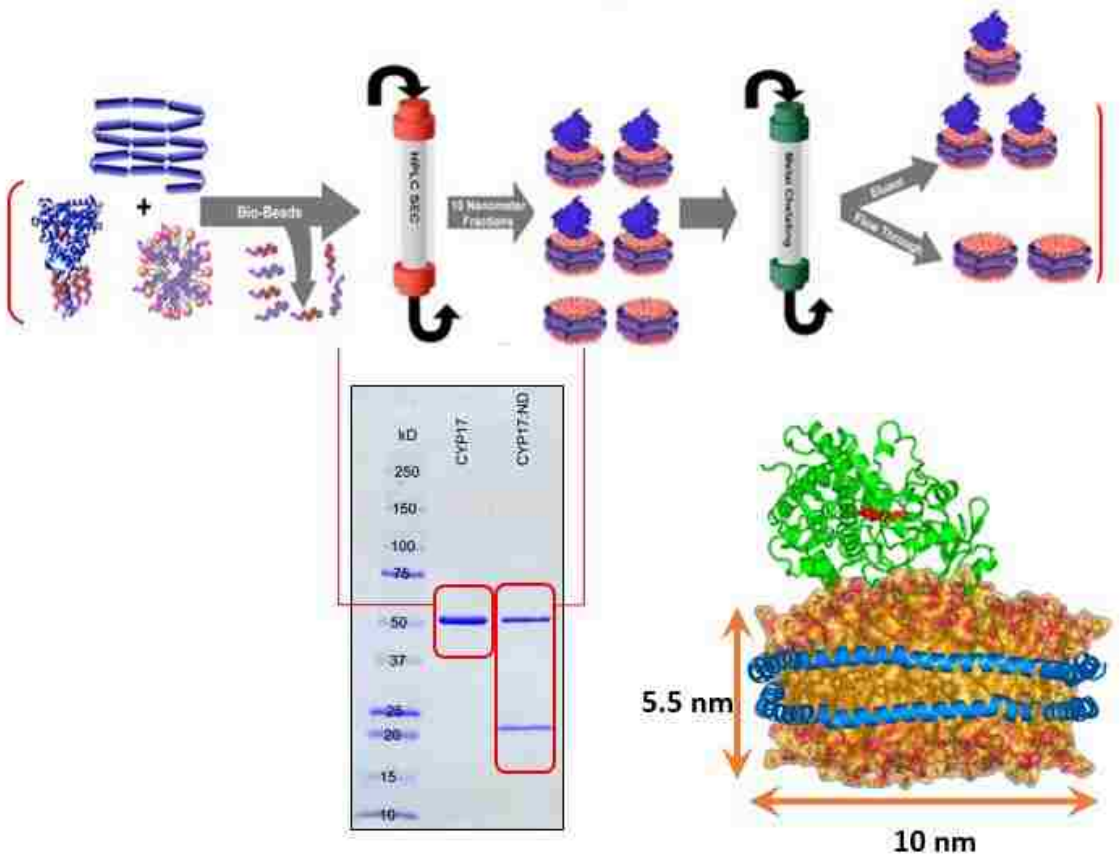

Figure 3.2.3 Preparation of CYP17 nandiscs.

3.2.2 Reconstitution of cyt b_5 with manganese protoporphyrin IX

Cyt b_5 was reconstituted with Mn-protoporphyrin IX according to previously published protocol,[83] with the following changes: After performing buffer exchange with G-25 column to separate unbound Mn-protoporphyrin IX, the eluate was run through a DEAE-cellulose column, equilibrated with 25 mM Tris acetate (pH 8.0), 1 mM EDTA and 10 mM sodium cholate. A linear salt gradient was formed using the equilibration buffer supplemented with 1 M NaCl. Mn-b_5 fractions which were characterized on the basis of their observed Rz ratios, were pooled and rigorously dialyzed against 100 mM potassium phosphate buffer (pH 7.4) and flash frozen in liquid nitrogen before being stored at 80C until use.

3.3.3 Preparation of Raman samples

3.3.3.1 Preparation of ferric form

CYP17A1 incorporated in Nanodiscs in 100 mM potassium phosphate buffer (pH 7.4) was concentrated to 200 μM and 2-foldexcess of Mn-b_5 was added from a 400 μM solution in the same buffer. The resultant solution incubated at 37C for 15 min. As shown in Figure 3.2.4, both cyp17 and Mn b_5 are successfully incorporated into nanodiscs, with their distinct bands. Substrate was added to each sample from methanolic stocks such that the final concentration was 420 μM.[98] Finally, ultrapure glycerol was added to a concentration of 15% (v/v); i.e., the final concentration of CYP17A1 was calculated to be 85 μM. The samples were flash frozen in liquid nitrogen and stored at 80C until analyzed.

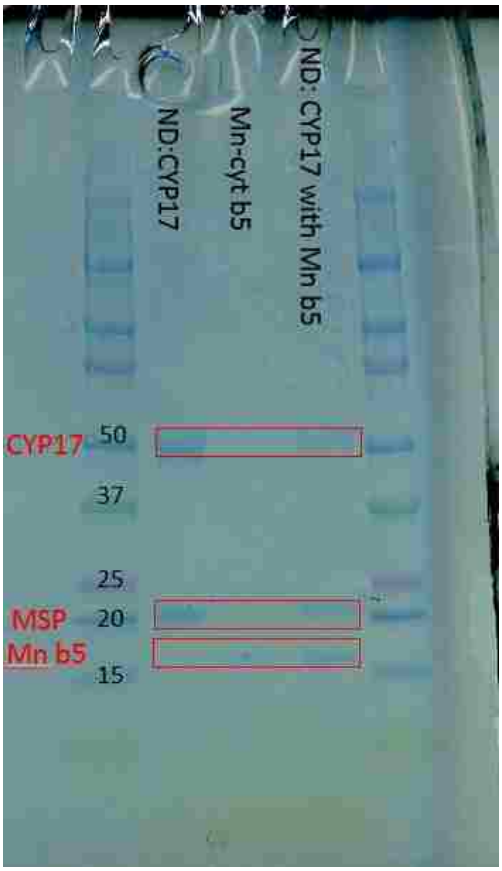

Figure 3.2.4 SDS-PAGE gel of ND: CYP17 with Mn b_5.

3.3.3.2 Preparation of ferrous dioxygen adduct

To better investigate effects of cytochrome b_5 on the H-bonding interactions in the CYP17 distal pocket, two substrates, 17α-hydroxyprogesterone (OH-PROG) or 17α-hydroxypregnenolone (OH-PREG) were incubated with ND: CYP17 samples in presence Mn b_5. Samples for rR spectroscopy measurement contain 250 μM ND: CYP17, 0.1 M potassium phosphate, pH 7.4, 0.2 M NaCl, and 400 μM of 17α-hydroxyprogesterone or 17α-hydroxypregnenolone (Sigma Aldrich). Solutions were prepared in distilled 30% (v/v) glycerol in H_2O buffer. Starting with the degassing samples by connecting the NMR tube to the vacuum line, then refilling the argon gas. This process is repeated for three

times to eliminate the possibility that presence of oxygen. Samples were reduced under anaerobic conditions by titrating with a 0.9~1 fold molar excess of sodium dithionite in the presence of 6.25 μM methyl-viologen. It is important to note that the carefully performed titration ensures the reduction only performs on CYP17 as the redox potential of the enzyme is more positive than Mn b_5. Each sample reduced at room temperature and then transferred to a dry ice-ethanol bath held at -20 °C where it was cooled for 2 minutes. Oxy-ferrous complexes were formed by bubbling $^{16}O_2$ or $^{18}O_2$ for 7 seconds, followed by rapid freezing in liquid N_2.

3.3.4 Resonance Raman Measurement

To determine the effect of cyt b_5 on the heme stretching modes in ferric CYP17A1, we employed the Mn reconstituted form of cyt b_5. This was done to prevent interference from the heme of cyt b_5 as was done previously by Mak *et al* in rR studies on CYP2B4.[98 99] We acquired resonance Raman spectra after adding 2-fold and 4-fold excess of Mn b_5. The high frequency spectra were acquired using the 406.7 nm excitation line from a Krypton ion laser (Coherent Innova Sabre Ion Laser) and changes in the ν(Fe-S) stretching mode were investigated 356.4 nm excitation line from the same laser, a wavelength known to selectively enhance this mode.[39] Resonance Raman spectra of frozen dioxygen samples were obtained using the 413.1 nm excitation line from a Kr+ laser, which effectively enhances internal modes of the Fe-O-O fragment. Each oxy sample was measured for 12hrs to obtain a better S/N signal, with a very low power maintained at 1mW on the sample. The rR spectra of all samples were measured using a Spex 1269 spectrometer equipped with a Spec-10 LN liquid nitrogen-cooled detector

(Princeton Instruments, NJ). The laser power was adjusted to ~10 mW. All samples were measured in a spinning NMR tube to avoid local heating and protein degradation. The spectra were collected using a 180° backscattering geometry, and the laser power was focused on the sample with a line image using a cylindrical lens. Spectra were calibrated with data acquired for fenchone and processed with Grams/32 AI software (Galactic Industries, Salem, NH).

3.3 Results and Discussion

3.3.1 NADPH oxidation and catalytic turnover of 17ahydroxypregnenolone in the presence of cyt b_5 or Mn-b_5 (Collaboration with Dr. Sligar's group)

The rates of NADPH oxidation and product formation in the presence of cyt b_5 and Mn-b_5 were compared to the rates in the absence of any added cyt b_5. The presence of cyt b_5 increases the product formation rate ~5 fold, while the addition of Mn-b_5 does not cause any change (Fig. 3.3.1 A). The rates of NADPH oxidation were close in value in all three cases, 54 ± 1.3 min^{-1} for cyt b_5, 51 ± 1.0 min^{-1} for Mn-b_5 and 46 ± 1.9 min^{-1} for reactions in the absence of any b_5. The efficiency of coupling was calculated as the ratio of product formation rate to the rate of NADPH consumption. This was seen to be maximal in the reactions with cyt b_5, while reactions with no b_5 and with Mn-b_5 had similar coupling efficiency (Fig. 3.3.1 B).

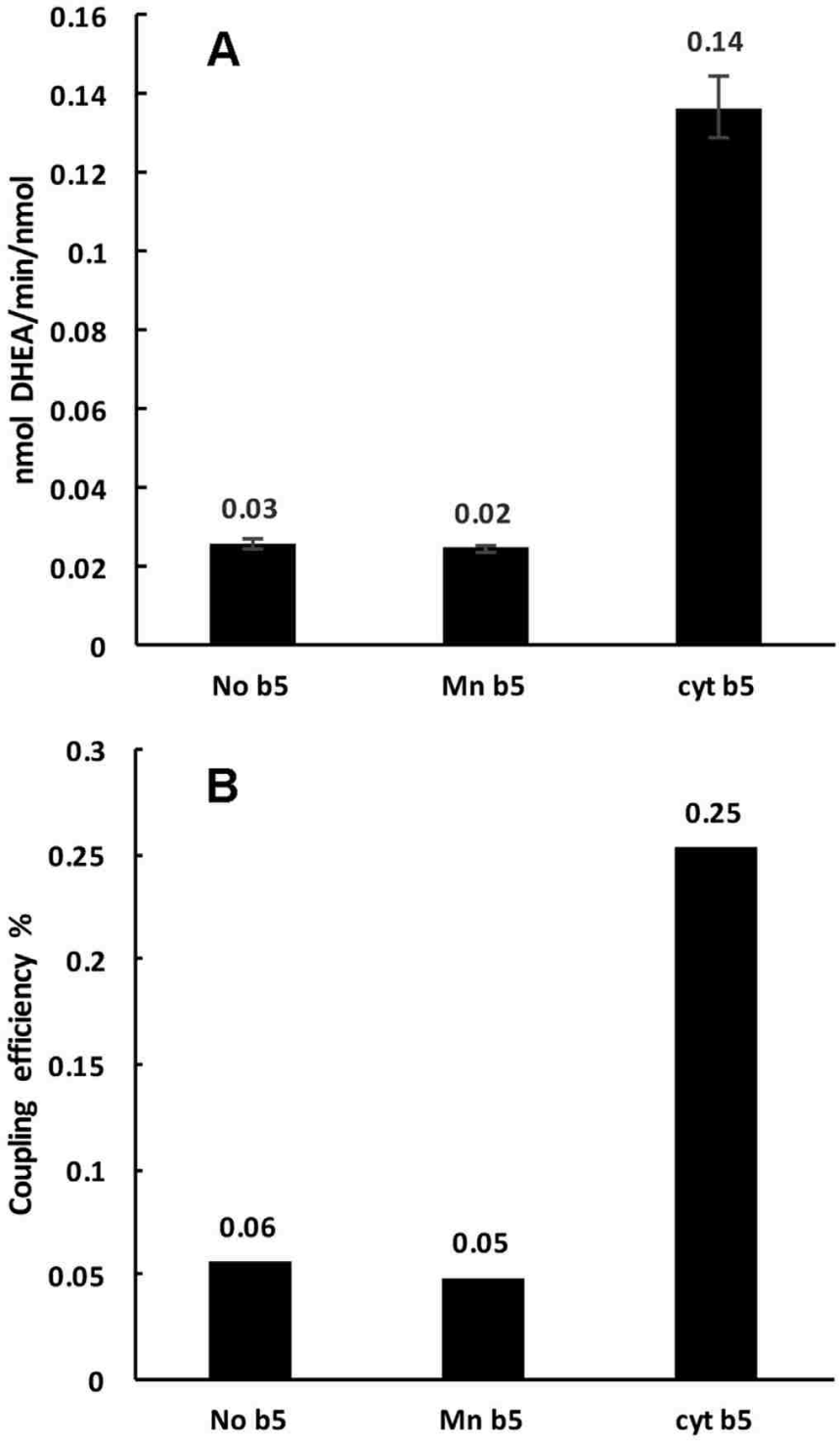

Figure 3.3.1 Comparison of CYP17A1 catalyzed lyase reactions with 17a-hydroxy-pregnenolone as substrate, with no cytochrome b_5 present, or with Mn-b_5, or native cytochrome b_5. (A) DHEA product formation rates (B) Coupling efficiencies (calculated as the percent ratio of amount of product formed to the amount of NADPH consumed).

3.3.2 Resonance Raman spectroscopy on Mn b_5 binding to ferric CYP17A1

As was reported in an earlier work,[100] binding of pregnenolone to substrate-free CYP17A1 causes a spin state conversion from almost pure low spin (LS) to largely high spin (HS) form, while binding of 17α-hydroxypregnenolone generates a lower HS fraction. The persistence of more LS component being attributed to the tendency of the 17α-hydroxy fragment of the substrate to directly interact with the heme iron or promote retention of distal pocket water molecules. In the present work, additions of Mn-b_5 to substrate-bound forms of CYP17A1, creating 2-fold excesses relative to the enzyme, cause relatively small increases of the LS component in these samples. This is reflected in the resonance Raman (rR) spectra illustrated in Fig. 3.3.2 for the samples bearing a 2-fold excess of Mn-b_5. As can be seen in trace B, pregnenolone bound CYP17A1 interacting with Mn-b_5 shows a spectrum similar to that for the sample without Mn-b_5 (trace A); they both exhibit a strong isolated ν_3 mode at 1488 cm^{-1} and a small signal for LS population near 1500 cm^{-1}. Employing a procedure developed in our laboratory by Mak et al., it is possible to estimate the spin state population using the intensity ratio of IHS/ILS equal to 1.24.[101] Using this value, the HS population of pregnenolone bound CYP17A1 in the presence of a 2-fold excess of Mn-b_5 is calculated to be 80%, close to the value observed in the absence of Mn-b_5. Similarly, it is noted that the HS component changes from ~57% to ~50% when a 2- fold excess of Mn-b_5 was added into 17α-hydroxypregnenolone bound CYP17A1 (Fig. 3.3.2 right panel, trace D). These remained nearly the same even in the presence of 4-fold Mn-b_5, indicating that all of CYP17A1 binding sites for cyt b_5 have been occupied. In addition to the relatively minor effects on

spin state populations, as can be seen in Fig. 3.3.2, it is important to emphasize that the frequencies observed for both the low energy and high energy internal modes of the heme prosthetic group do not shift relative to those observed for the corresponding samples without Mn-b_5, implying that the interaction with Mn-b_5 does not induce significant structural changes of the heme macrocycle or its peripheral substituents in the substrate-bound ferric enzyme. Though minimal effects were observed for spin state populations and heme structure, it is noted that association of CYP17A1 with Mn-b_5 increases the strength of Fe-S linkage, demonstrating the formation of a CYP17A1: Mn-b_5 complex. This is evident from viewing the inserts for the low-frequency spectra in Fig. 3.3.2, where the ν (Fe-S) stretching modes occurring in samples with the excess Mn-b_5 appear at 350 cm^{-1}, while those previously reported for the same samples of CYP17A1 in Nanodiscs without Mn-b_5 appear at 347 cm^{-1}.[100]

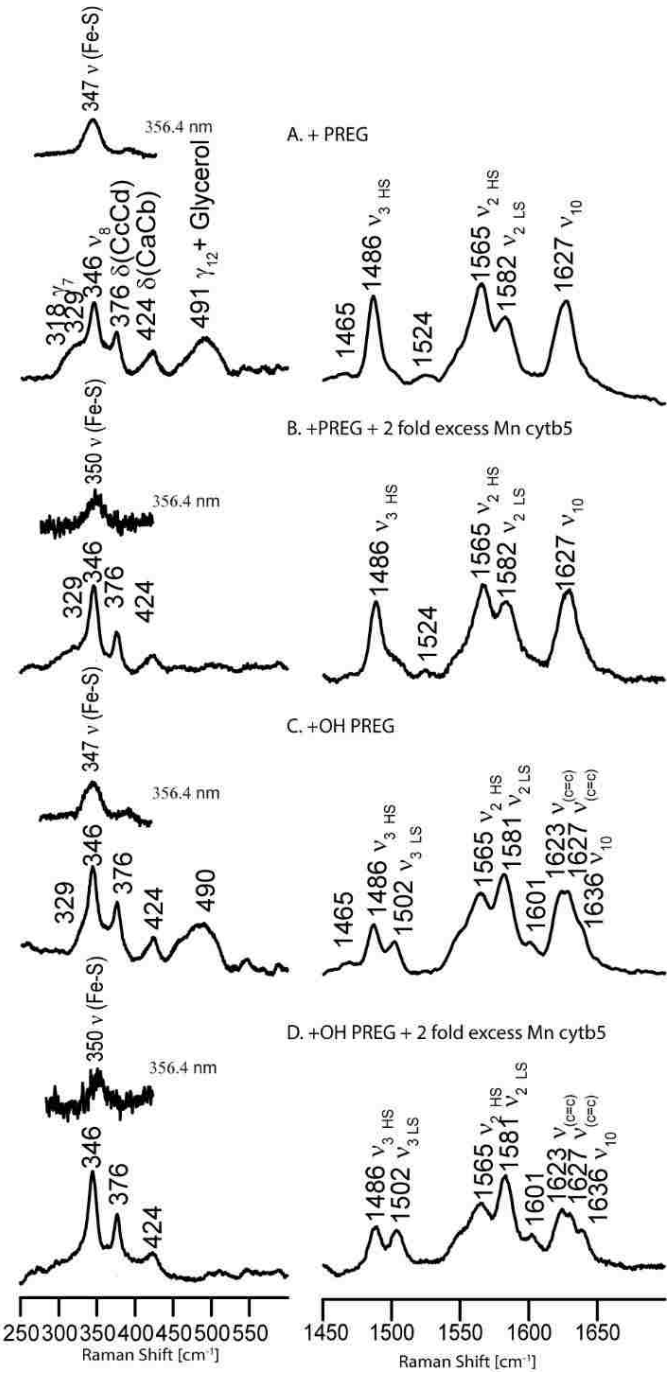

Figure 3.3.2 Resonance Raman Spectra of CYP17A1 +/- Mn b_5 in 100 mM potassium phosphate buffer (pH 7.4) containing 15% (v/v) glycerol. The right panel shows the high-frequency region of the acquired spectra, while the left panel shows the low frequency region; the spectra were acquired using the 406.7 nm excitation line from a Krypton ion laser, noting that the inset bands in the low frequency region were acquired with the 356.4 nm excitation line from the same laser, a wavelength that selectively enhances the ν(Fe-S) stretching mode.[39] Spectra traces in B and D are the resulting traces after subtraction of spectra obtained for samples containing the equivalent concentration of Mn b_5 in 15% (v/v) glycerol in buffer.

3.3.3 rR spectroscopy characterization of ferrous dioxygen intermediates of hydroxylated substrates bound to CYP17 in the presence of Mn b_5

In previous rR studies on CYP17 dioxygen adduct performed by our group, different H-bonding interactions in the active site with a key Fe-O-O fragment of the enzyme intermediates are demonstrated for OH-PROG and OH-PREG, which proves to be a key factor that can control substrate processing.[102] As mentioned earlier, CYP17 is able to catalyze the lyase reaction on both OH-PROG and OH- PREG cleaving the 17–20 carbon–carbon bond to form dehydroepiandrosterone and androstenedione; however, it is interesting to see that androgen formation is 50-fold greater with OH-PREG than for OH-PROG, with the rR spectra of the dioxygen adducts of CYP17 offering a plausible explanation for this differential behavior. As shown in Figure 3.3.3 and Figure 3.3.4, if we just have PROG and PREG bound in the active site, virtually identical iron oxygen and O-O stretching frequency. This is not surprising because they are known to dock similarly. However, if OH-PROG and OH- PREG are bound in the enzyme, both of the O-O stretching is shifting down slightly, but there is a quite significant difference in iron oxygen stretching modes, the ν(Fe-O) frequency for OH-PROG going up and the frequency for OH-PREG goes down, relatively to the ~535 cm^{-1} value seen for PROG and PREG. That's important, because DFT calculations showed that hydrogen bonds to the proximal O of the Fe-O_P-O_T fragment can cause a decrease of Fe-O stretching mode whereas H-bonding to the terminal O will shift up the Fe-O stretching mode. More importantly, computational works done by Haris and Shaik show this kind of H-bonding promotes lyase reaction, allowing the nucleophilic attack of the peroxo intermediate on the 20-carbonyl.[103,104] So this alone can explain why OH-PREG is much more effectively

transformed to lyase product than is OH PROG. So resonance Raman to be an effective way to detect subtle but functionally significant changes in the distal pocket environment.

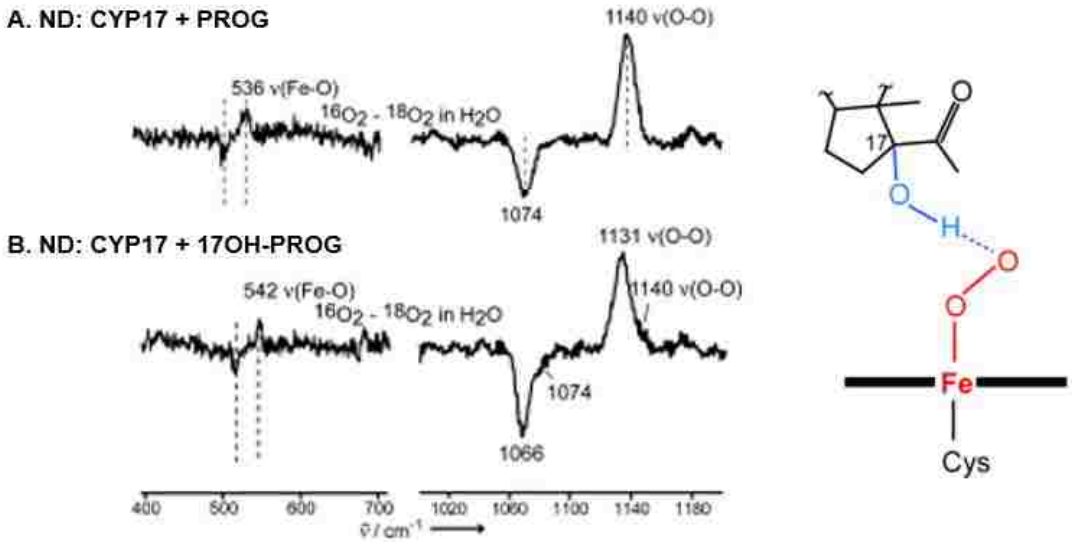

Figure 3.3.3 The rR spectra of PROG- and 17-OH-PROG-bound O_2 adducts of ND: CYP17 in H_2O buffer (Trace A and B, respectively).

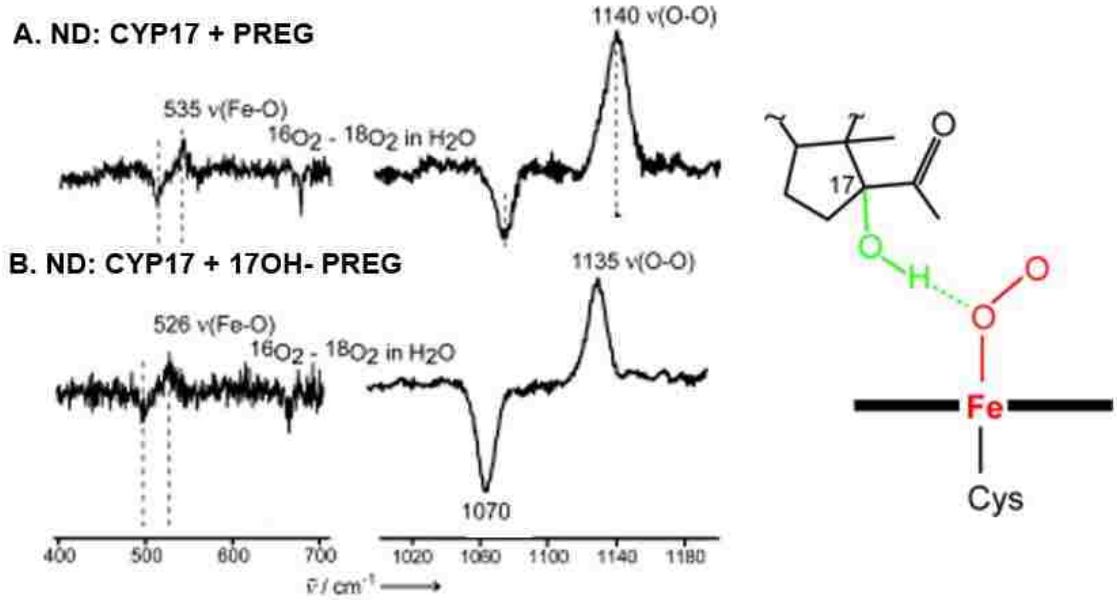

Figure 3.3.4 The rR spectra of PREG- and 17-OH-PREG-bound O_2 adducts of ND: CYP17 in H_2O buffer (Trace A and B, respectively).

Though the presence of redox partner Mn cyt b_5 does not appear to have a significant effect on heme structure, based on the results present earlier in this chapter, a more careful rR study applied to the OH-PROG and OH-PREG bound ND: CYP17 ferrous dioxygen complexes in presence of Mn cyt b_5 was conducted here, attempt to detect these subtle active site structural change caused by this redox partner. Shown in Figure 3.3.5, is the rR spectra for the OH-PROG bound ND: CYP17 dioxygen complex in presence of a two-fold excess of Mn cytb_5. The key $\nu(^{16}O\text{-}^{16}O)$ mode still appears at 1131 cm^{-1}, as confirmed by the $^{16}O_2/^{18}O_2$ difference spectrum, while the $(^{18}O\text{-}^{18}O)$ stretching mode occurs at 1068 cm^{-1} (the expected 63cm^{-1} isotope shift). Expansion of this spectral region, and comparison with the spectrum acquired with $^{18}O_2$, shows evidence for a minor conformer of Fe-O-O fragment with the $\nu(^{16}O\text{-}^{16}O)$ mode occurring at 1140 cm^{-1}, which is apparently unshifted from the values observed for OH-PROG in the absence of this redox partner (Figure 3.3.3). Significantly, the sample prepared including the Mn cyt b_5 activates a new Fe-O-O conformer, with a $\nu(Fe\text{-}^{16}O)$ mode at 530 cm^{-1} and a corresponding $\nu(Fe\text{-}^{18}O)$ mode at 501 cm^{-1}. This suggests that the interaction with Mn cyt b_5 causes a partial transformation to a conformer which provide an H-bonding interaction with the proximal oxygen, a structure which favor the lyase reaction. Though the main compact of the redox partner was shown to be as an electron transfer role from earlier functional studies,[105] subtle allosteric role of the Mn cyt b_5 is indicated on OH-PROG bound enzyme.

Corresponding spectral data for 17-OH PREG bound enzyme in presence of Mn b_5 is shown in Figure 3.3.6. The $\nu(^{16}O\text{-}^{16}O)$ and $\nu(Fe\text{-}^{16}O)$ modes are observed at 1135 cm^{-1} and 526 cm^{-1}, corresponding to the isotope band $\nu(^{18}O\text{-}^{18}O)$ and $\nu(Fe\text{-}^{18}O)$ occur at

1070 cm^{-1} and 497 cm^{-1}, which are unshifted from their values in the sample without the redox partner. Thus, addition of Mn cyt b_5 does not cause any spectral difference, the lack of effects on the Fe-O-O fragment further suggesting that the electron transfer role of the redox partner dominates for this substrates.

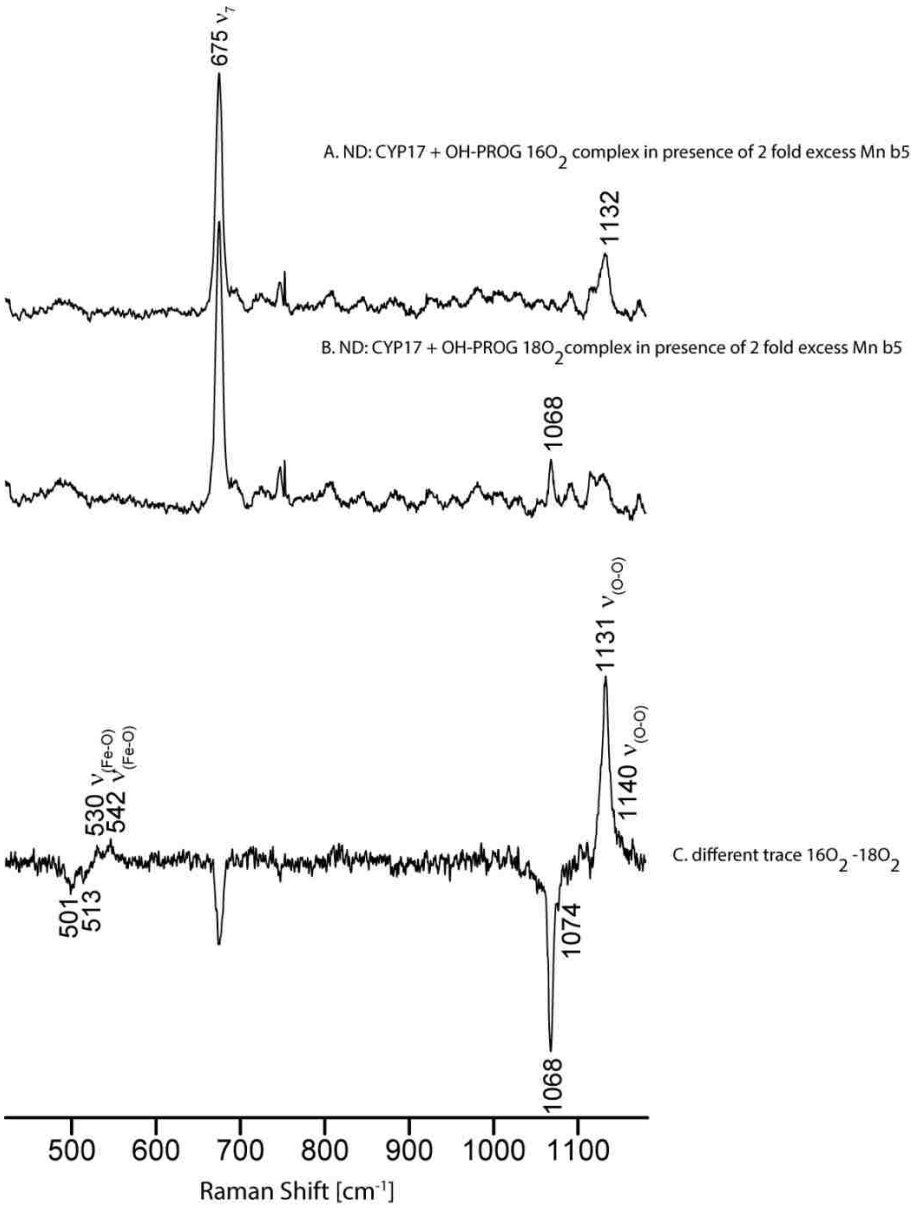

Figure 3.3.5 rR spectra of OH-PROG bound ND: CYP17 oxy complex in presence of 2 fold excess of Mn b_5 in mid-frequency region. Spectra were measured at liquid nitrogen temperature with excitation line at 413.1 nm. (A) OH-PROG bound ND: CYP17 $^{16}O_2$ complex, (B) OH-PROG bound ND: CYP17 $^{18}O_2$ complex, (C) difference spectra: trace A-trace B.

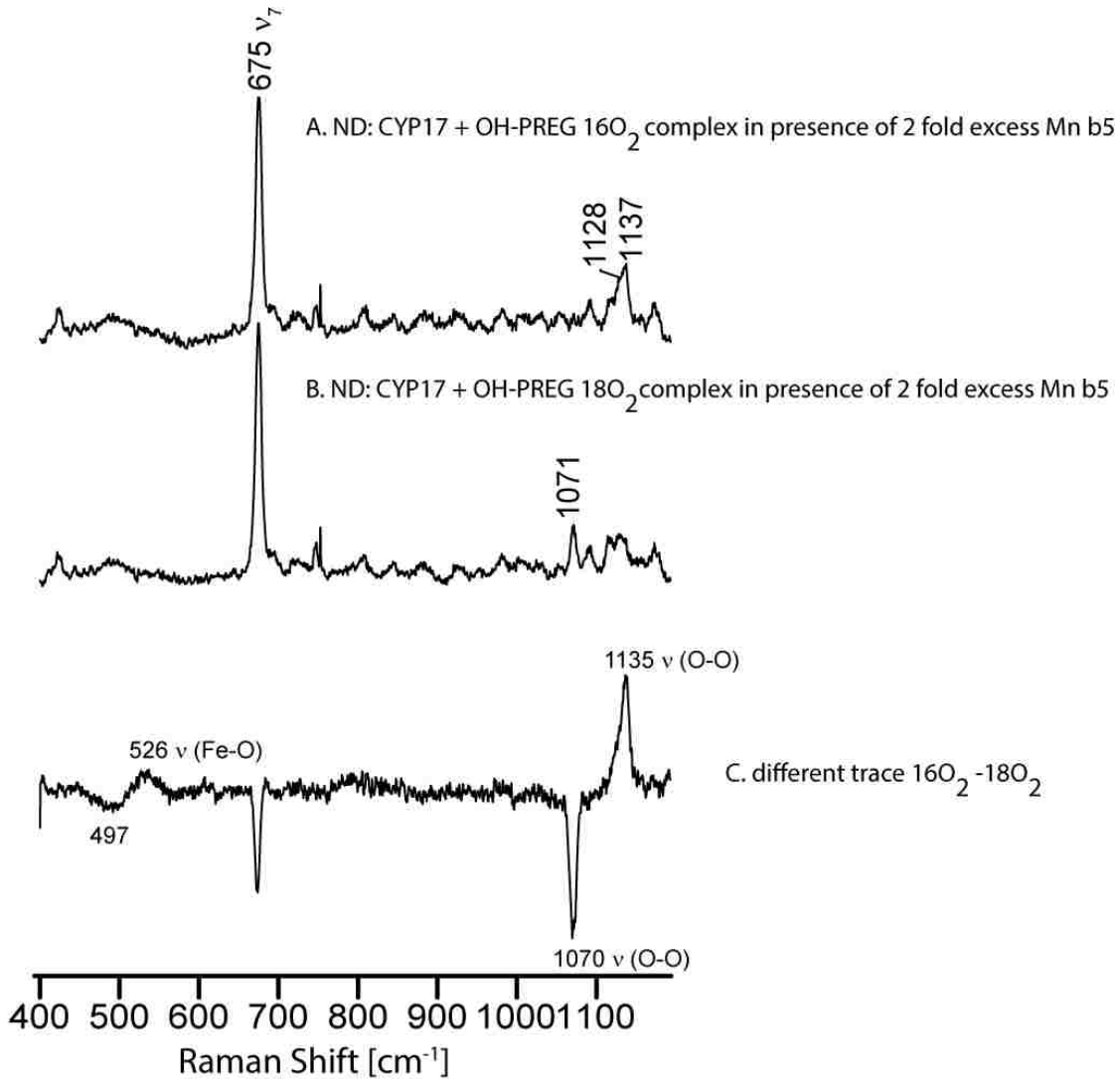

Figure 3.3.6 rR spectra of OH-PREG bound ND: CYP17 oxy complex in presence of 2 fold excess of Mn b_5 in mid-frequency region. Spectra were measured at liquid nitrogen temperature with excitation line at 413.1 nm. (A) OH-PREG bound ND: CYP17 $^{16}O_2$ complex, (B) OH-PREG bound ND:CYP17 $^{18}O_2$ complex, (C) difference spectra: trace A-trace B.

3.3.4 Discussion

CYP17A1 is a critical enzyme in steroidogenesis, lying at the branch point of glucocorticoids synthesis and androgen synthesis. It performs hydroxylation on the pregnene-nucleus to form hydroxylated products which can either be diverted to glucocorticoid synthesis, or undergo a C-C bond lyase reaction to produce androgens. Cytochrome b_5 is known to be the chief regulator of CYP17A1 reactivities in vivo, yet the nature of interactions of CYP17A1 with cyt b_5 is not clearly understood. Cyt b_5 is known to enhance the lyase reactions from 5 to 10 fold. Whether cyt b_5 acts as an allosteric modulator or if it functions as a second electron donor has long been debated,[88 89] and conflicting reports from various groups are complicated by the fact that these studies were carried out in uncontrolled conditions where aggregation states and stoichiometries of interactions were not known.[88 106 107] Scott and coworkers have used solution NMR with soluble forms of the proteins to study the conformational changes occurring in CYP17A1 bound to lyase substrates upon cyt b_5 binding and associated them with an allosteric role for cyt b_5,[108 102] although not directly addressing a possible redox role. The application of Nanodisc technology to this system is therefore an effective solution, enabling us to study reactions in controlled stoichiometries in a native-like membrane environment.

We reconstituted cyt b_5 with Mn-protoporphyrin IX, which is known to be redox inactive under these conditions,[83] and tested the rate of lyase reaction in 17α-hydroxypregnenolone in the presence and absence of cyt b_5, and also in the presence of Mn-b_5. Reactions with Mn-b_5 showed no enhancement of the rate of DHEA formation, which suggests very strongly that cyt b_5 has a definite redox donor role in the CYP17A1

lyase chemistry. Importantly, presence of cyt b_5 increases the coupling efficiency about 5-fold. Given the relatively high redox potential of cyt b_5 (~0 mV NHE),[81] its redox role is limited to reduction of the oxy-complex,[82] giving rise to the nucleophilic peroxo-species, the reactive intermediate responsible for carbon-carbon bond scission.[109 110] An enhanced reduction rate of the oxy-complex is expected to increase the steady-state concentration of the peroxoanion, which in the absence of cyt b_5 is depleted through non-productive release of hydrogen peroxide. Our resonance Raman data with Mn-b_5 binding to ferric CYP17A1 indicate no major structural changes of the heme planar modes, whereas on the proximal side, Fe-S bond was observed to get strengthened when Mn-b_5 was bound. Clearly, Mnb5 binds to CYP17A1, but is incapable of enhancing the lyase activity, the latter being enhanced if the native iron containing cyt b_5 is bound. The ferrous dioxygen adduct of OH-PROG CYP17 in presence of a 2 fold Mn cyt b_5 exhibits slight change in the active site, showing allosteric role of redox partner. However, the rR data of oxy OH-PREG enzyme with Mn cyt b_5 strongly supports the electron transfer role. Taken together, these experiments provide strong evidence that cyt b5 is serving as a redox partner in CYP17A1 catalytic cycle, most likely delivering a second electron to the oxy-complex and facilitating formation of the peroxo-ferric complex, which recent evidence shows to be the catalytically active intermediate in the lyase reaction.[109] This result is in agreement with conclusions on the role of cyt b_5 in CYP2B4 catalysis.[111],[89] Although our results cannot disprove the presence of functionally important allosteric interactions between cyt b_5 and CYP17A1, the lack of any effect of Mn-b_5 on the rate of turnover of 17α-hydroxypregnenolone, as compared with 5-fold acceleration of this

reaction in the presence of cyt b_5, suggests that these allosteric interactions do not play significant role in the human CYP17A1 mediated catalysis of lyase reaction.

Chapter 4. Resonance Raman studies on Cytochrome P450 from Bacillus megaterium (P450 BM3) and some biotechnologically important mutants

4.1 Introduction

The cytochromes P450 comprise a huge class of heme containing monooxygenases which collectively exhibit a diverse range of chemical reactivity in numerous organisms, facilitating important physiological functions, including the metabolism of pharmaceuticals and various toxic compounds.[9, 45] One essential catalytic activity of these enzymes is the insertion of an atom of molecular oxygen into a relatively inactive C-H bond, thereby effecting a hydroxylation reaction on otherwise inert substrates; e.g. fatty acids.[31] Furthermore, over the past several decades, a number of bacterial P450s have been shown to play key roles in many physiological processes; e.g. antibiotic synthesis and catabolism of complex molecules (e.g. steroids). Moreover, typically they display diverse regio- and stereoselectivity in the oxidation of a wide range of substrates,[112] a finding which has attracted growing attention from an industrial perspective, especially through use of protein engineering as an effective approach for important applications of microbial P450s in biotechnology.

The bacterial enzyme P450 BM3 first isolated from *Bacillus megaterium*, catalyzes the hydroxylation and epoxidation of hydrophobic long-chain fatty acids.[113] There is currently high interest in this enzyme owing to its remarkably high monooxygenase catalytic activity, which results mainly from the fact that it possesses a covalently linked, high activity cytochrome P450 reductase (CPR) partner, such an

arrangement providing extremely efficient electron transfer between the CPR and the P450.[114] Furthermore, its demonstrated ability (in wild-type and mutant forms) to catalyze oxidation of diverse substrates with high degrees of regio- and stereo-selectivity greatly enhances its potential for biotechnologically useful applications.[115] Examples include the utility of BM3 mutants in converting testosterone to 2β-hydroxytestosterone and 2β-hydroxytestosterone,[116] and particularly in producing human drug metabolites, such as those from PPI (proton pump inhibitor) drug molecules. These kinds of industrially important molecules are typically prepared by complicated and expensive methods of traditional synthetic chemistry.[117] Indeed, much effort has already been devoted to studies of this particular BM3 mutants to synthesize metabolites of omeprazole (OMP) (Figure 4.1.1), and of other PPI molecules.[118] With reference to the P450 BM3 heme domain crystal structure (Figure 4.1.2), the role of active site residues have been extensively explored,[119] with residues near the active site pocket, including Phe[87]and Ala[82], having been targeted in attempts to alter substrate selectivity and enzyme activity.[120] For example, Phe[87] is located over the heme cofactor and plays a key role in interacting with the ω-methyl group of the fatty acid substrate, preventing its oxidation. Mutating the phenylalanine provides new space close to the heme cofactor to allow binding of novel substrates. The A82F mutant causes moderate destabilization of the BM3 heme domain structure by inducing a conformational change.[121] Collectively, these effects lead to pronounced changes in the substrate specificity profile of the F87V/A82F double mutant. It is of note that both of the A82F and F87V single mutants demonstrate affinity for omeprazole, as measured by the development of high-spin heme in these samples on titration with omeprazole, with K_d values of 1.67 ± 0.05 μM and 49.0 ± 2.7

μM, respectively.[120] However, the combined mutations lead to much higher affinity for omeprazole in the F87V/A82F double mutant (K_d = 0.212 ± 0.014 μM). All of the mutants catalyze hydroxylation on the 5-methyl group of omeprazole, with the F87V/A82F double mutant being the most productive enzyme. The 5-hydroxylation of omeprazole is the same reaction catalyzed by CYP2C19, the major human omeprazole metabolizing P450.[120] The effects of various alterations on the structure and environment in the active site of these mutants are of great interest.

Among the many diverse spectroscopic methods, resonance Raman (rR) spectroscopy has proven itself to be a highly effective approach by which the active site environment of a heme protein can be interrogated. This technique can selectively enhance the heme vibrational modes by adjusting the excitation line close to the heme absorption bands.[2, 122] Information such as oxidation state and spin state of the heme iron can be readily obtained using the so-called marker modes, which appear in the high wavenumber region of the vibrational spectrum, while the low wavenumber region can provide important insight into the interactions between protein residues and the peripheral heme groups; i.e., the vinyl and propionate substituents. This is important, because the relative orientation of these groups can affect the reactivity of heme.[123] Moreover, this technique is particularly useful for analyzing changes in the disposition of exogenous axial ligands caused by binding of substrates, and for examining differences in the active site environment, including distal pocket polarity and steric interactions, imposed by the substrate or amino acid residues.[57]

In the present study, rR spectroscopy is used to probe heme structure and coordination environment for selected mutants (A82F, F87V and the F87V/A82F double

mutant) of the BM3 heme domain in their substrate-free and substrate-bound forms. The substrate selected is omeprazole (OMP), which was shown to bind to the mutant forms of the BM3 heme domain by UV-visible spectral titration, but which did not induce any significant shift towards high-spin heme iron in the wild type BM3 heme domain. Specifically, rR spectral data were acquired for the substrate free (SF) and OMP-bound forms of the wild type and mutant BM3 heme domains. Furthermore, the rR of ferrous CO adducts were also collected and analyzed in order to interrogate how omeprazole substrate binding affects the vibrational modes of the Fe-CO molecular fragment, data which reveal important details about the active site architecture. Collectively, these studies provide insight on how these 'gatekeeper' mutants influence substrate selectivity, affinity and protein-heme interactions within the BM3 heme domain active site.

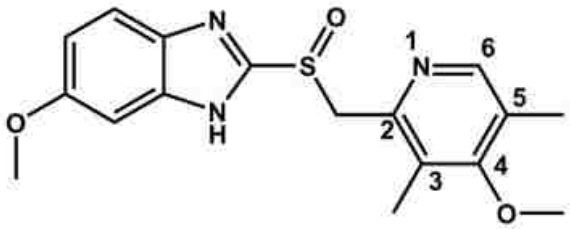

Figure 4.1.1. Structure of human drug OMP (omeprazole). Hydroxylation on the 5-methyl group is performed by engineered variants of P450 BM3 mutants.

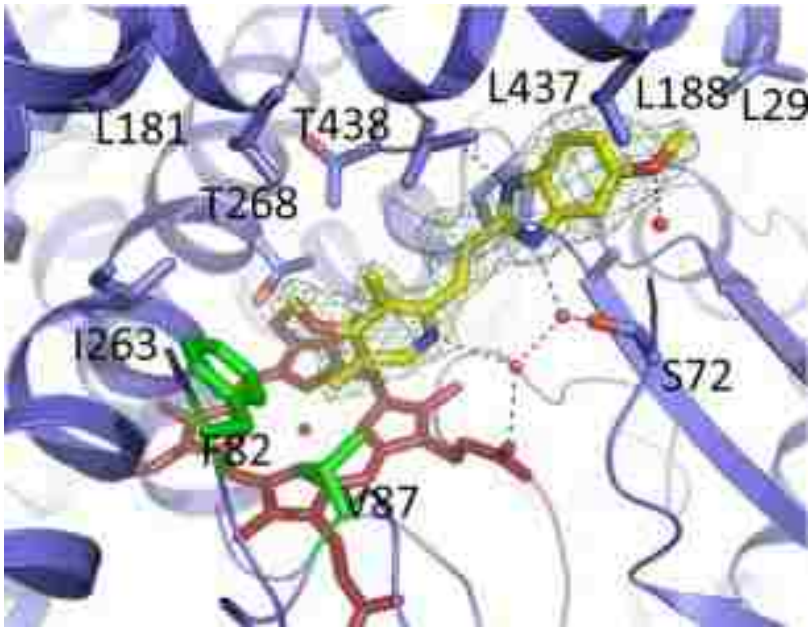

Figure 4.1.2. Structure of omeprazole bound A82F/F87V double mutant of P450 BM3. Key residues are shown as blue sticks. Phe82 and Val87 are shown in green, close to the heme. Other important residues include Ser72, which participates in a hydrogen bonding network involving active site water molecules, benzimidazole and pyridinyl group nitrogens, and a heme propionate. Leu437 also hydrogen bonds to the other benzimidazole group nitrogen atom through its backbone carbonyl group, while Thr268 plays a key role in proton delivery to heme iron-oxo species during the P450 catalytic cycle. (PDB #: 4KEY)[120]

4.2 Experimental

4.2.1 Samples preparation for rR measurement

Samples of P450 BM3 heme domain and its mutants, generated using previously described procedures,[120] were used to prepare samples for rR measurements. Specifically, 50 μL of 100 μM P450 BM3 (heme domain) samples of the substrate-free wild type, the single mutants A82F and F87V BM3, and the double mutant F87V/A82F heme domains were transferred into NMR tubes for rR measurements. The substrate stock solution was prepared by dissolving 9 mg of omeprazole in 450 μL of DMSO to reach a concentration

of 56.4 mM. The substrate/enzyme ratio is 5.6/1 in substrate-bound samples. The sample was centrifuged and the transparent supernatant solution was transferred to an NMR tube for rR measurement.

The carbon monoxide complexes of the heme domain of ferrous BM3 (wild type and mutant heme domaims) were prepared with and without the substrate, omeprazole. To prepare these samples, NMR tubes were sealed with a rubber septum and CO gas was introduced to the solution using a long needle for 20 minutes to remove oxygen. Then samples were reduced with a 2-fold excess of degassed sodium dithionite solution and CO gas was further bubbled for an additional 10 minutes before measuring the rR spectra.

4.2.2 Resonance Raman measurement

The ferric sample was measured with the 406.7 nm excitation line from a Kr^+ laser (Coherent Innova Sabre Ion Laser) while the spectra of the Fe(II)-CO adducts were acquired with the 441.6 nm line from a He-Cd laser (IK Series He−Cd laser, Kimmon Koha Co., Ltd.). All spectra were measured using a Spex 1269 spectrometer equipped with a Spec-10 LN liquid nitrogen-cooled detector (Princeton Instruments, NJ). The slit width was 150 μm and the laser power incident on ferric samples was ~10 mW, while the power used for ferrous-CO samples was adjusted to ~1 mW at the samples to prevent CO photo-dissociation. Rayleigh scattering was removed from the Raman signal by using an appropriate notch filter (Kaiser Optical). The samples were placed in a N_2–driven spinning NMR tube and the spectra were collected by using a 180° backscattering geometry with a cylindrical lens to achieve a line focus on the tube. Spectra were

calibrated with data acquired for fenchone and processed with Grams/32 AI software (Galactic Industries, Salem, NH).

4.3 Results and discussion

4.3.1 Effects of omeprazole binding on the ferric form of WT P450 BM3 heme domain and its mutants

The rR spectra of the ferric wild-type substrate-free enzyme and its omeprazole-bound form are shown in Figure 4.3.1. The spectrum of the substrate-free sample (trace A) exhibits the oxidation state marker mode ν_4 at 1372 cm^{-1} and the ν_3 and ν_2 spin-state markers at 1501 and 1585 cm^{-1}, respectively, confirming the presence of a pure six coordinate low-spin (6cLS) species. The spectrum of the BM3 heme domain with omeprazole (trace B) exhibits a spectral pattern essentially identical to that of the substrate-free sample, indicating that the addition of omeprazole causes no changes to the heme spin state or to the macrocyclic core structure. As shown in Figure 4.3.1, comparisons of both the low-wavenumber and high-wavenumber rR spectral data also confirm the lack of significant changes induced by omeprazole, as judged by the virtually identical rR spectra shown in traces A and B. Thus, the rR spectra of ferric wild type BM3 heme domain show no indication of heme spectral changes upon addition of OMP, a finding which is consistent with earlier published results, where optical titrations showed no evidence for binding of OMP to WT BM3.[120]

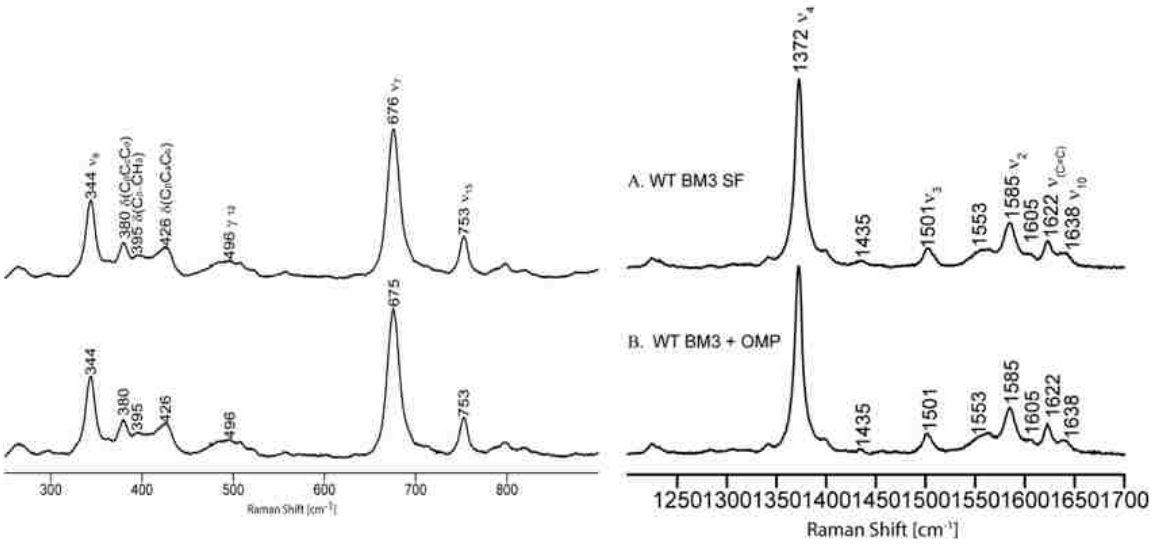

Figure 4.3.1 rR spectra of various form of wild type P450 BM3. (A) substrate-free form (B) OMP-bound. Left panel shows the low-wavenumber region while the right panel shows the high-wavenumber region.

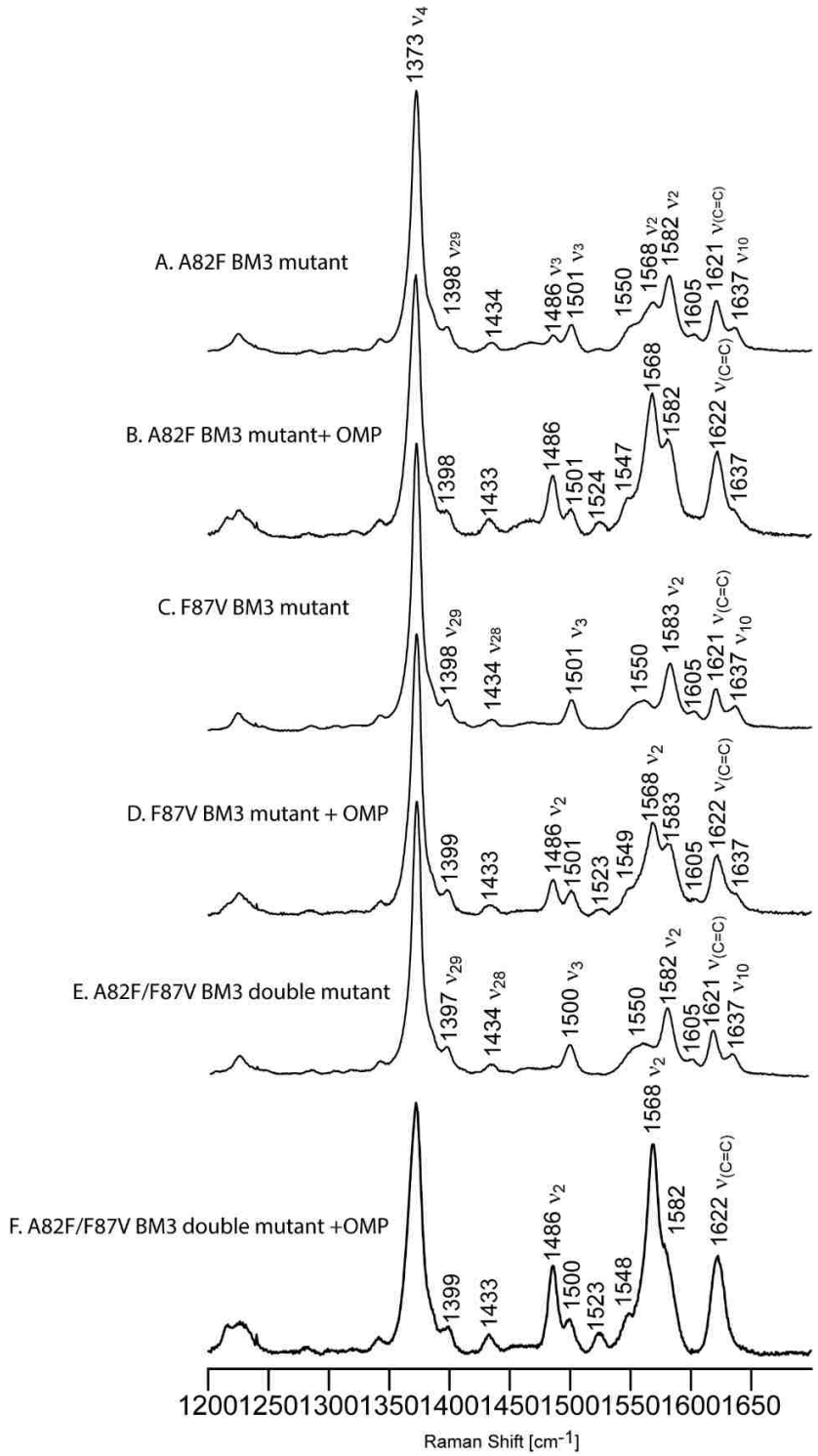

Figure 4.3.2. High wavenumber rR spectra of substrate-free ferric P450 mutants and their substrate bound forms. (A) A82F substrate-free form. (B) Omeprazole bound A82F. (C) F87V substrate-free form. (D) Omeprazole bound F87V. (E) A82F/F87V double mutant substrate-free form. (F) A82F/F87V double mutant omeprazole bound form. All spectra were normalized to the ν_4 mode.

4.3.2 Active site structural changes of P450 BM3 mutants induced by omeprazole binding

The high-wavenumber rR spectrum of substrate-free A82F BM3 heme domain mutant is shown in Figure 4.3.2 (A), where assignments of the observed bands are given, all of which are consistent with earlier published data for CYP101A1 (the camphor hydroxylase P450cam) and the general behavior of ν (C=C) modes.[124-125] The strongest peak occurs at 1373 cm^{-1} and is assigned as the oxidation state marker band, ν_4, confirming that the protein is in the ferric state. The spin state marker bands, ν_3, ν_2 and ν_{10}, occur at 1501 cm^{-1}, 1582 cm^{-1} and 1637 cm^{-1} respectively, consistent with a six coordinate, LS heme iron. However, weaker peaks at 1486 cm^{-1} and 1568 cm^{-1} indicate the presence of a small percentage of a high spin five coordinate (5cHS) species. It is possible to estimate the spin state population in this sample using previously derived relative rR scattering cross section of the ν_3 modes for the 6c LS and 5c HS species, as determined for both forms of P450cam, and as described by Mak et al.[101] Using this procedure, the HS percentage is calculated to be 30%. In contrast with most other substrate-free P450s (which often yield a more extensive LS population), this A82F mutant retains a significant percentage of HS state, even after having been passed through a Lipidex column to facilitate removal of any lipid substrate. X-ray crystallography data[120] reveal that the structure of the substrate-free A82F heme domain is significantly different from that of the substrate-free WT BM3 heme domain. Specifically, a displacement of the FG helix region is seen, which disrupts the contacts between the FG helices and the I helix, leading to the reorientation of hydrophobic residues within the

active site and a conformational change in the P450. It appears likely that this dramatic structural change may affect the organization of the cluster of water molecules in the distal pocket above the heme, as a consequence of the movement of I helix; i.e., hydrogen-bonding networks are disrupted and rearranged, altering the positions of water molecules. Thus, the substrate-free A82F mutant exists naturally in equilibrium between the LS and HS state.

Typically, binding of substrates to the cytochromes P450 causes a ferric heme iron spin state change from 6cLS towards 5cHS owing to the disruption of the water cluster in the distal pocket and through the displacement of the axial water ligand. Usually, there is a corresponding increase in the heme Fe^{III}/Fe^{II} redox potential that helps facilitate electron transfer to the heme iron from the relevant redox partner.[126] As shown in Figure 4.3.2 (B), addition of OMP to the A82F mutant causes significant changes in the high-wavenumber rR spectrum. Two ν_3 modes, observed at 1486 cm^{-1} and 1501 cm^{-1}, show that the OMP-bound form also exists in an equilibrium between the 5cHS and 6cLS forms, respectively. The relative intensity of the HS ν_3 (1486 cm^{-1}) band is larger compared to the LS ν_3 (1502 cm^{-1}) mode, indicating a higher population of the HS component, estimated to be 65%.[101] This spin state mixture is also reflected in alterations in the ν_2 and ν_{10} bands; i.e., the ν_2 bands occur at 1568 cm^{-1} (HS) and 1582 cm^{-1} (LS). In the WT P450 BM3 protein, the Ala82 residue is located in a peripheral position in the active site. However, mutating Ala82 to a bulky phenylalanine leads to a substantial conformational change, altering positions of key active site residues (Figure 4.3.3), In particular, the Phe87 residue adopts a different conformation in which its side chain flipped from a parallel position to a near perpendicular orientation relative to the heme

plane, as compared to wild type BM3 heme domain in its complex with N-palmitoylglycine substrate (NPG) (PDB: 1JPZ). This structural change provides a closer contact of the phenylalanine side chain with the pyridinyl moiety of OMP, inducing a reorientation of substrate, leading to an increased HS component.

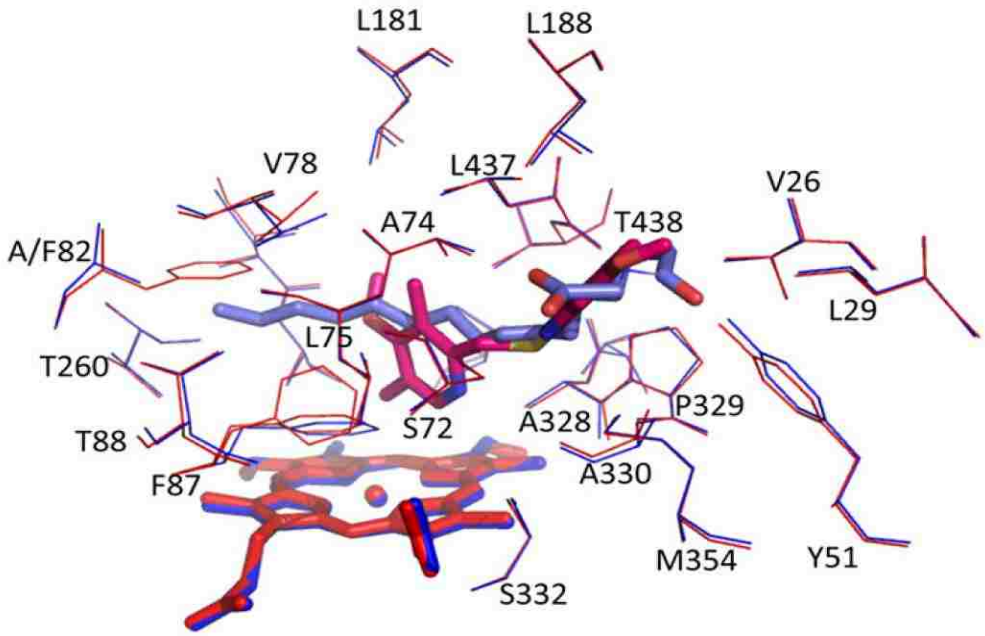

Figure 4.3.3 Stereoviews of A82F/OMP BM3 heme domain active site (PDB 4KEW in red) with WT/NPB BM3 active site (PDB 1JPZ in blue). Key amino acid residues in lines.

Similar studies of the F87V P450 BM3 heme domain mutant were conducted, with the high-wavenumber region of the substrate-free form (Figure 4, trace C) exhibiting features characteristic of the ferric state, with the ν_4 oxidation state marker occurring at 1373 cm^{-1}. The spin state marker bands, including ν_3 at 1501 cm^{-1}, ν_2 at 1583 cm^{-1} and ν_{10} at 1637 cm^{-1}, are indicative of a pure 6cLS state, consistent with heme iron coordination by a water molecule associated with a distal pocket cluster of water molecules.[127] The feature observed at 1621 cm^{-1} is confidently assigned to the ν(C=C) stretching mode of the peripheral vinyl group, with this wavenumber corresponding to an

in-plane vinyl stretching mode.[128] Binding of OMP to F87V BM3 causes a partial conversion from 6cLS to 5cHS, as shown in Figure 4.3.2 (trace D), with the 5cHS markers being observed at 1486 (ν_3), 1568 (ν_2), and 1622 cm^{-1} (ν_{10}) (the last being overlapped with vinyl ν(C=C) mode(s)). The weak 6cLS markers seen at 1501 and 1583 cm^{-1} persist in the spectrum, confirming the presence of residual low spin species. Overall, the increase of the HS component (56%) indicates the ability of this mutant to allow access of OMP to the heme distal pocket.

Turning attention to the substrate-free A82F/F87V double mutant, the enzyme exhibits a pure ferric 6cLS state, as evidenced by an isolated band at 1500 cm^{-1}. Binding of OMP to the double mutant gives rise to a relatively large HS component, exhibiting a ν_3 feature at 1486 cm^{-1}, as shown in Figure 4.3.2 (trace F). The intensity analysis referenced above[16] provided a calculated ratio of 68% of the HS form. It is noted that the wavenumbers of the vinyl stretching modes in the spectra of substrate-bound samples are difficult to establish because of their overlap with the HS ν_{10} mode; i.e., the ν_{10} mode for 5cHS is expected to occur near 1623 cm^{-1}.[129,130]

Summarizing the results obtained for the ferric proteins in the high-wavenumber region of the rR spectra, while binding of OMP is rigidly restricted for WT BM3, all of the F87V, A82F and F87V/A82F mutants show a considerable spin state conversion upon binding OMP, consistent with entry of OMP into the active site. However, a significant percentage of 6cLS species exists, possibly resulting from the incomplete expulsion of water molecules from the pocket and retention of an axial water ligand in minor proportion of the enzymes. However, a substrate conformation in which the pyridinyl nitrogen atom of OMP is in a position to coordinate with the heme, thereby generating a

LS species, cannot be ruled out. The percentages of the HS fractions for all of the BM3 heme domain samples (in substrate-free and OMP-bound forms) are summarized in the Table 1. These results obtained from resonance Raman data are in good agreement with earlier published binding data based on optical studies of OMP binding. These K_d data are also included in Table 1, clearly demonstrating that the F87V, A82F and combined F87V/A82F double mutations enable this fatty acid hydroxylase enzyme to act as a catalyst for OMP hydroxylation. The A82F substrate-free sample shows ~30% HS content, whereas the DM shows negligible HS content after treatment with Lipidex. It is likely that the introduced Val87 residue in the F87V/A82F double mutant alters distal pocket organization such that the spin-state equilibrium is perturbed as a result of reorganization of water molecules in the environment of the heme.

Table 4.3.1. P450 BM3 wild-type and mutant heme domain spin state populations, calculated by cross section ratio 1.24. The table shows the high spin proportion of the different mutants, along with K_d values for OMP binding to mutant heme domains. NA indicates that no evidence of binding was found.

Protein	substrate	resonance Raman (%HS)	K_d values from optical data[120]
Wild type	SF	0%	
Wild type	OMP	0%	NA
A82F	SF	30%	
A82F	OMP	65%	1.67± 0.05
F87V	SF	0%	
F87V	OMP	56%	49± 2.7
A82F/F87V DM	SF	0%	
A82F/F87V DM	OMP	68%	0.212± 0.014

Low frequency Resonance Raman spectra. The low-wavenumber region of rR spectra can provide important information about the disposition of heme peripheral groups. Specifically, the propionate groups usually exhibit their vibrational modes in the

region of ~360-380 cm^{-1}, providing insight into their interactions with the protein, mainly involving hydrogen bonding interactions with the surrounding amino acid residues which causes rR shifts to higher wavenumbers. In the 400-440 cm^{-1} region, the bending modes of vinyl groups occur, with the lower wavenumber mode (near 410 cm^{-1}) corresponding to the in-plane orientation, while the higher wavenumber mode (near 440 cm^{-1}) is associated with an out-of-plane distortion.[131, 132] In addition, structure sensitive in-plane and out-of-plane (γ_i) heme deformation modes occur in this region.[133, 134]

As shown in Figure 4.3.4, trace A, the substrate-free A82F BM3 low-wavenumber rR spectrum shows the normal heme skeletal modes: ν_7 (676 cm^{-1}), ν_{15} (753 cm^{-1}) and ν_8 (344 cm^{-1}). According to more detailed assignments of the rR spectra of other P450s, such as P450cam,[125] the bands observed at 364 cm^{-1} and 380 cm^{-1} are assigned to the bending modes of two heme propionate groups, while the band at 429 cm^{-1} is assigned to an out-of-plane vinyl bending mode, which can be correlated with the vinyl stretching mode observed at 1621 cm^{-1} in Figure 4. The binding of OMP causes an increase in the intensity of the 365 cm^{-1} bending mode of propionate group(s), indicating structural reorientation and a perturbed hydrogen bonded propionate group(s). A similar pattern was observed in the spectrum of substrate bound P450 BM3, this mode is originally assigned as an out-of-plane γ_6 mode by Deng et al,[135] which is induced by binding of the substrate. However, Schelvis and coworkers[132] assign this substrate activated mode to be a new propionate mode, result from a disrupted H-bonding between 7-propionate and lysine amino acid residue (Lys69), supported by crystallographic data.[136] Finally, as confirmed by Mak et al by employing a deuterated heme and a carefully performed deconvolution procedure, this feature is believed to contain contributions from both the γ_6 and propionate mode.[125]

Another bending mode of the propionate group(s) is observed at the same position as in the substrate-free form (at 380 cm^{-1}). Two bending modes of vinyl groups are detected at 414 cm^{-1} and 430 cm^{-1}.[124] Additionally, it is noted that a heme out-of-plane mode $\gamma_{7,}$ occurring at 312 cm^{-1}, is activated after binding of OMP, which apparently induces an out-of-plane distortion of the heme, i.e. the enhancement of out-of-plane modes arises from an out-of-plane heme distortion of the equilibrium structure of the heme macrocycle.[26,27,137]

Similar patterns are seen for the F87V mutant and for the A82F/F87V double mutant heme domains (Figure 4.3.4, trace C-F). In both cases, introduction of OMP (Figure 4.3.4 trace D and F) causes significant change in their low-wavenumber regions compared to the substrate-free forms.

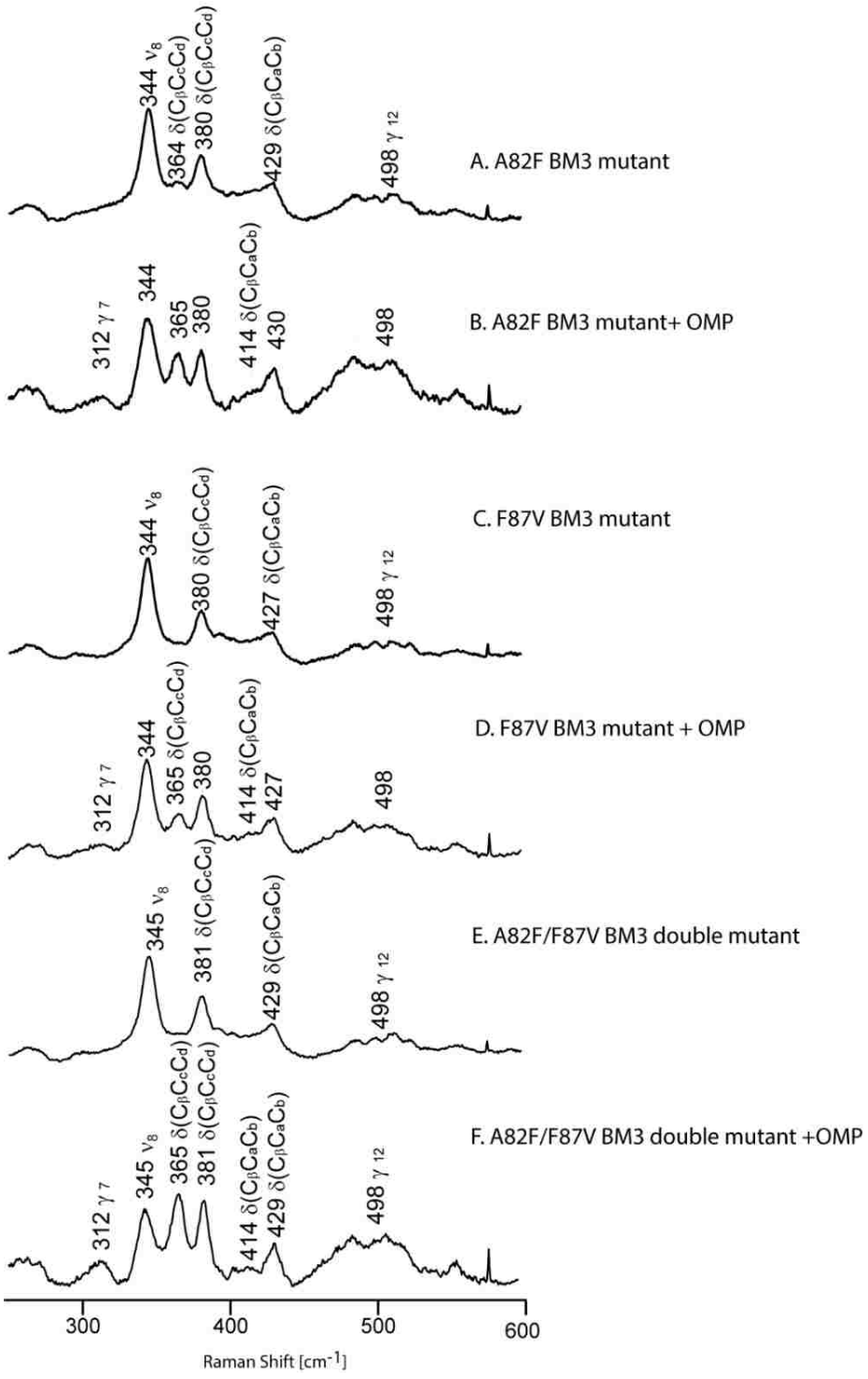

Figure 4.3.4. Low frequency rR spectra of substrate-free ferric P450 mutants and their substrate bound forms. (A) A82F substrate-free form. (B) Omeprazole bound A82F. (C) F87V substrate-free form. (D) Omeprazole bound F87V. (E) A82F/F87V double mutant substrate-free form. (F) A82F/F87V double mutant omeprazole bound form. All spectra were normalized to the ν_7 mode.

4.3.3 Ferrous CO P450 BM3 wild-type and mutant (A82F, F87V, A82F/F87V DM) and their interaction with substrate.

Cytochromes P450 are able to bind gaseous diatomic ligands, such as CO, NO and O_2, among which the ferrous-CO adducts are relatively more stable, facilitating detailed rR spectroscopic studies.[59] This is fortunate, because the behavior of the observable ν(Fe-C) and ν(C-O) stretching modes of the Fe-C-O fragment can provide quite useful information about steric hindrance and H-bonding interactions imposed upon the Fe-C-O fragment by the substrate or by surrounding amino acids within the active site.[138] The effects of such interactions are directly related to corresponding interactions with the Fe-N-O and Fe-O-O fragments of the more unstable NO and O_2 adducts. The interaction between the heme iron and the bound CO involves heme dπ back- bonding to the π* orbital of the CO ligand, strengthening the Fe-C bond while weakening the C-O bond; this is reflected by an increased Fe-C stretching wavenumber and a decreased ν(C-O) stretching mode, leading to the well-documented inverse linear correlation plot, discussed in more detail later.[57,139]

The low wavenumber rR spectra of the ferrous CO adduct of wild type substrate-free BM3 heme domain is shown in Figure 4.3.5 (Trace A, left panel). The most intense band in this region, besides the ν_7 mode, is the ν(Fe-C) band seen at 471 cm^{-1}. In accordance with earlier work performed, including ^{13}CO labeling, the band at 559 cm^{-1} is assigned to the δ(Fe-C-O) bending mode, with the corresponding ν(C-O) mode occurring at 1943 cm^{-1}, as shown in Figure 4.3.5 (Trace A, right panel).

A similar spectral patten is seen in the low wavenumber region of the rR spectra of wild type BM3 with OMP (Figure 4.3.5, trace B), where the ν(Fe-C) stetching mode occurs at 471 and the ν(C-O) mode at 1943 cm^{-1}. Thus, introduction of OMP into the wild type BM3 does not cause any significant change in the distal pocket, which is consistent with other documented lack of evidence for the binding of OMP to the wild-type BM3. It is emphasized that this seemingly "redundant" information is actually useful, because it is possible that binding of a substrate may not cause significant changes in the spin state of the ferric form, but much less likely that binding of substrate would not affect the modes of the Fe-C-O fragment in the P450. Thus, the absence of changes in these modes provides stronger confirmation of the lack of OMP binding in the active site.

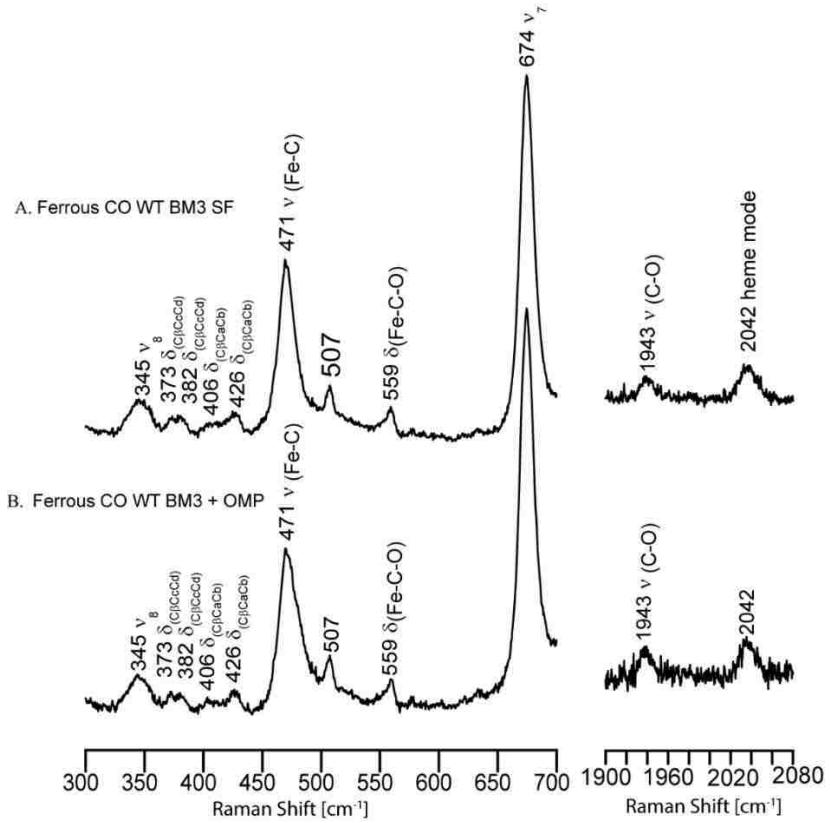

Figure 4.3.5 The rR spectra of ferrous CO adducts of wild type BM3, the low frequency spectra is shown in left panel, and the high frequency is in right panel. (A) Wild type substrate-free (B) wild-type OMP bound. Spectra were measured with 442 nm excitation line and normalized to the ν_7 modes.

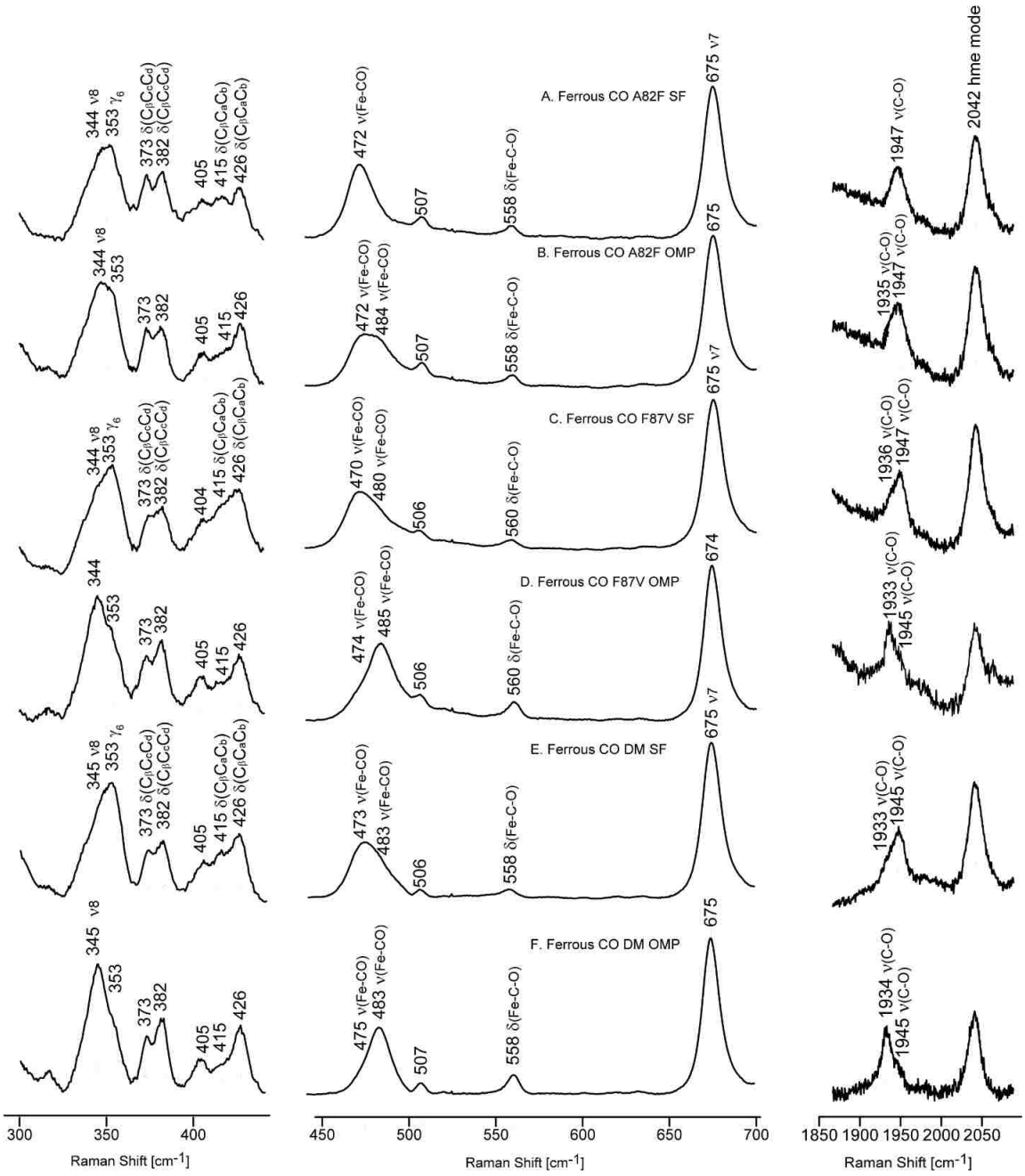

Figure 4.3.6 The low frequency (left panel), middle frequency (mid-panel) and high frequency (right panel) rR data of ferrous CO adduct of P450 BM3 mutants. (A) A82F substrate-free form. (B) Omeprazole bound A82F. (C) F87V substrate-free form. (D) Omeprazole bound F87V. (E) A82F/F87V double mutant substrate-free form. (F) A82F/F87V double mutant omeprazole bound form. All spectra were normalized to the ν_7 mode.

Figure 4.3.6 shows the rR spectra of the ferrous CO adduct of the BM3 mutants in both the low wavenumber (left panel) and the high wavenumber regions (right panel). It is important to note that binding of OMP to the ferrous CO forms of all these mutants has no impact on the heme core modes, including the propionate modes and the orientation of vinyl modes (Figure 4.3.6, left panel). This means that the bound substrate OMP mainly interacts with the Fe-CO fragments within the active sites of the BM3 mutant heme domains.

While the effect of OMP binding on the heme moiety is minimal, binding of OMP has a significant impact on the Fe-C-O fragments of all of these mutants. As seen in the low-wavenumber spectrum of the substrate-free form of the A82F ferrous CO adduct (Figure 4.3.6, trace A**)**, a single ν (Fe-CO) stretching mode occurs at 472 cm^{-1}, with the corresponding ν(C-O) mode being seen at 1947 cm^{-1}, It is notable that these values are quite similar to those of the substrate-free form of the WT heme domain (i.e., 472/1943 cm^{-1}). However, addition of OMP causes substantial changes, as shown in Figure 4.3.6, trace B. While the 472/1947 cm^{-1}pair persists, a new ν (Fe-CO) stretching mode is seen at 484 cm^{-1}, with its corresponding ν(C-O) mode occurring at 1935 cm^{-1}; i.e., a new Fe-C-O conformer is formed upon OMP binding. It should be recalled that, while the Phe87 residue of the WT protein (with NPG substrate bound) lies almost parallel to the heme plane (Figure 4.3.3), this residue assumes a nearly perpendicular orientation with respect to the heme plane for the A82F mutant; i.e., presumably the newly observed conformer (with the 484/1935 cm^{-1} pair of Fe-C-O modes) results from this reorientation of the Phe87 fragment.

In the case of the F87V BM3 mutant, it is interesting to note that while the ferric substrate-free heme domain showed no evidence for heterogeneity, there are two ν(Fe-CO) stretching modes seen in the spectrum of the CO adduct, observed at 470 and 480 cm^{-1}, with the corresponding ν(C-O) modes occurring at 1947 cm^{-1} and 1936 cm^{-1}, respectively (Figure 4.3.6, trace C). Based on relative intensities, the ν(C-O) mode at 1947 cm^{-1} corresponds to the 470 cm^{-1} ν(Fe-CO) mode and the 1936 cm^{-1} feature is correlated with the 480 cm^{-1} ν(Fe-CO) mode. Obviously, this behavior is consistent with the well-documented inverse wavenumber relationship. As the less bulky valine was introduced to replace the phenylalanine sidechain, a more open distal pocket provides an environment with greater opportunities for conformational flexibility of the Fe-C-O fragment. The effect of OMP binding on the F87V mutant, now devoid of the intrusive phenyl group, has a rather dramatic effect on the Fe-CO linkage, leading to a high population of a fragment participating in a relatively strong H-bonding interaction, as evidenced by the 485/1933 cm^{-1} pair of bands, an interaction presumably associated with the OMP substrate.

Given this apparent key role for the F87V mutation in regulating active site environment, it is not surprising that the vibrational mode patterns for the Fe-C-O fragment for the double mutant are virtually identical to those observed for the F87V mutant (within a couple wavenumbers and having quite similar relative intensities). The most likely candidates for a strongly polar group associated with substrate binding are the methyl ether substituent of the pyridinyl frament or, perhaps less likely, the S=O group, either of which is likely to associate with a distal pocket water molecule, polarizing it to serve as an effective H-bond donor.

The wavenumbers of the ν(Fe-C) and ν(C-O) stretching modes for the ferrous-CO adducts of all of the P450 BM3 heme domain variants studied here, including the substrate-free and OMP-bound forms, are collated in Table 4.3.2. The resulting plot of the ν(Fe-C) vs ν(C-O) values, (Figure 4.3.7) yields the expected inverse correlation.[140] In Figure 4.3.7, the correlation line for nitric oxide synthase, NOS, (green line) [141,142] is displaced above the P450 line, owing to correspondingly higher ν(Fe-C) stretching modes that result from the fact that a proximal pocket tryptophan residue provides an H-bond donor fragment to the proximal thiolate ligand of NOS, weakening the Fe-S linkage. Below this line lies the line for P450cam (blue line),[59,143,144] which possesses a more strongly electron donating thiolate proximal ligand, leading to relatively high ν(Fe-S) stretching modes occurring near 350-355 cm^{-1}.[39] The data points for the P450 BM3 heme domain and mutants yield a line close to that of P450cam (red line), but with a slightly greater slope, reflecting a wider variation in distal pocket polarity; this observation is consistent with the higher polarity of the OMP substrate compared to the collection of less polar substrates in the study of P450cam.

In conclusion**,** the resonance Raman data presented here show that the binding of OMP causes a substantial increase in distal heme-pocket polarity in the BM3 F87V, A82F and F87V/A82F mutant heme domains. The addition of OMP has no effect on the Fe-C-O fragment in the wild-type P450 BM3 heme domain, confirming earlier results indicating that OMP does not enter the heme pocket.[120] The F87V mutation has a strong impact on the modes of the Fe-C-O fragment, an observation consistent with the structural changes enabled by this mutation within the heme distal pocket. In general, the data acquired here highlight the ability of these mutations to effectively influence protein

structure and so to alter the substrate selectivity of BM3, as demonstrated by their introducing catalytic activity towards OMP and related PPI drugs.[120, 118] These rR studies provide important new structural insights into BM3 mutants that have gained novel functions in PPI drug metabolism through changes to P450 conformational state and active site organization produced through introduction of the A82F and F87V mutations, respectively. These BM3 mutants catalyze the 5-hydroxylation of OMP (and oxidation of other PPI drugs), generating the same metabolite produced by human P450 2C19, as well as other human P450-type metabolites (e.g. from rabeprazole and lansoprazole) that should make these drug metabolites more readily available as standards for tests required for FDA compliance.

Table 4.3.2 The frequencies of ν(Fe-C) and ν(C-O) stretching modes for P450 BM3 proteins. The numbers in the column represents points in **Figure 4.3.7**.

	P450 BM3	ν (Fe-C) cm^{-1}	ν(C-O) cm^{-1}
1	wild type substrate-free	471	1943
2	wild type + OMP	471	1943
3	A82F substrate-free	472	1947
4	A82F + OMP	472	1947
5	A82F + OMP	484	1935
6	F87V substrate-free	470	1947
7	F87V substrate-free	480	1936
8	F87V+ OMP	474	1945
9	F87V+ OMP	485	1933
10	A82F/F87V substrate-free	473	1945
11	A82F/F87V substrate-free	483	1933
12	A82F/F87V + OMP	475	1945
13	A82F/F87V + OMP	483	1934
	CYP101		
14	substrate-free	464	1963
15	+ norcamphor	473	1947
16	+ adamantanone	474	1942
17	+ camphoroquione	476	1941
18	+ fenchone	480	1945
19	+ camphor	481	1940
20	+ tetramethylcyclohexanone	485	1934
	NOS		
21	nNOS Substrate-free	487	1949
22	nNOS Substrate-free	501	1930
23	nNOS + Arg	503	1929
24	nNOS + OH-Arg	502	1928
25	NOS_{FL} substrate-free	487	1945

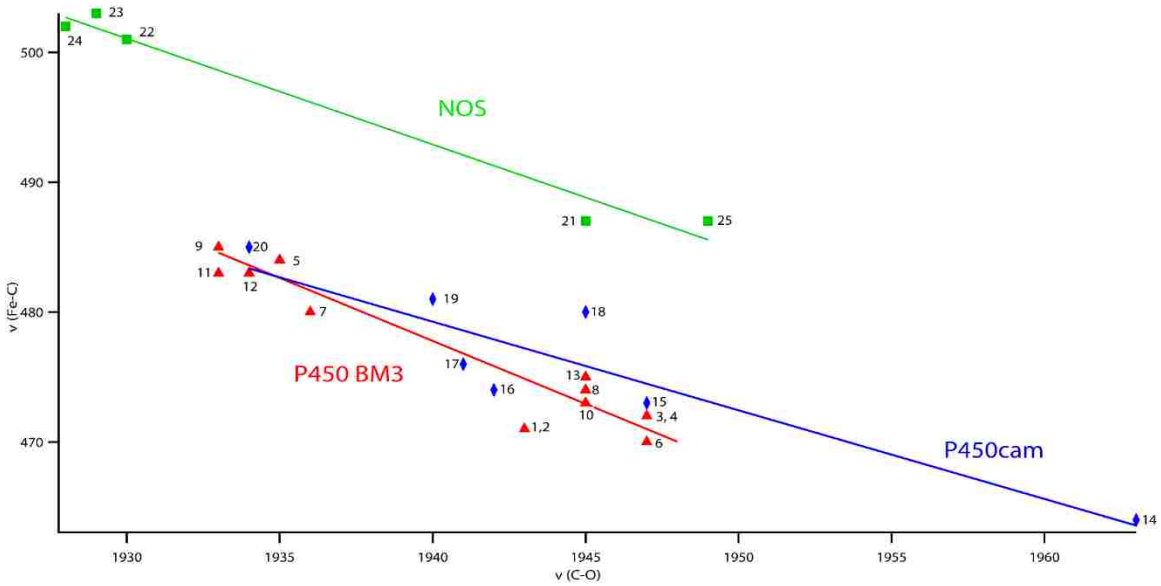

Figure 4.3.7. Diagrams showing an inverse correlation for P450 BM3 (wild type and mutants), P450cam and NOS in substrate free and substrate bound form. The numbers represent proteins listed in Table 4.3.2. The red triangles show points for P450 BM3 (red line), the blue diamonds for P450cam (blue line), and green squares for NOS (green line).

Chapter 5 Resonance Raman investigations on cytochromes P450 peroxygenase: Ole T (CYP152L1) and P450 Staph (CYP152L2)

5.1 Introduction

While the majority of known cytochromes P450 use NAD(P)H-dependent reductase systems and the O_2-bound intermediate to eventually produce Compound I, several P450s have evolved to exploit the so-called "peroxide-shunt" pathway, where reaction of the ferric heme with H_2O_2 directly produces "Compound 0", which rapidly converts to Compound I, a mechanism which bypasses any need for partner reductases, prompting the designation of peroxygenases for these P450s, the mechanism is shown in Figure 5.1.1 (grey arrows).[145] In contrast to other monooxygenase P450s that use the oxygen as oxidizing agent (double-headed arrow in Figure 5.1.1), these peroxygenases utilize H_2O_2 to facilitate substrate oxidation to replace the need for solubilized oxygen and the complex reductase system. Needless to say, this efficient peroxide activation route has attracted great interest for biotechnological purpose.[146]

Two of these, one from *Bacillus subtilis*, CYP152A1 ($P450_{BS\beta}$), and the other, from *Sphingomonas paucimobilis*, CYP152B1 ($P450_{SP\alpha}$), employ H_2O_2 to efficiently catalyze the hydroxylation of long chain fatty acids (FAs).[145, 147] While $P450_{SP\alpha}$ catalysis is highly specific, with nearly exclusive hydroxylation at the α position, $P450_{BS\beta}$ catalyzes hydroxylations at both the α (40%) and β (60%) positions.[145] Another peroxygenase, recently isolated from Jeotgalicoccus and characterized by Rude et al,[148] is 41% identical in sequence to $P450_{BS\beta}$ and 37% to $P450_{SP\alpha}$. The authors designated this

enzyme as a CYP152 P450 family member (i.e., CYP152L1), whose commonly used name is Ole T. While reasonably close in sequence with the other CYP152 members mentioned above, Ole T displays a much different catalytic activity. Like $P450_{SP\alpha}$ and $P450_{BS\beta}$, Ole T also has high affinity for long chain FAs; however, instead of catalyzing hydroxylations at α and β positions, Ole T catalyzes a remarkable transformation of FAs, converting them into linear and branched chain terminal alkenes involving a C-C_α bond cleavage process, as shown in Figure 5.1.2.[149]

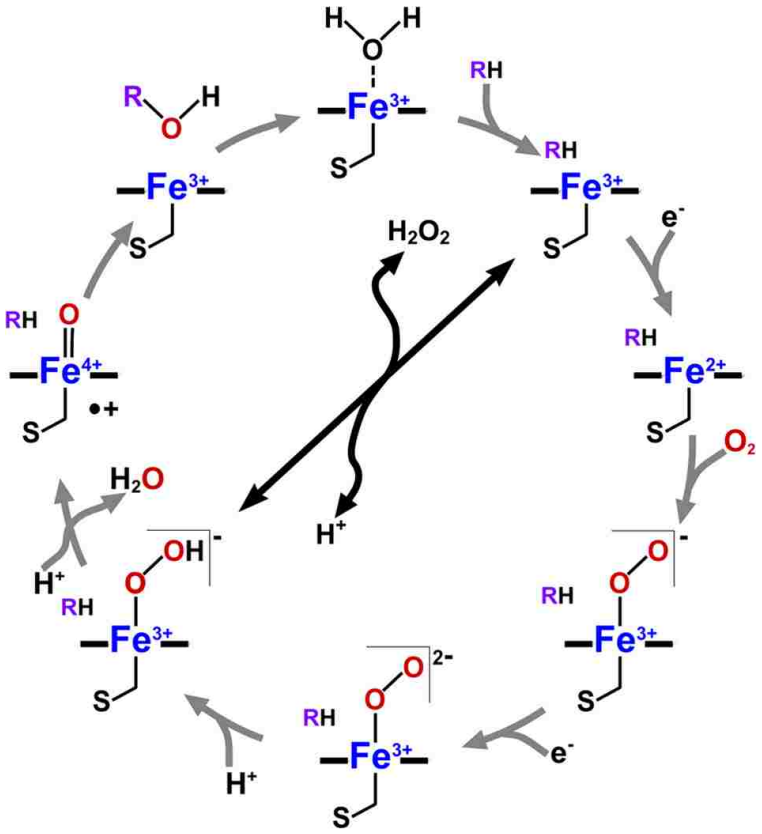

Figure 5.1.1 The catalytic mechanism for Ole T and general P450.[149]

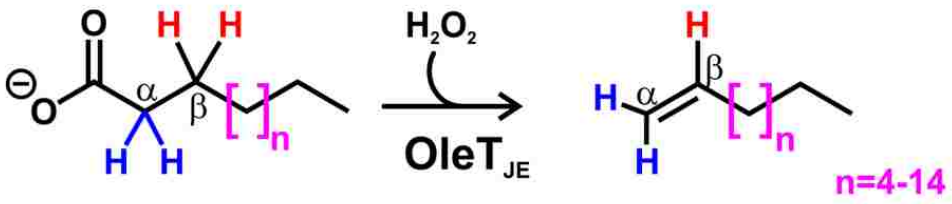

Figure 5.1.2 The C-C cleavage reaction catalyzed by Ole T.

In order to better understand the stark differences in catalytic activities, direct comparisons have been made for crystal structures of Ole T,[149] and $P450_{BS\beta}$,[145] revealing a similar substrate binding mode in which the fatty acid carboxylate is tethered via electrostatic interactions to an active site arginine (Arg245). A most interesting difference in the two structures is the replacement of Q85 in the $P450_{BS\beta}$ enzyme with a potentially H-bonding H85 in the case of Ole T. Attempts to relate the effects of this residue replacement to possible mechanistic differences have been made. However, our collaborator, Professor Thomas Makris and his group, have shown that introducing the H85Q mutation into Ole T does not diminish conversion of C_{20} FA to nonadecene. These and other spectroscopic and kinetic studies have led Professor Makris to consider other possible mechanisms.[150] In presence of per-deuterated eicosanoic acid (C20D FA) with excess H_2O_2, a Compound I species is accumulated to a high level with its optical spectroscopic characters being similar to those observed spectra (Soret band 370nm and an additional band at 690nm).[52] In a parallel experiment, the protiated native substrate bound Ole T failed to permit accumulation of Compound I. Such an apparent kinetic isotope effect strongly suggests that a hydride removal from C_β position initiates fatty acid decarboxylation performed by Compound I.[149] The newly proposed mechanism is shown in Figure 5.1.3, following by H abstraction from C20 fatty acid by Compound I, a

substrate radical and a Fe (IV) Compound II species are generated, either a substrate biradical or carboncation is produced involving a single electron transfer to Compound II, which can be further rearranged to generate the alkene products.[151]

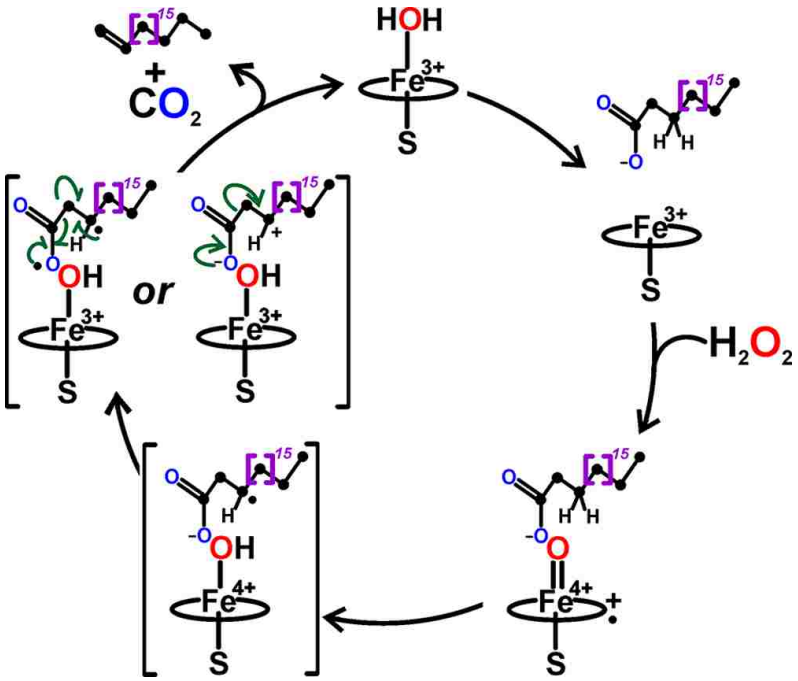

Figure 5.1.3. Proposed mechanism for Ole T decarboxylation reaction catalyzed by P450 Compound I.

The other CYP152 family enzyme, CYP152L2 from *Staphylococcus massiliensis*, named as P450 staph (abbreviated as CYP-SA), is a close orthologue to the P450 Ole T CYP152L1 with 61% identity shared. Both enzymes have highly similar properties and perform highly similar reactions. Although here are a couple of differences on the protein surface, the active site is very similar. The one main difference is that CYP-SA is much more stable than Ole T, this is a huge advantage as Ole T has a big precipitation/P420 issue upon thawing/freezing and reduction process, thus trapping the unstable intermediate on this analogy could be extremely informative on both enzymes.

The general purpose of this project is to use resonance Raman spectroscopy to track how well the O_2 driven pathway works with peroxygenase enzymes, as there is always a large interest in seeing if Ole T can turn over with O_2 and electrons, which could be much easier for biofuel generation in *organisms* since it is difficult to leverage H_2O_2 in cells. Thus, rR experiments are planned on Ole T (CYP152L1) and CYP-SA (CYP152L2) in presence of per-deuterated eicosanoic acid substrate, which will be quite useful in providing information, such as potential heme macrocycle distortions and reorientation of peripheral substituents, it will be also interesting to investigate how the substrate position affects the disposition of the diatomic ligand, including the Fe-CO and Fe-O-O fragments, which can lead to a better understanding of both the Fe-S strength in the proximal side and the H-bonding environment in distal pocket.

5.2 Experimental

5.2.1 Sample preparation

The following samples were kindly provided by our collaborator, Dr. Thomas Makris from the University of South Carolina University, including: 1) 290 μM Ole T, in clean ES complex with deuterated eicosanoic acid (C20D FA) in 250 mM phosphate buffer (pH=7.5) with 250mM NaCl, prepared in H_2O. 2) 200 μM CYP-SA in 200 mM phosphate buffer (pH=7.5), containing 30% purified glycerol (v/v).

Some of P450s and/or fatty acid substrate precipitates out of solution upon thawing, and those samples were centrifuged to eliminate the precipitations before use. Ferric samples were prepared by directly transfering 50uL of protein to an NMR tube. The ferrous samples were prepared by adding degassed sodium dithionate solution into the argon equilibrated protein samples, where monitoring the 642nm Q band in Uv-vis spectra, until it completely disappears. This is all done at room temperature.

5.2.1.1 Ferrous CO samples for rR measurement

The ferrous CO adducts of both Ole T and CYP-SA enzymes were prepared in exactly the same way with the presence of methyl viologen to facilitate reduction (molar ratio of protein to MeV is 5:1). Specifically, 50μL of CYP-SA protein was placed in NMR tube (WG-5 Economy, Wilmad) which was sealed with a rubber septum (Sigma Aldrich, Milwaukee, WI). After degassing with CO gas for 15 minutes, the proteins were reduced by injecting a stoichiometric amount of sodium dithionite solution, which is

prepared freshly in degassed buffer. Then the sample was further equilibrated with CO gas by bubbling for an additional 10 mintues to ensure full converstion.

5.2.1.2 Ferrous dioxygen adduct preparation

Oxy samples were prepared by using the vaccum line in our lab, on which the NMR tube could be easisly connected with sealed connection parts. Starting with the ferric substrate-bound samples, vaccum was applied to the tube first and then refilling with Ar gas, repeating this process for several times to ensure there is no presence of oxygen. Sodium dithionite solution was titrated to the enzyme through a long needle attached to a syringe, until the 642 nm band disappeared in the Q region of Uv-vis spectra. Again, the enzyme is reduced in presence of Methyl Viologen. Then, reduced CYP-SA sample tubes were transferred to a dry ice-ethanol bath held at -20°C to be cooled down for 1 minute. Oxy-ferrous complexes were made by bubbling $^{16}O_2$ or $^{18}O_2$ for 10 seconds, followed by rapid freezing in liquid N_2 to avoid auto-oxidation.

However, lots of efforts were taken on making oxy Ole T under different conditions; i.e., $^{16}O_2$ or $^{18}O_2$ gas was bubbled into the reduced Ole T at different temperatures to find the suitable conditions of oxy complex formation, including -20°C, -15°C, -12°C, -10°C and 4°C, with a mixing time ranging from 10-20s. The procedure of making oxy compound is exactly same as state above.

5.2.2 Resonance Raman Measurement

The spectra of ferric samples was obtained using a 406.7nm excitation line and the spectra of ferrous and oxy samples were measured using 413.1nm line, both lines

being provided by a Kr+ laser (Coherent Innova Sabre Ion Laser). And the spectra of the ferrous CO sample, were acquired with the 441.6 nm excitation line from a He-Cd laser (IK Series He-Cd laser, Kimmon Koha CO., Ltd.). The RR spectra of all samples were measured using a Spex 1269 spectrometer equipped with a Spec-10 LN liquid nitrogen-cooled detector (Princeton Instruments, NJ). The slit width was 150 μm, and the laser power for ferric sample was kept around 10mW, whereas for the ferrous CO and oxy complex, the power was adjusted to ~1 mW. All samples were measured in a spinning NMR tube and a cylindrical focusing lens to avoid local heating and protein degradation. It is emphasized that, the oxy adducts were measured at 77K, in a home-designed glass dewer filled with liquid nitrogen. Spectra were calibrated with fenchone and processed with Gram/32 AI software (Galactic Industries, Salem, NH).

5.3 Results and Discussion

5.3.1 Results of ferric Ole T protein with deuterated eicosanoic acid (C20D fatty acid)

The high-frequency rR spectrum of substrate-free (SF) Ole T is shown in Figure 5.3.1 (trace A). The peak occurs at 1373 cm^{-1}, assigned as the oxidation state marker band, ν_4, indicating the protein is in ferric state. The spin state markers ν_3 and ν_2 mode occurs at 1502 and 1581 cm^{-1}, confirming the presence of a pure six-coordinated low spin (6cLS) form. The modes observed at 1619 and 1628 cm^{-1} were assigned to two vinyl stretching vibrations. Addition of the substrate, C20D fatty acid, to the enzyme caused a

large degree of conversion from LS to HS component, as reflected by the relatively higher intensity of high spin ν_3 (1488 cm^{-1}) band than the low spin ν_2 mode (1502 cm^{-1}); the HS component is estimated to be 70% by employing the value of I_{HS}/I_{LS} determined to be 1.24.[101] This spin state mixture is also reflected by alterations in the ν_2 and ν_{10} bands; i.e., the ν_2 bands occur at 1565 cm^{-1} and 1637 cm^{-1}. However, it is difficult to estimate the mix spin state mixture from the ν_{10} band since the high spin state ν_{10} band usually overlaps with the vinyl stretching mode which occurs at 1623 cm^{-1}.

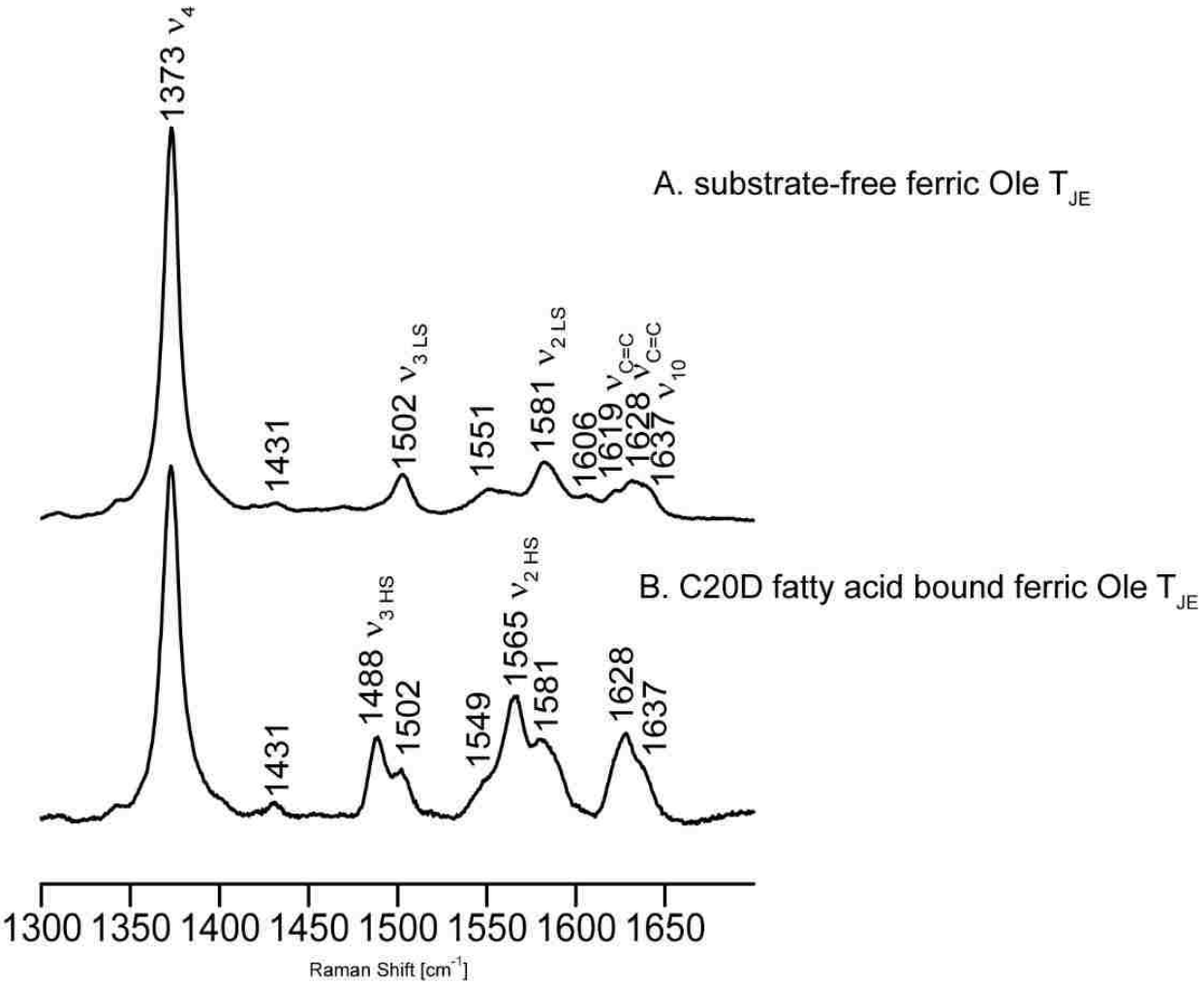

Figure 5.3.1 The high frequency rR spectra of Ferric Ole T protein. (A) substrate-free Ole T (B) C20D-bound Ole T. Spectra were normalized to the ν_4 mode at 1374 cm^{-1}.

The low-frequency rR spectrum of SF Ole T is shown in Figure 5.3.2 (trace A). The assigned heme skeletal modes are ν_7 (676cm^{-1}), ν_{15} (752 cm^{-1}) and ν_8 (348 cm^{-1}). A shoulder of ν_7, appearing at 695 cm^{-1}, can be allocated to γ_{20}. According to the complete assignments of other heme proteins, including globins and Cytochromes P450, the bands observed in the region of 365-380 cm^{-1} are typically assigned to the bending modes of the heme propionate groups,[125] though they are more properly interpreted as heme deformation modes that involve significant contributions from the propionate bending coordinates as well as δ (C_β-CH_3) motions: herein, the bands occuring at 372 and 382 cm^{-1} are assigned as heme propionate bending modes. Likewise, bands appearing between 400-440 cm^{-1} are assigned to "vinyl bending" modes,[128] with frequencies observed at 414 and 426 cm^{-1}, values which are in good agreement with the observations of two vinyl stretching modes observed in the high frequency region, as mentioned earlier.

Binding of the C20D fatty acid substrate does not induce a significant change in the heme skeletal vibrations, ν_8, ν_{15} and ν_7, at 348 cm^{-1}, 752 cm^{-1}, 676 cm^{-1} respectively, in the low-frequency region, as shown in Figure 5.3.2 (trace B). However, it can be seen that one propionate bending mode occurs at lower frequency (372 cm^{-1}) decreased relative intensity compared to the other higher frequency bending mode. It is generally agreed that this lower frequency propionate bending mode is associated with the greater hydrogen-bonding network between the propionate and surrounding amino acid residue. One possible explanation for this is the H-bond network is disrupted and thus showing the deactivation of one propionate bending mode or, more likely that both propionates have similar environments.

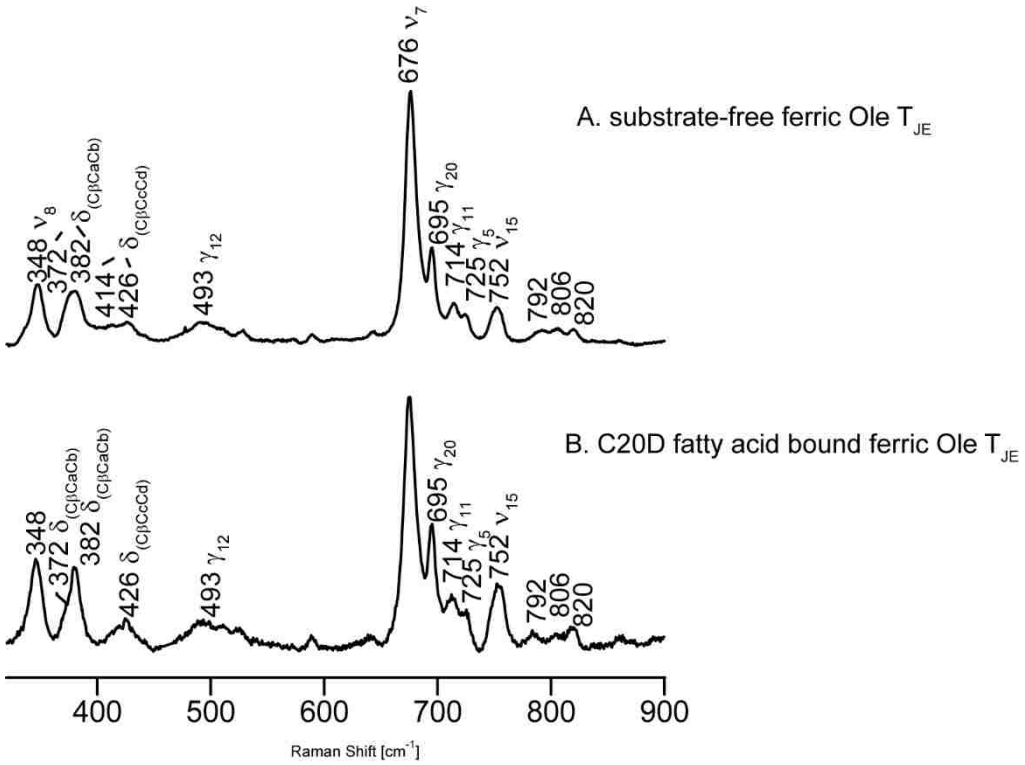

Figure 5.3.2 The low frequency rR spectra of Ferric Ole T protein. (A) substrate-free Ole T (B) C20D-bound Ole T. Spectra were normalized to the ν_7 mode at 676 cm^{-1}.

5.3.2 Results of ferric CYP-SA protein with deuterated eicosanoic acid (C20D fatty acid)

The high-frequency RR spectra of ferric state P450-SA is shown in Figure 5.3.3, noting that the band appearing at 1468 cm^{-1} is attributable to glycerol. The ν_4 mode was seen at 1373 cm^{-1}, which indicates the sample is in ferric state. Furthermore, the spin state marker, ν_3 mode at 1504 cm^{-1} shows the presence of 6cLS state. There is also a relatively higher intensity 5cHS component observed (ν_3 at 1490 cm^{-1}). This spin state mixture is also reflected by alterations in the ν_2 and ν_{10} bands; i.e., the ν_2 bands occur at 1571 cm^{-1} and 1584cm^{-1}, which the ν_{10} bands occur at 1632 and 1642 cm^{-1}. It is also important to

notice two vinyl stretching mode occurs at 1623 cm^{-1} and 1632 cm^{-1} (the last being overlapped with ν_{10}).

The low-frequency region of rR spectra of CYP-SA is shown in Figure 5.3.4. The assigned heme skeletal modes are ν_7 (675cm^{-1}), ν_{15} (754 cm^{-1}) and ν_8 (345 cm^{-1}). A strong shoulder of ν_7 appearing at 694 cm^{-1} can be allocated to γ_{20}. According to the complete assignments of other heme proteins, including globins and Cytochromes P450, the bands observed at 365 and 380 cm^{-1} are assigned to the bending modes of the heme propionate groups,[125] Similarly, bands appearing between 400-440 cm^{-1} are assigned to "vinyl bending" modes, which occurs at 412 and 425 cm^{-1}. It is interesting to note that in this C20A bound sample, the intensity of heme out-of-plane modes are relatively strong; i.e., γ_7 and γ_{12} occurs at 322 cm^{-1} and 492 cm^{-1}, which implies a greater oop distortion of heme macrocycle compared to Ole T.[152] Collectively, it can be concluded that CYP-SA heme cofactor possesses a ruffled, highly distorted posture reflected by relatively intense oop modes seen in rR spectra.

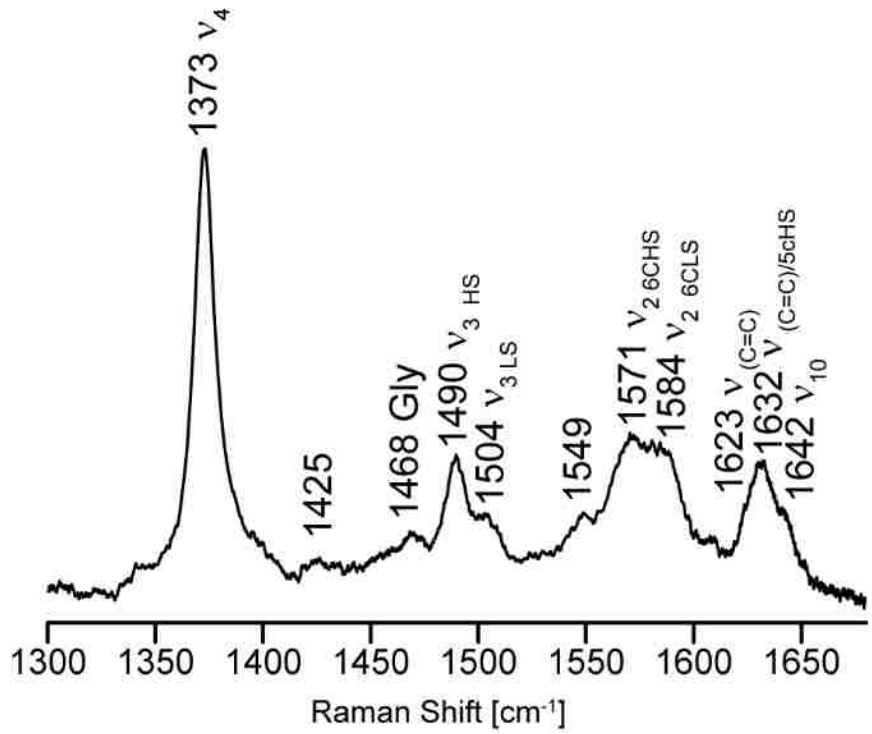

Figure 5.3.3 High-frequency rR spectra of P450-SA. Spectra were measured at room temperature with excitation line at 406.7 nm.

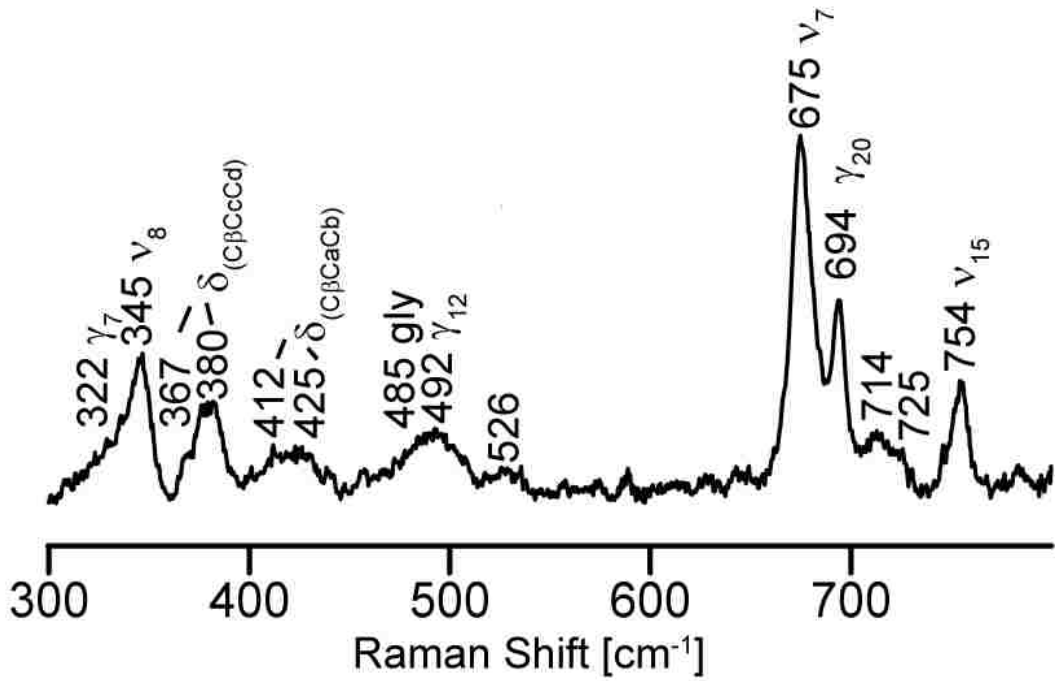

Figure 5.3.4 Low-frequency rR spectra of P450-SA. Spectra were measured at room temperature with excitation line at 406.7 nm.

5.3.3 Ferrous-CO samples of Ole T and CYP-SA characterized by resonance Raman Spectroscopy

One of the most important factors that control the reactivity of Cytochromes P450 is the strength of linkage between the heme iron and the proximal cysteine thiolate. Interrogation of the ferrous CO adducts of heme proteins using rR has been proven to be an effective probe of this linkage, including the proximal active site environment, especially H-bonding interactions with surrounding amino acid residues. Basically, the strength of Fe-S ligand can be reflected from trans-axial exogenous ligand with measurable changes in the internal modes for the Fe-CO fragment, which depend on extent of dπ (Fe) to CO (π*) backbonding donation. In order to better understand the structural factors involved in CYP152 family, the rR spectroscopy is performed on ferrous CO CYP152 complexes.

The rR spectra of ferrous CO Ole T substrate-free complex is shown in Figure 5.3.5, trace A, with the left panel showing the low frequency spectra, indicating the presence of two Fe-CO fragments, with the ν(Fe-C) frequencies observed at 467 and 479 cm^{-1}. The presence of two conformers is confirmed by the observation of the two corresponding ν(C-O) modes being observed at higher frequency at 1939 and 1957 cm^{-1} (Figure 5.3.5, trace A right panel). In contrast, binding of a long chain C20D fatty acids to Ole T with its polar carboxylate group lying close to the heme iron, gives rise to only one distinct Fe-C feature, which appears at 476 cm^{-1}, with its correlated C-O stretching mode occurring at 1941 cm^{-1} (Figure 5.3.5, trace B). It can be suggested that a more constrained distal pocket is formed as the bulky long chain fatty acid is anchored into the

active site, allowing less space for Fe-CO movement, consistent with only one conformer. Similarly, only one Fe-CO stretching mode (479 cm^{-1}) is detected for the C20D bound CYP-SA CO complex, with the associated ν(C-O) mode seen at 1949 cm^{-1} (Figure 5.3.6).

To gain more insight into the electrostatic and H-bonding effects in the active site of the enzyme, a plot of the inverse backbonding correlation line between ν(Fe-C) and ν(C-O) frequencies is shown in Figure 5.3.7. The data points for Ole T and CYP-SA samples are shown in yellow and purple dots, respectively, along with similar plots for other previously reported cytochrome P450cam (in blue line),[143,59, 139,139] mammalian nitric oxide synthase (NOS) in grey lines[142,141] and the histidine ligated myoglobin (Mb) variants with differing distal residues (orange line).[153,154,155,156] The values for all the points are listed in Table 5.3.1. The data points for these myoglobin variants are highly informative; as is well-known, the His64 residue in wild-type Mb provides a weak H-bond donor to the Fe-CO fragment, and replacing the His64 with a more hydrophobic residue can lead to a downshift data points along the backbonding line. However, mutation of His64 to a stronger H-bond donor residue can shift the point up (left).[157] Thus, the increased polarization effect in distal pocket can be reflected by the position of data points. Compared with the histidine ligated myoglobin variants, P450cam possesses a stronger donor thiolate ligand from a cysteine side chain, which is expected to decrease ν(Fe-C) frequency via sigma competition, thus showing a backbonding line below the Mb line. Consistent with the trend, the NOS enzymes, which have a proximal cysteine residue, exhibit a line between these two lines owing to the fact that they possess a proximal H-bond donor with tryptophan residues, this lead to a lowered thiolate donor

strength, thus exhibiting a separate line between P450cam and Mb backbonding lines. Considering all the data points for CYP152L enzymes herein, it is important to notice all these data points fit very well on the correlation line for P450cam, showing a similar Fe-S strength and proximal environment. On the other hand, the C20D bound samples yield a higher position along the line, suggesting the increased polarity in the distal pocket, which can be well postulated that the H-bonding interaction is enhanced by the introduction of the polar carboxyl group of the substrate.

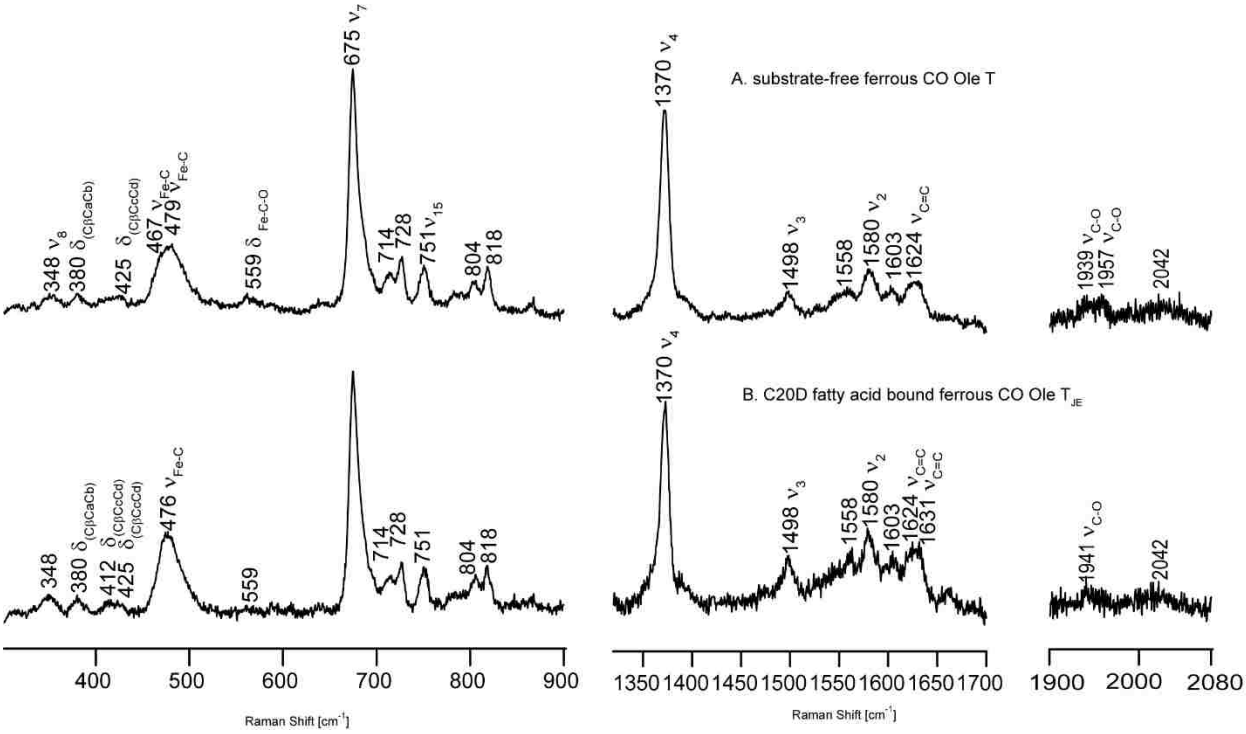

Figure 5.3.5 rR spectra of Ole T CO complex. Spectra were measured at room temperature with excitation line at 441.6 nm. Left panel shows Low-frequency region, middle panel presents high frequency, and right panel shows the region where the C-O stretching mode occurs.

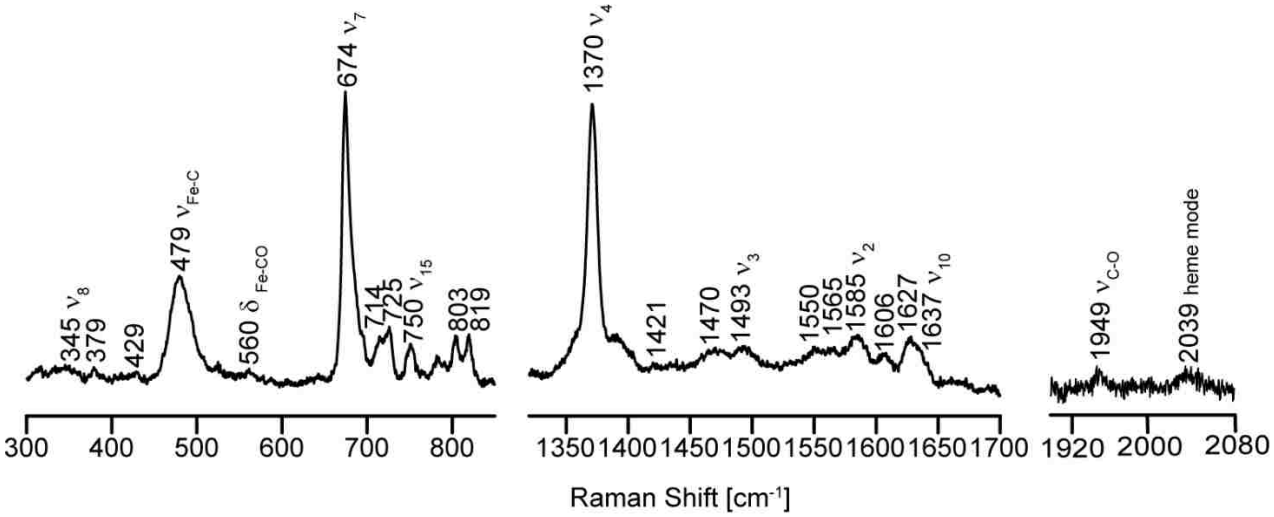

Figure 5.3.6 rR spectra of C20D fatty acid bound CYP-SA complex. Spectra were measured at room temperature with excitation line at 441.6 nm. Left panel shows Low-frequency region, middle panel presents high frequency, and right panel shows the region where the C-O stretching mode occurs.

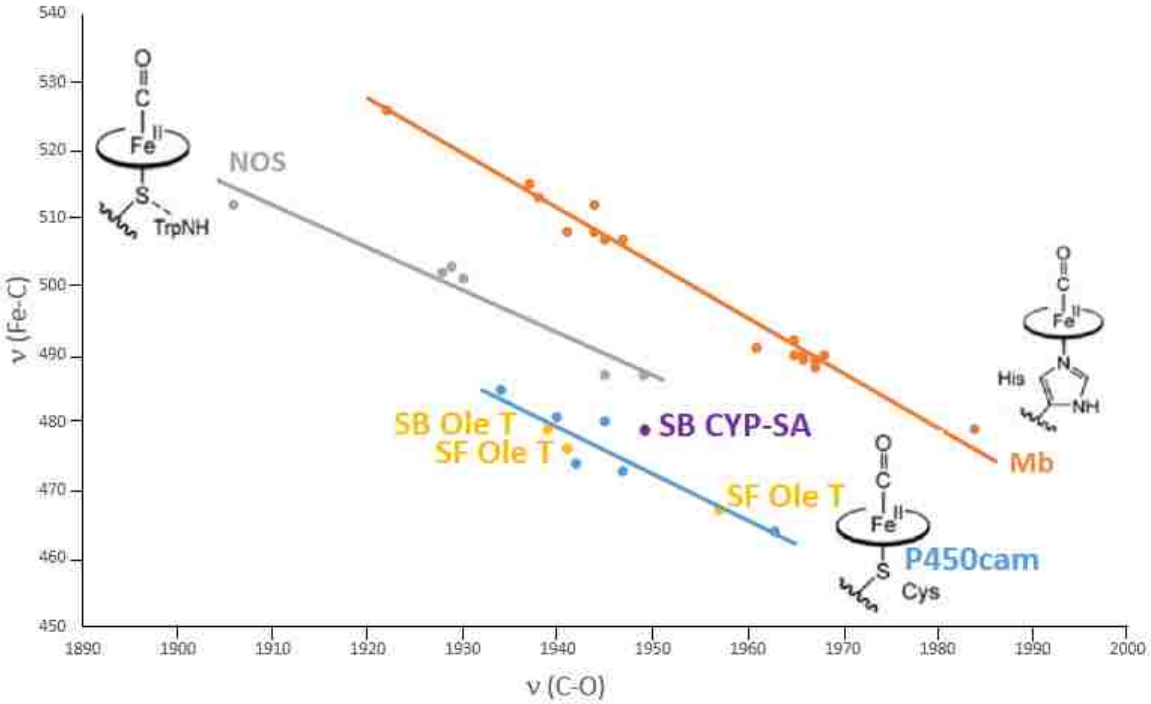

Figure 5.3.7 backbonding correlations of FeCO adducts in different heme proteins which yielding various axial ligands: blue line – thiolate ligated P450cam, grey line – thiolated ligated with Tryptophan backbone H bond NOS, orange line- myoglobin variants with differing distal residues. The data points for Ole T CO complex are shown in yellow dots while the CYP-SA CO data point is shown in purple.

Table 5.3.1 values of all the points for plotting Figure 5.3.5 are listed below. References are cited in the content.

P450 cam	ν(C-O) cm^{-1}	ν(Fe-C) cm^{-1}
substrate-free	1963	464
+ norcamphor	1947	473
+ adamantanone	1942	474
+ camphoroquione	1941	476
+ fenchone	1945	480
+ camphor	1940	481
+tetramethylcyclohexanone	1934	485
Mb		
WTSW	1937	515
WTSW pH=8.4	1944	512
WTSW pH=7.0	1947	507
WTSW pH=2.6	1966	489
WTh	1941	508
WTp	1944	508
H64Qh	1945	507
H64Gh	1965	492
H64ASW	1966	490
H64VSW	1967	488
H64ISW	1968	490
H64LSW	1965	490
V68Th	1961	491
V68Np	1922	526
F46VSW	1967	489
L29F/H64QSW	1938	513
H64V/V68Tp	1984	479
nNOS		
substrate-free	1949	487
substrate-free	1930	501
+ Arg	1929	503
+ HO-Arg	1928	502
iNOS substrate-free	1945	487
iNOS + Arg	1906	512
CYP152 enzyme		
Ole T substrate free	1957	467
Ole T substrate free	1939	479
Ole T C20D bound	1941	476
CYP-SA C20D bound	1949	479

5.3.4 rR investigations on ferrous-dioxygen adduct of Ole T and CYP-SA

As discussed earlier in this dissertation, the rR technique applied to oxy intermediates of CYP17 had shown the impressive potential to detect the subtle active site structure perturbation especially the H-bond interactions with the Fe-OO fragment.[91] Specifically, H-bonding to the proximal O of the Fe-O_P-O_T fragment causes decrease of Fe-O stretching mode, in this case, the H-O^P interaction is expected to inhibit bond cleavage and prolong the lifetime of the peroxo intermediate, allowing nucleophilic attack on susceptible substrates leading to the C-C bond cleavage lyase reaction.[158] H-bonding to the terminal O will shift up the Fe-O stretching mode, and the H-O^T interaction promotes O-O bond protonation and cleavage, finally yielding Compound I intermediate, which effective mediate hydroxylation reactions.[159] Needless to say, such a powerful technique is able to detect subtle structure variations that can dramatically impact enzyme function.

The original plan is to prepare and trap the ferrous dioxygen adducts of Ole T and characterize it and following intermediates in the P450 enzyme cycle with rR spectroscopy. However, although a lot of effort was spent trying to prepare and trapp the dioxygen adduct, under different conditions, as summarized in section 5.2.1.2. Since all the samples are freezing immediately after mixing with oxygen, the complex formation can only be examined by rR spectroscopy which the samples could be measured in liquid nitrogen temperature using home design setup in our lab. After long rR spectral acquisition time on these frozen samples, there was no evidence obtained for dioxygen adduct formation. These disappointing results led us to reconsider various possibilities for the failure to generate fragile oxy samples. The first step of the cycle begins with the

substrate-bound ferric samples, where rR spectra is earlier shown in Figure 5.3.1. The presence of 70% HS form in this sample eliminates our worry about whether this organic substrate could reach sufficient concentrations to sheathe the highly concentrated enzyme (200 μM), However, it is important to notice that these samples quite readily generate precipitation due to the excess amount of organic fatty acid substrate present. So the reduction process on substrate-bound form were carefully checked before dioxygen bubbling. The collected rR data for ferrous form is shown in Figure 5.3.8, the intense sharp peak ν_4 in high frequency region occurs at 1358 cm^{-1}, indicating the P420 form formation (inactive form of enzyme which the CO adduct exhibits a Soret band at 420nm); i.e., the ferrous P450 form typically has a ν_4 occuring at 1347cm^{-1}. A similar pattern is seen in the camphor bound CYP101 P420, the ν_4 mode shifts from 1372 to 1361 cm^{-1} upon the reduction.[127] Under this situation with quick P420 formation upon reduction, trapping oxygen adduct would be difficult.

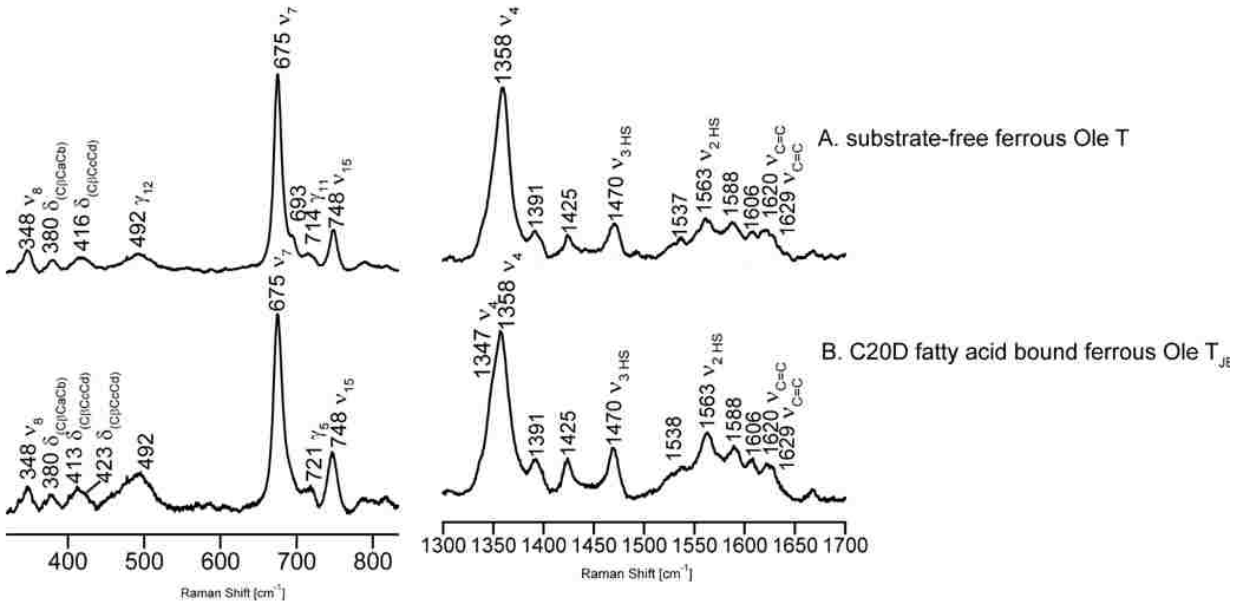

Figure 5.3.8 rR spectra of ferrous substrate-free and C20D bound enzyme. Left panel shows low frequency and right panel shows the high frequency region.

While the other CYP152 enzyme, CYP-SA, shares highly similar active site structure with Ole T, it is much more stable than Ole T, without any P420 conversion and substrate precipitation issues. Thus, the study the dioxygen adduct of CYP-SA is an alternative way to gain useful information. The 413.1 nm excitation line from Krypton laser is selected as the closest line to the Soret band of oxy CYP-SA (428 nm). Due to the low S/N of these frozen samples, the modes of Fe-O-O fragment were identified using difference traces of O_2 isotope, the resultant spectra being seen in Figure 5.3.9. As seen in trace C, an $\nu(Fe-^{16}O)$ occurs at 513 cm^{-1} with the $\nu(Fe-^{18}O)$ seen at 486 cm^{-1}, which is shifted down by 27 cm^{-1} (calculated to be 25cm^{-1}). Usually, the frequency of ν (Fe-O) can be modulated by direct H-bonding interactions between the bound oxygen and neighboring residues. It is interesting to notice that the frequency of Fe-O is unusually low, compared with other Cytochrome P450s whose frequencies typically occur in the region 526-542 cm^{-1}.[91, 63, 109] It can be postulated that the significant reduction in the ν (Fe-O) frequency is caused by a relative strong distal hydrogen bonding to the proximal oxygen of $Fe-O_P-O_T$ fragment, this could be consistent with a lowering of the tendency for the O-O bond cleavage, allowing the enzyme to utilize a peroxo intermediate as the oxidizing species. One puzzling observation is that, there is no appreciable O-O stretching mode detected in the higher frequency region (1000-1700 cm^{-1}). It is believed that the distal interactions can alter the mechanism of enhancement by changing the energy level of $Fe-O_2$ molecular orbital, thus the silence of O-O stretching mode could be either attributed to the ruffled heme plane, or it can be suggested that the Fe-O-O unit is highly bent, showing steric interactions between Fe-OO fragment and steric bulk of substrate/residues of distal pocket.

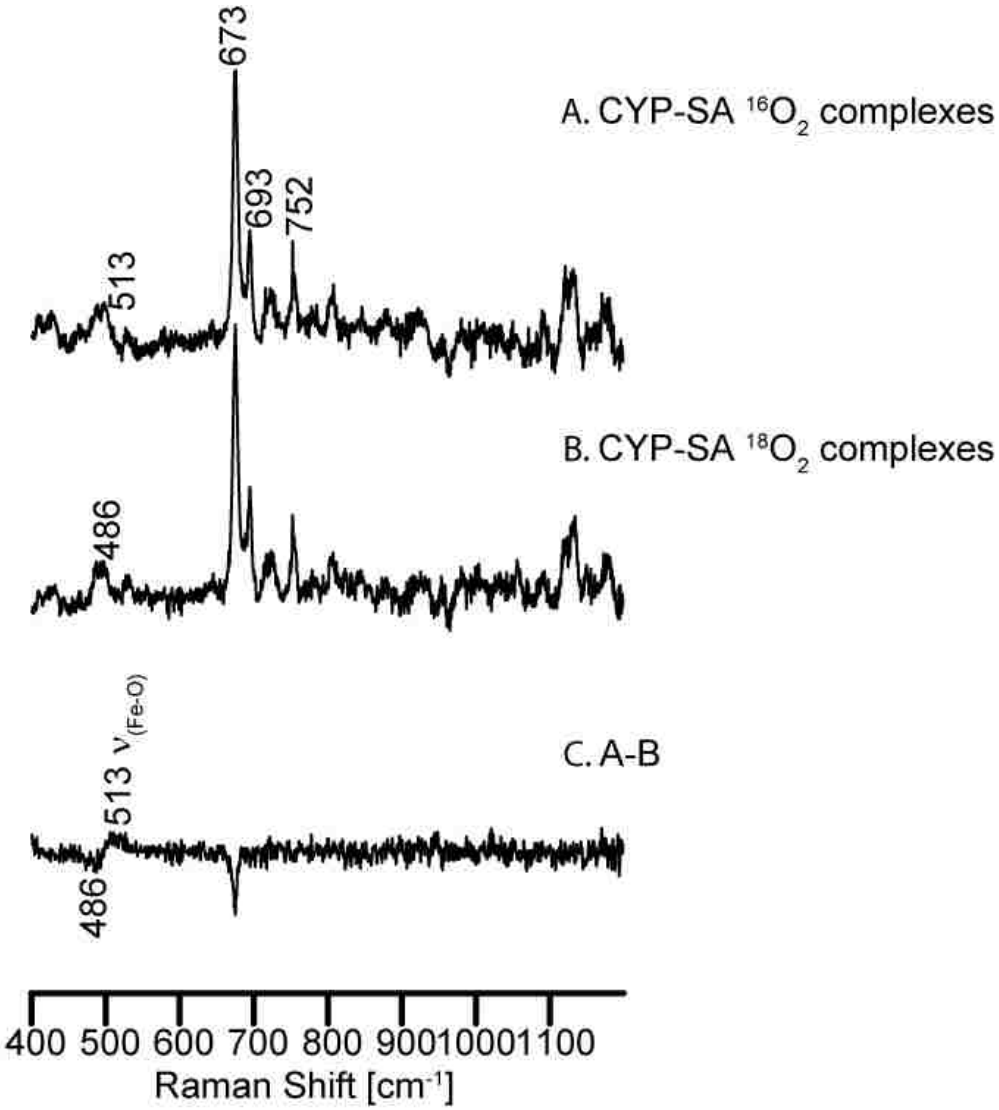

Figure 5.3.9 rR spectra of P450-SA oxy complex in mid-frequency. Spectra were measured at liquid nitrogen temperature with excitation line at 413.1 nm. (A) CYP-SA $^{16}O_2$ complex, (B) CYP-SA $^{18}O_2$ complex, (C) difference spectra: trace A-trace B.

In summary, the results presented here provide a general idea of the effect of the C20D fatty acid on the active site structure, including the spin state conversion and vinyl and changes of protein interaction with vinyl and propionate groups of heme. The rR data of ferric OleT indicates the introduction of bulky fatty acid substrates cause the reorientation of propionate group, while the CYP-SA C20D bound data strongly

suggesting a ruffled, highly distorted heme cofactor. Both of the CO complexes of Ole T and CYP-SA indicate a strong Fe-S linkage like P450cam, while the presence of the C20D fatty acid substrates bring the additional H-bonding in the distal pocket. Though not yet successful in trapping the Ole T dioxygen complex, the ferrous dioxygen adduct of the Ole T analogue, CYP-SA, seems to suggest the presence of a strong hydrogen bond donor to the proximal oxygen of Fe-O_P-O_T fragment, suggesting a mechanism that could involve a stabilized peroxo species is the oxidizing species.

Chapter 6 Conclusion

Heme proteins play an important role in many biological processes, they all recruit a heme cofactor into the enzyme active site to display a remarkably diverse range of chemical activity. These include the electron transport proteins, oxygen transport proteins, heme sensor proteins and the most interesting, catalytic proteins, which can effect quite remarkable chemical transformations under physiological conditions. Among all these heme containing enzymes, cytochromes P450 and peroxidases are of great interest for study in our lab. Within the catalytic cycles of these proteins, highly reactive intermediates are generated; these actually dictate the chemical reactivity, but historically it has proven very difficult to structurally characterize these fleeting species. Fortunately, resonance Raman spectroscopy has emerged as a very effective technique to study structural changes of these crucial intermediates.

Cytochromes P450 exist in many organisms throughout the biosphere, from bacteria to humans. However, most of the significant progress in understanding the mechanisms of P450s was made by studying the bacteria P450s, as they are soluble and easily isolated compared to the mammalian P450s. Chapter 2 describes the methods used for the expression and purification of a bacteria P450, CYP101A1, which hydroxylates the substrate, camphor. In this work, CYP101 was used as a vehicle to gain important experience in protein expression and purification as well as providing a relatively stable enzyme to gain valuable expertise in acquiring resonance Raman spectral data. Indeed, this enzyme has served as the paradigm of cytochrome P450 structure and function during the past 5 decades.

Cytochrome P450 is a broad class of heme monooxygenase enzymes, which catalyze various oxidative transformations. Mammalian P450s can be classified into two main sub-classes, one is involved with drug metabolism and the other comprises enzymes that participate in steroidogenic processes. Chapter 3 of this dissertation focuses on one of these steroidogenic P450s, CYP17A1, which not only catalyzes hydroxylation reactions, but also promotes C-C bond cleavage reactions; i.e., lyase reactions. Cytochrome b_5 is known to be a key regulator of this latter activity by a mechanism that is not well understood. Here, nanodisc technology is used to prepare functional dyads of these proteins and resonance Raman spectroscopy is effectively employed to structurally characterize protein-protein interactions. Results of careful functional studies show no impact of (redox inactive) Mn b_5 on the lyase reaction, indicating mainly an electron transfer role for cytochrome b5 in the lyase reaction. While resonance Raman spectroscopic studies showed that Mn b_5 binding does not affect the heme skeletal modes, they do reveal a slight increase the strength of the Fe-S bond, as well as a weakening of the Fe-O bond of OH-PROG bound CYP17, while that of the enzyme complex with the lyase substrate, OH-PREG, remains unaffected.

Chapters 4 and 5, focus on cytochromes P450 that are attracting growing attention from an industrial prospective, especially the exploring of protein engineering as an effective approach for important applications in biotechnology. The bacterial fusion enzyme, P450 BM3 (CYP102A1), which includes a fused reductase domain, is a good target of exploration for biotechnologically useful purposes, especially its A82F, F87V and the double mutant, which enhance the affinity for the human P450 drug metabolite, omeprazole (OMP). Here again, as in Chapter 3, rR spectroscopy was useful in showing

OMP does not bind in the active site of WT BM3, does bind and cause rR-detected structural changes within the active sites of the A82F, F87V and double mutations of P450 BM3.

Chapter 5 describes initial studies conducted to investigate P450 peroxygenase enzymes [CYP152L1 (Ole T) and CYP152L2 (CYP-SA)], both of which are able to convert fatty acids to terminal alkenes. They use a "peroxide-shunt" pathway, generating crucial intermediates via reaction of the ferric heme with H_2O_2, following a mechanism which bypasses any need for partner reductases, an attractive activation route for biotechnological applications. The acquired rR data documented a 70% HS component upon binding of the substrates, also showing that the introduction of bulky fatty acid substrates causes the reorientation of a propionate group on Ole T enzyme, while inducing a ruffled, highly distorted heme cofactor in the CYP-SA C20D bound enzyme. Spectra of the CO complexes of Ole T and CYP-SA indicate a strong Fe-S linkage, comparable to that of P450cam. In future studies it will also be of great interest to document any differences in the key Fe-O-O fragments of the "precursor" to the Compound I intermediate. Though unsuccessful in trapping the Ole T dioxygen complex, preliminary studies of the ferrous dioxygen adduct of the Ole T analogue, CYP-SA, provides evidence for a strong hydrogen bond to the proximal oxygen of $Fe\text{-}O_P\text{-}O_T$ fragment, an observation that is consistent with a stabilized peroxo intermediate.

Overall, the extensively rR studies performed here on quite different heme proteins demonstrate how useful such studies can be in revealing how enzyme reactivity can be profoundly affected by subtle structural changes.

Appendix: Analysis of Heme Iron Coordination in DGCR8: The Heme-Binding

Portions of this chapter have appeared in the paper:

Girvan, H. M,; Bradley, J. M.; Cheesman M. R.; Kincaid, J. R,; **Liu, Y**.; Czarnecki, K,; Fisher, K,; Leys, D,; Rigby, S. E. J,; Munro, A. M,; "Analysis of Heme Iron Coordination in DGCR8: The Heme-Binding Component of the Microprocessor Complex" *Biochemistry*, **2016**, *55*, 5073–5083

1. Background of DGCR8

This is a small project which cooperating with Dr. Munro's group, which aims to use resonance Raman spectroscopy in our laboratory as an assist tool to help identifying the coordination environment of DGCR8. The work was publish in ACS Journal of Biochemistry.[72]

Micro RNAs are a small non-coding RNAs which are only ~22 nucleotides which plays a significant role in the regulation of cellular function in animals and plants and in certain viruses. They can prevent translation process by binding with messenger RNA.[160] As shown in Figure A1, mature miRNA needs to be processed from primary miRNA by a series of cleavage steps to reach the activation in gene regulation. Firstly, a pri-miRNA is cleaved in the nucleus into an intermediate called the precursor miRNA by the RNase III enzyme Drosha, this process will not happen with the assistance of DGCR8. Then the precursor miRNA was transported to cytoplasm and finish the further cleavage steps with the help of different types of enzymes.[161]

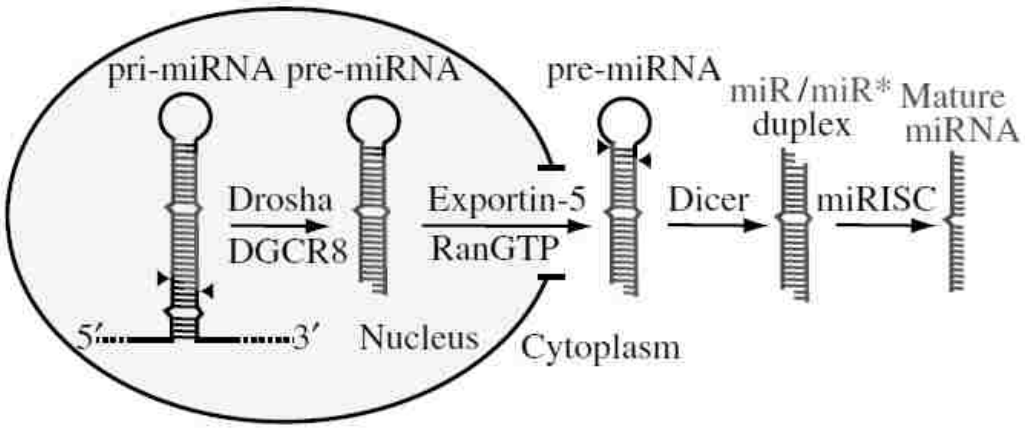

Figure A1. Process of generating mature microRNA.

Earlier studies reported spectroscopic data consistent with bis-cysteine ligation of the heme iron and suggested that a single heme was coordinated by Cys352 side chains from both DGCR8 proteins in a dimer.[162]

DGCR8 is the first example of a heme binding protein with two endogenous cysteine side chains serving as axial ligands. This special the heme environment of DGCR8 attracts more interest and thus resonance Raman and Uv-vis spectroscopy are effective tools to probe the structure in different forms.

2. Uv-vis spectroscopic analysis of DGCR8.

The Uv-vis spectra of ferric state of DGCR8 is shown in Figure A2 (red line), it is showing a hyperporphyrin spectrum with the main soret peak at 450 nm and the second feature at 367 nm. In the visible region, the ferric heme exhibits a broad absorption feature with a peak at 557 nm and a shoulder at 586 nm. This is consisted with the spectrum of a ferric bis-Cys heme ligated model complex.

The reduced DGCR8 is shown in green lines with the Soret band at 427 nm and 531, 559 nm band in visible region. Dawson's group conducted a lot of work on spectroscopic investigations of heme axial coordination using a mutated myoglobin with no axial heme coordination from the polypeptide. Using either cyclopentanethiol to mimic bis-cysteine coordination, they determined the spectroscopic properties of these complexes.[163] In both cases, the addition of the neutral ligand yields an UV−vis spectrum with properties similar to those of the spectrum of the ferrous Δ276 DGCR8 protein, suggesting that, in the ferrous state, DGCR8 is coordinated by neutral axial ligand or ligands, prospectively through CysH/CysH coordination.

Again the ferrous CO complex have a soret feature at 420nm, which is generally considered to be the species arising from protonation of proximal thiolate ligand to the thiol form. However, the histidine ligated heme protein also have a similar spectrum in their ferrous CO form. Thus, the absence of a Soret band at 450 nm thus strongly suggests that in its ferrous, CO-bound state the DGCR8 heme iron is not coordinated to the protein by a thiolate ligand but instead via a neutral thiol or a histidine.

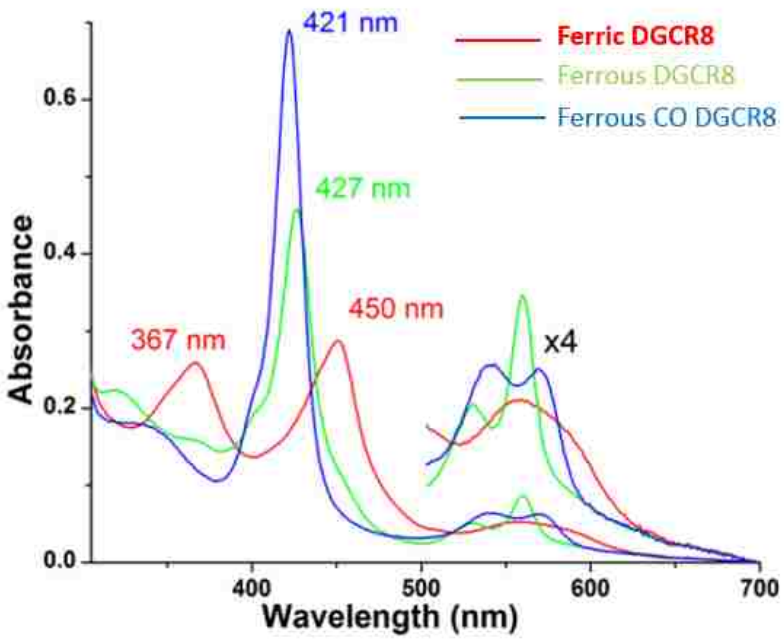

Figure A2 Uv-vis spectra of DGCR8. Ferric DGCR8 is in red, ferrous form is in green while the Ferrous-CO complex form is in Blue.

3. Resonance Raman spectroscopic analysis of DGCR8.

A. Preparation of samples for resonance Raman measurements.

The concentration of ferric DGCR8 sample was 85 μM in 50 mM Tris (pH=8.0), 500 mM KCl containing 10% glycerol. The 50 μL ferric sample was transferred into an NMR tube for measurements. The ferrous form of the protein, dissolved in the glycerol containing buffer, was then generated by first degassing the DGCR8 sample under oxygen-free nitrogen, before adding a 20-fold molar excess of sodium dithionite and the redox mediators methyl viologen (MV) and benzyl viologen (BV) to final concentrations of 0.3 μM and 1 μM, respectively, these additives being dissolved in the same glycerol containing buffer. Reduction of the hemoprotein was monitored by electronic absorption

spectrophotometry in the UV-visible region, noting that full reduction required up to one hour. The ferrous-CO complex was then prepared by saturation of a sample of DGCR8 with CO prior to the addition of sodium dithionite and the BV and MV mediators (as was done for the ferrous, CO-free sample). Formation of the DGCR8 ferrous-CO complex was monitored by observation of the electronic absorption spectrum to ensure complete formation of the CO complex.

It is noted that a second sample of the ferric enzyme was prepared in glycerol-free buffer and studied in an effort to resolve an apparent conflict with previous reports regarding spin state populations (*vide infra*).[36] This second sample was prepared in the same buffer, but lacking glycerol, by adding 50 µL of the glycerol free buffer (50 mM Tris (pH=8.0), 500 mM KCl) to 50 µL of the sample in the original (with 10% glycerol) buffer contained in a centrifugal filter cartridge (10K molecular weight cut-off) and concentrating the 100 µL resulting solution to 50 µL using a microcentrifuge at 8000 rpm at 4 °C. This process was repeated 8 times to ensure the buffer was completely exchanged.

B. Resonance Raman Measurements.

The ferric DGCR8 sample was measured with the 441.6 nm excitation line from a He-Cd laser (IK Series He−Cd laser, Kimmon Koha CO., Ltd.), while the ferrous DGCR8 sample was measured with the 415 nm line provided by a Kr^+ laser (Coherent Innova Sabre Ion Laser). The spectra of the Fe(II)-CO adducts were acquired with the 441.6 nm line. The RR spectra of all samples were measured using a Spex 1269 spectrometer equipped with a Spec-10 LN liquid nitrogen-cooled detector (Princeton

Instruments, NJ). The slit width was 150 μm, and the laser power was adjusted to ~30 mW at the laser for the ferric and ferrous samples, while the power of ~1 mW was maintained for the CO adducts to minimize photo dissociation. All samples were measured in a spinning NMR tube to avoid local heating and protein degradation. The spectra were collected using a 180° backscattering geometry, and the laser power was focused on the sample with a line image using a cylindrical lens. Spectra were calibrated with data acquired for fenchone and processed with Grams/32 AI software (Galactic Industries, Salem, NH). Data were collected at 4 (± 2) °C by placing the samples in a homemade quartz Dewar flask filled with cold water and monitoring during the measurements using a thermocouple.

C. Results for ferric DGCR8

The high frequency region of ferric DGCR8 sample is presented in Figure A3 (A). The region includes the oxidation state and spin state markers. As shown in Figure A3 (A), the high frequency spectrum of the DGCR8 sample exhibits the oxidation state marker mode, ν_4, at 1375 cm^{-1} and the ν_3 spin-state marker at 1506 cm^{-1}, confirming the presence of a ferric 6-coordinate low-spin state, in agreement with results from other methods used in this work. While there are some small differences (3-6 cm^{-1}) in frequencies between our results and those reported in the earlier published data from Barr *et al*,[164] they can be atributed to the one-point spectral calibration method used in the published work compared to the multipoint calibration used in the present studies; slight differences in relative intensities of bands between the two works are attributable to the fact that two different excittaions lines were used (441.6 vs 457.9 nm). A more

worrisome discrepancy is the fact that a weak 1471 cm^{-1} band seen in the earlier work was taken as evidence for a 5-coordinate high spin component. Indeed, in the present work a band is also observed in Figure A3 near this frequency (1465 cm^{-1}), but is assigned to an internal mode of glycerol, whose concentration is 10% (volume/volume) in our sample; it is noted that samples studied in the published report also contained 10% glycerol. In order to verify the assignment of this 1465cm^{-1} feature to glycerol, further experiments were conducted on a DGCR8 sample containing no glycerol. The inset in Figure A3 (A) shows spectra of the ferric DGCR8 sample containing 10% glycerol buffer (a), a sample in the same buffer without glycerol (b) and their difference spectrum (c). In the difference spectrum, all the heme modes were cleanly cancelled out, revealing only the 1465 cm^{-1} glycerol band. Thus, we assigned this band to the 10% glycerol present in the original protein solution, confirming the interpretation that the ferric protein samples studied here contain an insignificant amount of 5-coordinate HS state. The low frequency region of the RR spectrum is shown in Figure A4 (A) which is as the supporting information attached in published article.

D. Results for ferrous DGCR8

In the ferrous state, the high-frequency region (Figure A3 B) exhibited the oxidation state marker band (ν_4) at 1362 cm^{-1} and the spin-state marker band (ν_3) at 1495 cm^{-1}, indicating a low-spin 6-coordinated ferrous heme protein. Again, the weak broad glycerol band near 1465 cm^{-1} was observed. In the earlier work, a 1470 cm^{-1} band was observed and assigned to the ν_3 mode of a 5-coordinate HS component, again prompting the conclusion of a mixture of 5- and 6-coordinate forms of the ferrous protein, as was

reported in that work for the ferric state.[164] While that 1470 cm^{-1} feature is reasonably close to the expected glycerol band, the frequency observed is slightly higher than expected. Considering it not to be a mis-calibrated glycerol band, the authors assigned it to the ν_3 mode of a HS component, also assigning a feature at 1579 cm^{-1} to the ν_2 mode of that HS component; however, this frequency is unusually high for a HS component. Acceptance of the 1470 cm^{-1} feature observed in the earlier work as confirmation of a HS component suggests that the sample studied there (the frog 278-498) does form a HS component, while the isoform of interest in this work (human 276-773) does not form a HS species, under the conditions studied here. The low-frequency rR spectrum of ferrous DGCR8 is shown in Figure A4 B.

E. Results for ferrous CO complex of DGCR8

As was pointed out above, the appearance of a Soret band near 420 nm for the ferrous CO adduct of DGCR8 is indicative of a 6-coordinate CO ligated heme bearing a neutral (e.g., thiol or histidine) trans-axial ligand. Resonance Raman spectra in the region between 1000-1650 cm^{-1}, provided in Figure A4 (C) of Supporting Information, reveal the oxidation state marker band (ν_4) at 1373 cm^{-1} and spin state marker band (ν_3) at 1497 cm^{-1}, consistent with values typically seen for these low spin CO adducts of cytochromes P450.[59, 69] The regions of the RR spectra of the Fe-CO and Fe-^{13}CO adducts of the DGCR8, wherein the ν(Fe-C) and ν(C-O) stretching modes occur, are shown in Figure A3 (C). In the lower frequency region a clean difference pattern emerges from a ν(Fe-^{12}C) mode appearing at 496 cm^{-1}, with its ^{13}C counterpart shifting to 490 cm^{-1}. The corresponding ν(C-O) bands appear at 1963 cm^{-1} for ^{12}C-O and at 1917 cm^{-1} for the ^{13}C

analogue. Finally, a clean difference pattern, with components at 575 and 557 cm^{-1}, reveal the δ(Fe-C-O) bending mode.

Figure A3 (D) shows the well-established inverse correlation plots for ν(Fe-C) vs ν(C-O) modes, which are useful for probing the nature of the distal heme pockets and proximal ligands.[57] Thus, the lowest line in the figure includes data for the cytochromes P450, which possess the strongly electron donating thiolate proximal ligand, leading to relatively high ν(Fe-S) stretching modes occurring near 350-355 cm^{-1}. Just above this line lies the correlation plot for NOS enzymes, which possess proximal pocket residues that provide H-bond donor fragments to the proximal thiolate ligand, weakening the Fe-S linkage; possessing lower ν(Fe-S) frequencies (337-343 cm^{-1}), these show correspondingly higher ν(Fe-C) stretching modes. Highest in the figure is the correlation line for histidine bound Fe-CO complexes. As was discussed above, actual protonation of the trans-axial thiolate to form a trans thiol-ligated species, as has been suggested for cytochromes P420,[165] would lead to an even weaker Fe-S bond and higher ν(Fe-C) stretching frequencies, compared to those seen for NOS adducts. Indeed, the points acquired for the P420 forms of iNOS and for CYP101,[127] as well as one for a well-characterized CO adduct of a heme model compound bearing a trans-axial thiol,[166] lie near the line corresponding to histidine ligated CO adducts.

It is interesting to note that these rR results described above for the ferrous CO adduct provide useful insight regarding the coordination status of the ferrous form. Thus, in the case of the ferrous heme adopting a thiol/thiolate coordination, where it is reasonably expected that the Fe-thiolate bond is stronger than the Fe-thiol bond, a CO complex of heme bearing a trans thiolate ligand would likely be formed, for which the

correlation point would fall near the line corresponding to cytochromes P450. However, the point determined herein for the CO adduct of DGCR8 clearly lies in the neighbourhood of these adducts bearing a trans-axial thiol ligand; i.e., near the line corresponding to histidine-ligated CO adducts. Thus, the rR data obtained here for the ferrous DGCR8 CO complex supports the conclusion that the ferrous form of this enzyme possesses a thiol/thiol coordination environment, rather than a thiol/thiolate formulation.

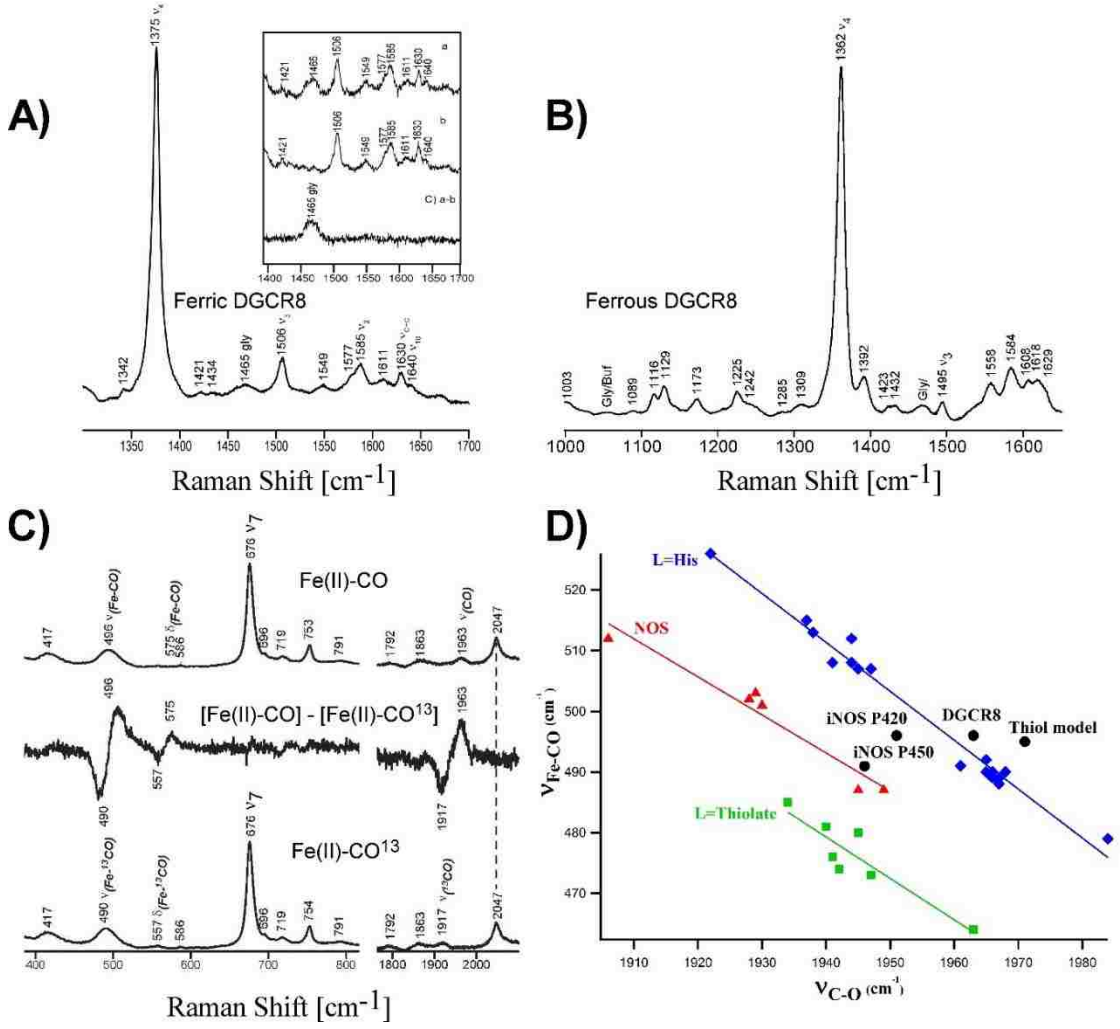

Figure A3 A) the high-frequency RR spectra for the ferric DGCR8 aquired with 442 nm laser lines. (85 μM ferric DGCR8, in TRIS pH 8.0, 500mM KCl, 10% glycerol). The inset shows the ferric DGCR8 in 10% glycerol buffer (a), ferric DGCR8 in same buffer without glycerol (b) and their difference traces (c); **B)** The high-frequency RR spectra for the ferrous DGCR8 acquired with the 415 nm laser line (85 μM DGCR8 reduced under inert atmosphere of N_2 with 20 time molar excess of sodium dithionate in the presence of methyl viologen and benzyl viologen); **C)** The low-frequency (left-panel) and high-frequency (right panel) RR spectral region of ferrous adducts of DGCR8. The middle trace in each panel shows $^{12}C^{16}O$ – $^{13}C^{16}O$ difference plot in the $\nu_{(Fe-C)}$ and $\nu_{(C-O)}$ regions (respectively in the left and right panels); **D**) The CO-backbonding correlation lines of P450 cam (L= thiolate), histidine ligated enzymes (L=his) and NOS (L- thiolate).[140] Data points (•) associated with heme- thiol model complex, DGCR8, iNOS P420 and iNOS P450.[166]

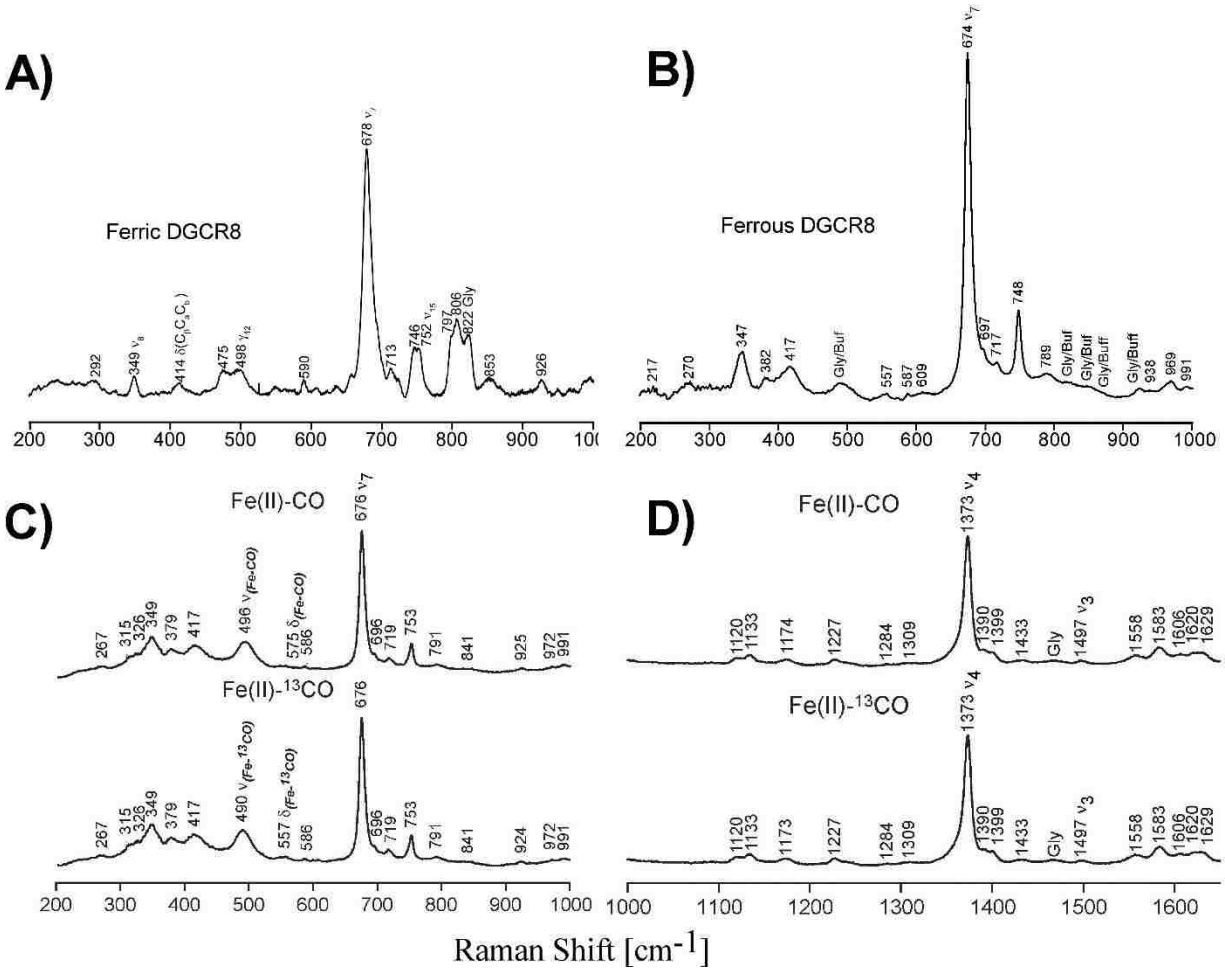

Figure A4 A) The low-frequency RR spectra for the ferric DGCR8 acquired with 442nm laser line. Experimental conditions same as in Figure A1 for the corresponding high-frequency regions; **B)** the low-frequency RR spectra for the ferrous DGCR8 acquired with the 415 nm laser line. Experimental condition as in Figure 3C; **C)** The low-frequency RR spectra of the carbon monoxide and its ^{13}CO isotopomer complex of DGCR8 acquired with the 415 nm laser line; **D)** The high-frequency RR spectra of the carbon monoxide and its ^{13}CO isotopomer complex of DGCR8 acquired with the 415 nm laser line.

References

1. Mowat, C. G.; Chapman, S. K., Multi-heme cytochromes - new structures, new chemistry. *Dalton T* **2005,** (21), 3381-3389.

2. Spiro, T. G., *Biological Application of Raman Spectroscopy*. Wiley, New York: 1988; Vol. 3, p 1-37.

3. Poulos, T. L.; Finzel, B. C.; Gunsalus, I. C.; Wagner, G. C.; Kraut, J., The 2.6-a Crystal-Structure of Pseudomonas-Putida Cytochrome-P-450. *J Biol Chem* **1985,** *260* (30), 6122-6130.

4. Antonini, E., *Hemoglobin and myoglobin in their reactions with ligands*. Elsevier, Amsterdam: 1971.

5. Schenkman, J. B.; Jansson, I., The many roles of cytochrome b(5). *Pharmacol Therapeut* **2003,** *97* (2), 139-152.

6. Chan, M. K., Recent advances in heme-protein sensors. *Curr Opin Chem Biol* **2001,** *5* (2), 216-222.

7. Aono, S.; Nakajima, H.; Saito, K.; Okada, M., A novel heme protein that acts as a carbon monoxide-dependent transcriptional activator in Rhodospirillum rubrum. *Biochem Bioph Res Co* **1996,** *228* (3), 752-756.

8. Ma, X. L.; Sayed, N.; Beuve, A.; van den Akker, F., NO and CO differentially activate soluble guanylyl cyclase via a heme pivot-bend mechanism. *Embo J* **2007,** *26* (2), 578-588.

9. Poulos, T. L., Heme Enzyme Structure and Function. *Chem Rev* **2014,** *114* (7), 3919-3962.

10. Spiro, T. G., Resonance Raman Spectroscopy: a New Structure Probe for Biological Chromophores. *Resonance Raman Spectroscopy* **1974,** *7*, 6.

11. Wajcman, H.; Kiger, L.; Marden, M. C., Structure and function evolution in the superfamily of globins. *Cr Biol* **2009,** *332* (2-3), 273-282.

12. Kendrew, J. C., A Three-Dimensional Model of the Myoglobin Molecule Obtained by X-Ray Analysis. *Nature* **1958,** *181*, 662.

13. Phillips, G. N.; Arduini, R. M.; Springer, B. A.; Sligar, S. G., Crystal-Structure of Myoglobin from a Synthetic Gene. *Proteins-Structure Function and Genetics* **1990,** *7* (4), 358-365.

14. Berg, J. M. T., J. L.; Stryer, L., *Biochemistry*. Sixth edition ed.; W. H. Freeman and Company: New York: 2007; p 183-192.

15. Ordway, G. A.; Garry, D. J., Myoglobin: an essential hemoprotein in striated muscle. *J Exp Biol* **2004,** *207* (20), 3441-3446.

16. Bowman, S. E. J.; Bren, K. L., The chemistry and biochemistry of heme c: functional bases for covalent attachment. *Nat Prod Rep* **2008,** *25* (6), 1118-1130.

17. Ferguson, S. J.; Stevens, J. M.; Allen, J. W. A.; Robertson, I. B., Cytochrome c assembly: A tale of ever increasing variation and mystery? *Bba-Bioenergetics* **2008,** *1777* (7-8), 980-984.

18. Reedy, C. J.; Gibney, B. R., Heme protein assemblies. *Chem Rev* **2004,** *104* (2), 617-649.

19. Monson, E. K.; Ditta, G. S.; Helinski, D. R., The Oxygen Sensor Protein, Fixl, of Rhizobium-Meliloti - Role of Histidine-Residues in Heme-Binding, Phosphorylation, and Signal-Transduction. *J Biol Chem* **1995,** *270* (10), 5243-5250.

20. Coyle, C. M.; Puranik, M.; Youn, H.; Nielsen, S. B.; Williams, R. D.; Kerby, R. L.; Roberts, G. P.; Spiro, T. G., Activation mechanism of the CO sensor CooA - Mutational and resonance Raman spectroscopic studies. *J Biol Chem* **2003,** *278* (37), 35384-35393.

21. Kosowicz, J. G.; Boon, E. M., Insights into the distal heme pocket of H-NOX using fluoride as a probe for H-bonding interactions. *J Inorg Biochem* **2013,** *126*, 91-95.

22. Zhao, Y.; Schelvis, J. P. M.; Babcock, G. T.; Marletta, M. A., Identification of histidine 105 in the beta 1 subunit of soluble guanylate cyclase as the heme proximal ligand. *Biochemistry-Us* **1998,** *37* (13), 4502-4509.

23. Zhao, Y. D.; Hoganson, C.; Babcock, G. T.; Marletta, M. A., Structural changes in the heme proximal pocket induced by nitric oxide binding to soluble guanylate cyclase. *Biochemistry-Us* **1998,** *37* (36), 12458-12464.

24. Stone, J. R.; Marletta, M. A., Spectral and kinetic studies on the activation of soluble guanylate cyclase by nitric oxide. *Biochemistry-Us* **1996,** *35* (4), 1093-1099.

25. Denninger, J. W.; Marletta, M. A., Guanylate cyclase and the (NO)-N-./cGMP signaling pathway. *Bba-Bioenergetics* **1999,** *1411* (2-3), 334-350.

26. Greco, O.; Tozer, G. M.; Folkes, L. K.; Wardman, P.; Scott, S. D.; Marples, B.; Joiner, M.; Dachs, G. U., Horseradish peroxidase and indole-3-acetic acid for hypoxia- and radiation-regulated gene therapy of cancer. *Brit J Cancer* **2001,** *85*, 15-15.

27. Veitch, N. C., Horseradish peroxidase: a modern view of a classic enzyme.

Phytochemistry **2004,** *65* (3), 249-259.

28. Degrand, C.; Limoges, B.; Martre, A. M.; Schollhorn, B., Determination of horseradish peroxidase and a peroxidase-like iron porphyrin at a Nafion-modified electrode. *Analyst* **2001,** *126* (6), 887-891.

29. Klingenberg, M., Pigments of rat liver microsomes (Reprinted from Archives of Biochemistry and Biophysics, vol 75, pg 376-386, 1958). *Arch Biochem Biophys* **2003,** *409* (1), 2-6.

30. Garfinkel, D., Studies on pig liver microsomes I. Enzymic and pigment composition of different microsomal fractions (Reprinted from Archives of Biochemistry and Biophysics, vol 77, pg 493-509, 1958). *Arch Biochem Biophys* **2003,** *409* (1), 7-15.

31. David, F. V., *Cytochrome P450, Structure, Function and Mechanism*. Taylor and Francis Ltd: 1996; p 1-5.

32. Guengerich, F. P., New Trends in Cytochrome P450 Research at the Half-Century Mark. *J Biol Chem* **2013,** *288* (24), 17063-17064.

33. Nebert, D. W., The P450 superfamily: update on new sequences, gene mapping, and recommended nomenclature. *DNA and Cell biology* **1991,** *10* (1991), 1-14.

34. Hsu, P.-Y., Identification of Thromboxane Synthase Amino Acid Residues Involved in Heme-Propionate Binding. *Arch Biochem Biophys* **2000,** *383* (119-127).

35. Hannemann, F.; Bichet, A.; Ewen, K. M.; Bernhardt, R., Cytochrome P450 systems - biological variations of electron transport chains. *Bba-Gen Subjects* **2007,** *1770* (3), 330-344.

36. Gray, H. B.; Winkler, J. R., Electron flow through metalloproteins. *Bba-Bioenergetics* **2010,** *1797* (8), 1563-1572.

37. Laura, L. F., Cytochrome P450 Enzymes in Drug Metabolism and Chemical Toxicology. *Biochem Mol Biol Edu* **2006,** *34* (2), 33-74.

38. Peterson, J. A.; Graham, S. E., A close family resemblance: the importance of structure in understanding cytochromes P450. *Struct Fold Des* **1998,** *6* (9), 1079-1085.

39. Champion, P. M.; Stallard, B. R.; Wagner, G. C.; Gunsalus, I. C., Resonance Raman Detection of an Fe-S Bond in Cytochrome-P450cam. *J Am Chem Soc* **1982,** *104* (20), 5469-5472.

40. Stout, C. D., Cytochrome P450 Conformation Diversity. *Structure* **2004,** *12*, 1921-1922.

41. Gotoh, O., Substrate Recognition Sites in Cytochrome-P450 Family-2 (Cyp2)

Proteins Inferred from Comparative Analyses of Amino-Acid and Coding Nucleotide-Sequences. *J Biol Chem* **1992,** *267* (1), 83-90.

42. Hasemann, C. A.; Kurumbail, R. G.; Boddupalli, S. S.; Peterson, J. A.; Deisenhofer, J., Structure and Function of Cytochromes-P450 - a Comparative-Analysis of 3 Crystal-Structures. *Structure* **1995,** *3* (1), 41-62.

43. Groves, J. T., The bioinorganic chemistry of iron in oxygenases and supramolecular assemblies. *P Natl Acad Sci USA* **2003,** *100* (7), 3569-3574.

44. Bernhardt, R., Cytochrome P450: Structure, function, and generation of reactive oxygen species. *Rev Physiol Bioch P* **1996,** *127*, 137-221.

45. Munro, A. W.; Girvan, H. M.; McLean, K. J., Variations on a (t)heme - novel mechanisms, redox partners and catalytic functions in the cytochrome P450 superfamily. *Nat Prod Rep* **2007,** *24* (3), 585-609.

46. Poulos, T. L., Structural and functional diversity in heme monooxygenases. *Drug Metab Dispos* **2005,** *33* (1), 10-18.

47. David, F. V., *Cytochrom P450, Structure, Function and Mechanism*. Taylor and Francis Ltd: 1996.

48. Schlichting, I.; Berendzen, J.; Chu, K.; Stock, A. M.; Maves, S. A.; Benson, D. E.; Sweet, B. M.; Ringe, D.; Petsko, G. A.; Sligar, S. G., The catalytic pathway of cytochrome P450cam at atomic resolution. *Science* **2000,** *287* (5458), 1615-1622.

49. Denisov, I. G., *Methods in Molecular Biology*. Springer Science+Business Media New York: 2012; p 375-394.

50. Denisov, I. G.; Victoria, D. C.; Sligar, S. G., Cryoradiolytic reduction of heme proteins: Maximizing dose-dependent yield. *Radiat Phys Chem* **2007,** *76* (4), 714-721.

51. Jung, C., The mystery of cytochrome P450 Compound I A mini-review dedicated to Klaus Ruckpaul. *Bba-Proteins Proteom* **2011,** *1814* (1), 46-57.

52. Rittle, J.; Green, M. T., Cytochrome P450 Compound I: Capture, Characterization, and C-H Bond Activation Kinetics. *Science* **2010,** *330* (6006), 933-937.

53. John, T. G., Aliphatic Hydroxylation via Oxygen Rebound. Oxygen Transfer Catalyzed by Iron. *Jounal of American Chemistry Society* **1976,** *98* (3), 859-861.

54. McCleverty, J. A. M., T.J. , *Comprehensive Coordination Chemistry II From Biology to Nanotechnology*. Elsevier: New York, 2004; Vol. 2.

55. Jayaraman, V.; Rodgers, K. R.; Mukerji, I.; Spiro, T. G., Hemoglobin Allostery -

Resonance Raman-Spectroscopy of Kinetic Intermediates. *Science* **1995,** *269* (5232), 1843-1848.

56. Champion, P. M., *Biological Application of Raman Spectroscopy*. John Wiley and Sons: New York, 1988; p 43.

57. Spiro, T. G.; Soldatova, A. V.; Balakrishnan, G., CO, NO and O-2 as vibrational probes of heme protein interactions. *Coordin Chem Rev* **2013,** *257* (2), 511-527.

58. Yu, N., *Methods in Enzymology*. Academic Press: New York: 1988; Vol. 130, p 350-401.

59. Uno, T.; Nishimura, Y.; Makino, R.; Iizuka, T.; Ishimura, Y.; Tsuboi, M., The Resonance Raman Frequencies of the Fe-Co Stretching and Bending Modes in the Co Complex of Cytochrome P-450cam. *J Biol Chem* **1985,** *260* (4), 2023-2026.

60. Hu, S. Z.; Kincaid, J. R., Resonance Raman Characterization of Nitric-Oxide Adducts of Cytochrome-P450cam - the Effect of Substrate Structure on the Iron Ligand Vibrations. *J Am Chem Soc* **1991,** *113* (8), 2843-2850.

61. Hu, S. Z.; Kincaid, J. R., Resonance Raman-Spectra of the Nitric-Oxide Adducts of Ferrous Cytochrome P450cam in the Presence of Various Substrates. *J Am Chem Soc* **1991,** *113* (26), 9760-9766.

62. Macdonald, I. D. G.; Sligar, S. G.; Christian, J. F.; Unno, M.; Champion, P. M., Identification of the Fe-O-O bending mode in oxycytochrome P450cam by resonance Raman spectroscopy. *J Am Chem Soc* **1999,** *121* (2), 376-380.

63. Hu, S. Z.; Schneider, A. J.; Kincaid, J. R., Resonance Raman Studies of Oxycytochrome P450cam - Effect of Substrate Structure on Nu(O-O) and Nu(Fe-O2). *J Am Chem Soc* **1991,** *113* (13), 4815-4822.

64. Hu, S. Z.; Kincaid, J. R., Resonance Raman Studies of Oxycytochrome-P450cam. *Abstr Pap Am Chem S* **1990,** *200*, 413-INOR.

65. Kevan, L., Current Problems in the Localization and Solvation of Excess Electrons in Glasses. *J Phys Chem-Us* **1980,** *84* (10), 1232-1240.

66. Kappl, R.; Hohnberlage, M.; Huttermann, J.; Bartlett, N.; Symons, M. C. R., Electron-Spin and Electron Nuclear Double-Resonance of the [Feo2]- Center from Irradiated Oxyhemoglobin and Oxymyoglobin. *Biochim Biophys Acta* **1985,** *827* (3), 327-343.

67. Davydov, R.; Macdonald, I. D. G.; Makris, T. M.; Sligar, S. G.; Hoffman, B. M., EPR and ENDOR of catalytic intermediates in cryoreduced native and mutant oxy-cytochromes P450cam: Mutation-induced changes in the proton delivery system. *J Am*

Chem Soc **1999,** *121* (45), 10654-10655.

68. Denisov, I. G.; Sligar, S. G., Cytochromes P450 in Nanodiscs. *Bba-Proteins Proteom* **2011,** *1814* (1), 223-229.

69. Mak, P. J.; Denisov, I. G.; Grinkova, Y. V.; Sligar, S. G.; Kincaid, J. R., Defining CYP3A4 Structural Responses to Substrate Binding. Raman Spectroscopic Studies of a Nanodisc-Incorporated Mammalian Cytochrome P450. *J Am Chem Soc* **2011,** *133* (5), 1357-1366.

70. Denisov, I. G.; Baas, B. J.; Grinkova, Y. V.; Sligar, S. G., Cooperativity in cytochrome P450 3A4 - Linkages in substrate binding, spin state, uncoupling, and product formation. *J Biol Chem* **2007,** *282* (10), 7066-7076.

71. Grinkova, Y. V.; Denisov, I. G.; Sligar, S. G., Functional reconstitution of monomeric CYP3A4 with multiple cytochrome P450 reductase molecules in Nanodiscs. *Biochem Bioph Res Co* **2010,** *398* (2), 194-198.

72. Girvan, H. M.; Bradly, J. M.; Cheesman, M. R.; Kincaid, J. R.; Liu, Y. L.; Czarnecki, K.; Fisher, K.; Leys, D.; Rigby, S. E. J.; Munro, A. W., Analysis of Heme Iron Coordination in DGCR8: The Heme-Binding Component of the Microprocessor Complex. *Biochemistry-Us* **2016,** *55* (36), 5073-5083.

73. Gunsalus, I. C., Bacterial P-450cam methylene monooxygenase components: Cytochrome m, putidaredoxin, and putidaredoxin reductase. *Methods in Enzymology* **1978,** *52*, 166-188.

74. Ewing, G. W., *Analytical Instrumentation handbook*. New York, Marcel: 2003.

75. Manyumwa, M. E. Resonance Raman Spectroscopy of isotopically labeled cytochrome P450cam and low temperature measurements. Marquette University, 2005.

76. Shriver, D. F., The Backscattering Geometry for Raman Spectroscopy of Colored Materials. *Society of Applied Spectroscopy* **1974,** *28*, 319-323.

77. Oshino, N.; Imai, Y.; Sato, R., Function of Cytochrome-B5 in Fatty Acid Desaturation by Rat Liver Microsomes. *J Biochem-Tokyo* **1971,** *69* (1), 155-&.

78. Ingelmansundberg, M.; Johansson, I., Cytochrome-B5 as Electron-Donor to Rabbit Liver Cytochrome-P-450lm2 in Reconstituted Phospholipid-Vesicles. *Biochem Bioph Res Co* **1980,** *97* (2), 582-589.

79. Imai, Y.; Sato, R., Roles of Cytochrome B5 in a Reconstituted N-Demethylase System Containing Cytochrome-P-450. *Biochem Bioph Res Co* **1977,** *75* (2), 420-426.

80. Bonfils, C.; Balny, C.; Maurel, P., Direct Evidence for Electron-Transfer from Ferrous Cytochrome-B5 to the Oxyferrous Intermediate of Liver Microsomal Cytochrome-

P-450 Lm2. *J Biol Chem* **1981,** *256* (18), 9457-9465.

81. Rodgers, K. K.; Sligar, S. G., Surface Electrostatics, Reduction Potentials, and the Internal Dielectric-Constant of Proteins. *J Am Chem Soc* **1991,** *113* (24), 9419-9421.

82. Lipscomb, J. D.; Sligar, S. G.; Namtvedt, M. J.; Gunsalus, I. C., Autooxidation and Hydroxylation Reactions of Oxygenated Cytochrome P-450cam. *J Biol Chem* **1976,** *251* (4), 1116-1124.

83. Morgan, E. T.; Coon, M. J., Effects of Cytochrome-B5 on Cytochrome P-450-Catalyzed Reactions - Studies with Manganese-Substituted Cytochrome-B5. *Drug Metab Dispos* **1984,** *12* (3), 358-364.

84. Miller, W. L.; Auchus, R. J.; Geller, D. H., The regulation of 17,20 lyase activity. *Steroids* **1997,** *62* (1), 133-142.

85. Lee-Robichaud, P.; Akhtar, M. E.; Akhtar, M., Control of androgen biosynthesis in the human through the interaction of Arg(347) and Arg(358) of CYP17 with cytochrome b(5). *Biochem J* **1998,** *332*, 293-296.

86. Sondhi, V.; Owen, B. M.; Liu, J. Y.; Chomic, R.; Kliewer, S. A.; Hughes, B. A.; Arlt, W.; Mangelsdorf, D. J.; Auchus, R. J., Impaired 17,20-Lyase Activity in Male Mice Lacking Cytochrome b(5) in Leydig Cells. *Mol Endocrinol* **2016,** *30* (4), 469-478.

87. Sakai, Y.; Yanase, T.; Hara, T.; Takayanagi, R.; Haji, M.; Nawata, H., In-Vitro Evidence for the Regulation of 17,20-Lyase Activity by Cytochrome B5 in Adrenocortical Adenomas from Patients with Cushings-Syndrome. *Clin Endocrinol* **1994,** *40* (2), 205-209.

88. Auchus, R. J.; Lee, T. C.; Miller, W. L., Cytochrome b(5) augments the 17,20-lyase activity of human P450c17 without direct electron transfer. *J Biol Chem* **1998,** *273* (6), 3158-3165.

89. Guryev, O. L.; Gilep, A. A.; Usanov, S. A.; Estabrook, R. W., Interaction of apo-cytochrome b(5) with cytochromes P4503A4 and P45017A: Relevance of heme transfer reactions. *Biochemistry-Us* **2001,** *40* (16), 5018-5031.

90. Holmans, P. L.; Shet, M. S.; Martinwixtrom, C. A.; Fisher, C. W.; Estabrook, R. W., The High-Level Expression in Escherichia-Coli of the Membrane-Bound Form of Human and Rat Cytochrome B(5) and Studies on Their Mechanism of Function. *Arch Biochem Biophys* **1994,** *312* (2), 554-565.

91. Gregory, M.; Mak, P. J.; Sligar, S. G.; Kincaid, J. R., Differential Hydrogen Bonding in Human CYP17 Dictates Hydroxylation versus Lyase Chemistry. *Angew Chem Int Edit* **2013,** *52* (20), 5342-5345.

92. Denisov, I. G.; Grinkova, Y. V.; Lazarides, A. A.; Sligar, S. G., Directed self-assembly of monodisperse phospholipid bilayer nanodiscs with controlled size. *J Am Chem*

Soc **2004,** *126* (11), 3477-3487.

93. Mulrooney, S. B.; Waskell, L., High-level expression in Escherichia coli and purification of the membrane-bound form of cytochrome b(5). *Protein Expres Purif* **2000,** *19* (1), 173-178.

94. Marty, M. T.; Wilcox, K. C.; Klein, W. L.; Sligar, S. G., Nanodisc-solubilized membrane protein library reflects the membrane proteome. *Anal Bioanal Chem* **2013,** *405* (12), 4009-4016.

95. Ritchie, T. K.; Grinkova, Y. V.; Bayburt, T. H.; Denisov, I. G.; Zolnerciks, J. K.; Atkins, W. M.; Sligar, S. G., Reconstitution of Membrane Proteins in Phospholipid Bilayer Nanodiscs. *Method Enzymol* **2009,** *464*, 211-231.

96. Bayburt, T. H.; Grinkova, Y. V.; Sligar, S. G., Assembly of single bacteriorhodopsin trimers in bilayer nanodiscs. *Arch Biochem Biophys* **2006,** *450* (2), 215-222.

97. P. S. Chen, T. Y. T., and Huber. Warner, Microdetermination of Phosphorus. *Anal Chem* **1956,** *28* (11), 1956-1958.

98. Mak, P. J.; Im, S. C.; Zhang, H. M.; Waskell, L. A.; Kincaid, J. R., Resonance Raman studies of cytochrome P4502B4 in its interactions with substrates and redox partners. *Biochemistry-Us* **2008,** *47* (12), 3950-3963.

99. Gruenke, L. D.; Sun, J.; Loehr, T. M.; Waskell, L., Resonance Raman spectral properties and stability of manganese protoporphyrin IX cytochrome b(5). *Biochemistry-Us* **1997,** *36* (23), 7114-7125.

100. Mak, P. J.; Gregory, M. C.; Sligar, S. G.; Kincaid, J. R., Resonance Raman Spectroscopy Reveals That Substrate Structure Selectively Impacts the Heme-Bound Diatomic Ligands of CYP17. *Biochemistry-Us* **2014,** *53* (1), 90-100.

101. Mak, P. J.; Zhu, Q. H.; Kincaid, J. R., Using resonance Raman cross-section data to estimate the spin-state populations of cytochromes P450. *J Raman Spectrosc* **2013,** *44* (12), 1792-1794.

102. Petrunak, E. M.; DeVore, N.; Scott, E. E., Differential Interactions of Steroidogenic Cytochrome P450 17a1 with Its Substrates. *Drug Metab Rev* **2015,** *47*, 70-70.

103. Harris, D. L.; Loew, G. H., Theoretical investigation of the proton assisted pathway to formation of cytochrome P450 compound I. *J Am Chem Soc* **1998,** *120* (35), 8941-8948.

104. de Visser, S. P.; Ogliaro, F.; Sharma, P. K.; Shaik, S., What factors affect the regioselectivity of oxidation by cytochrome P450? A DFT study of allylic hydroxylation and double bond epoxidation in a model reaction. *J Am Chem Soc* **2002,** *124* (39), 11809-11826.

105. Duggal, R.; Liu, Y. L.; Gregory, M. C.; Denisov, I. G.; Kincaid, J. R.; Sligar, S. G., Evidence that cytochrome b(5) acts as a redox donor in CYP17A1 mediated androgen synthesis. *Biochem Bioph Res Co* **2016,** *477* (2), 202-208.

106. Naffin-Olivos, J. L.; Auchus, R. J., Human cytochrome b5 requires residues E48 and E49 to stimulate the 17,20-lyase activity of cytochrome P450c17. *Biochemistry-Us* **2006,** *45* (3), 755-762.

107. Akhtar, M.; Wright, J. N.; Lee-Robichaud, P., A review of mechanistic studies on aromatase (CYP19) and 17 alpha-hydroxylase-17,20-lyase (CYP17). *J Steroid Biochem* **2011,** *125* (1-2), 2-12.

108. Estrada, D. F.; Laurence, J. S.; Scott, E. E., Substrate-modulated Cytochrome P450 17A1 and Cytochrome b7(5) Interactions Revealed by NMR. *J Biol Chem* **2013,** *288* (23), 17008-17018.

109. Mak, P. J.; Gregory, M. C.; Denisov, I. G.; Sligar, S. G.; Kincaid, J. R., Unveiling the crucial intermediates in androgen production. *P Natl Acad Sci USA* **2015,** *112* (52), 15856-15861.

110. Gregory, M. C.; Denisov, I. G.; Grinkova, Y. V.; Khatri, Y.; Sligar, S. G., Kinetic Solvent Isotope Effect in Human P450 CYP17A1-Mediated Androgen Formation: Evidence for a Reactive Peroxoanion Intermediate. *J Am Chem Soc* **2013,** *135* (44), 16245-16247.

111. Im, S. C.; Waskell, L., The interaction of microsomal cytochrome P450 2B4 with its redox partners, cytochrome P450 reductase and cytochrome b(5). *Arch Biochem Biophys* **2011,** *507* (1), 144-153.

112. Newhouse, T.; Baran, P. S., If C-H Bonds Could Talk: Selective C-H Bond Oxidation. *Angew Chem Int Edit* **2011,** *50* (15), 3362-3374.

113. Ruettinger, R. T.; Fulco, A. J., Epoxidation of Unsaturated Fatty-Acids by a Soluble Cytochrome-P-450-Dependent System from Bacillus-Megaterium. *J Biol Chem* **1981,** *256* (11), 5728-5734.

114. Munro, A. W.; Leys, D. G.; McLean, K. J.; Marshall, K. R.; Ost, T. W. B.; Daff, S.; Miles, C. S.; Chapman, S. K.; Lysek, D. A.; Moser, C. C.; Page, C. C.; Dutton, P. L., P450BM3: the very model of a modern flavocytochrome. *Trends Biochem Sci* **2002,** *27* (5), 250-257.

115. Chen, M. S.; White, M. C., A predictably selective aliphatic C-H oxidation reaction for complex molecule synthesis. *Science* **2007,** *318* (5851), 783-787.

116. Ren, X. K.; Yorke, J. A.; Taylor, E.; Zhang, T.; Zhou, W. H.; Wong, L. L., Drug Oxidation by Cytochrome P450(BM3): Metabolite Synthesis and Discovering New P450

Reaction Types. *Chem-Eur J* **2015,** *21* (42), 15039-15047.

117. Kola, I.; Landis, J., Can the pharmaceutical industry reduce attrition rates? *Nat Rev Drug Discov* **2004,** *3* (8), 711-715.

118. Butler, C. F.; Peet, C.; McLean, K. J.; Baynham, M. T.; Blankley, R. T.; Fisher, K.; Rigby, S. E. J.; Leys, D.; Voice, M. W.; Munro, A. W., Human P450-like oxidation of diverse proton pump inhibitor drugs by 'gatekeeper' mutants of flavocytochrome P450 BM3. *Biochem J* **2014,** *460*, 247-259.

119. Sevrioukova, I. F.; Li, H. Y.; Zhang, H.; Peterson, J. A.; Poulos, T. L., Structure of a cytochrome P450-redox partner electron-transfer complex. *P Natl Acad Sci USA* **1999,** *96* (5), 1863-1868.

120. Butler, C. F.; Peet, C.; Mason, A. E.; Voice, M. W.; Leys, D.; Munro, A. W., Key Mutations Alter the Cytochrome P450 BM3 Conformational Landscape and Remove Inherent Substrate Bias. *J Biol Chem* **2013,** *288* (35), 25387-25399.

121. Whitehouse, C. J. C.; Bell, S. G.; Wong, L. L., P450(Bm3) (Cyp102a1): Connecting the Dots. *Chem Soc Rev* **2012,** *41* (3), 1218-1260.

122. Kitagawa, T.; Mizutani, Y., Resonance Raman-Spectra of Highly Oxidized Metalloporphyrins and Heme-Proteins. *Coordin Chem Rev* **1994,** *135*, 685-735.

123. Lee, K. B.; Jun, E. S.; Lamar, G. N.; Rezzano, I. N.; Pandey, R. K.; Smith, K. M.; Walker, F. A.; Buttlaire, D. H., Influence of Heme Vinyl-Protein and Carboxylate Protein Contacts on Structure and Redox Properties of Bovine Cytochrome-B5. *J Am Chem Soc* **1991,** *113* (9), 3576-3583.

124. Marzocchi, M. P.; Smulevich, G., Relationship between heme vinyl conformation and the protein matrix in peroxidases. *J Raman Spectrosc* **2003,** *34* (10), 725-736.

125. Mak, P. J.; Kaluka, D.; Manyumwa, M. E.; Zhang, H. Q.; Deng, T. J.; Kincaid, J. R., Defining resonance Raman spectral responses to substrate binding by cytochrome P450 from Pseudomonas putida. *Biopolymers* **2008,** *89* (11), 1045-1053.

126. Champion, P. M.; Gunsalus, I. C.; Wagner, G. C., Resonance Raman Investigations of Cytochrome P450cam from Pseudomonas-Putida. *J Am Chem Soc* **1978,** *100* (12), 3743-3751.

127. Wells, A. V.; Li, P. S.; Champion, P. M.; Martinis, S. A.; Sligar, S. G., Resonance Raman Investigations of Escherichia-Coli-Expressed Pseudomonas-Putida Cytochrome-P450 and Cytochrome-P420. *Biochemistry-Us* **1992,** *31* (18), 4384-4393.

128. Hu, S. Z.; Morris, I. K.; Singh, J. P.; Smith, K. M.; Spiro, T. G., Complete Assignment of Cytochrome-C Resonance Raman-Spectra Via Enzymatic Reconstitution

with Isotopically Labeled Hemes. *J Am Chem Soc* **1993,** *115* (26), 12446-12458.

129. Li, X. Y.; Czernuszewicz, R. S.; Kincaid, J. R.; Su, Y. O.; Spiro, T. G., Consistent Porphyrin Force-Field .1. Normal-Mode Analysis for Nickel Porphine and Nickel Tetraphenylporphine from Resonance Raman and Infrared-Spectra and Isotope Shifts. *J Phys Chem-Us* **1990,** *94* (1), 31-47.

130. Li, X. Y.; Czernuszewicz, R. S.; Kincaid, J. R.; Stein, P.; Spiro, T. G., Consistent Porphyrin Force-Field .2. Nickel Octaethylporphyrin Skeletal and Substituent Mode Assignments from N-15, Meso-D4, and Methylene-D16 Raman and Infrared Isotope Shifts. *J Phys Chem-Us* **1990,** *94* (1), 47-61.

131. Choi, S.; Spiro, T. G.; Langry, K. C.; Smith, K. M., Vinyl Influences on Protoheme Resonance Raman-Spectra - Nickel(Ii) Protoporphyrin-Ix with Deuterated Vinyl Groups. *J Am Chem Soc* **1982,** *104* (16), 4337-4344.

132. Chen, Z. C.; Ost, T. W. B.; Schelvis, J. P. M., Phe393 mutants of cytochrome P450BM3 with modified heme redox potentials have altered heme vinyl and propionate conformations. *Biochemistry-Us* **2004,** *43* (7), 1798-1808.

133. Huang, Q.; Schweitzer-Stenner, R., Non-planar heme deformations and excited state displacements in horseradish peroxidase detected by Raman spectroscopy at Soret excitation. *J Raman Spectrosc* **2005,** *36* (4), 363-375.

134. Shelnutt, J. A.; Song, X. Z.; Ma, J. G.; Jia, S. L.; Jentzen, W.; Medforth, C. J., Nonplanar porphyrins and their significance in proteins. *Chem Soc Rev* **1998,** *27* (1), 31-41.

135. Deng, T. J.; Proniewicz, L. M.; Kincaid, J. R.; Yeom, H.; Macdonald, I. D. G.; Sligar, S. G., Resonance Raman studies of cytochrome P450BM3 and its complexes with exogenous ligands. *Biochemistry-Us* **1999,** *38* (41), 13699-13706.

136. Li, H. Y.; Poulos, T. L., The structure of the cytochrome p450BM-3 haem domain complexed with the fatty acid substrate, palmitoleic acid. *Nat Struct Biol* **1997,** *4* (2), 140-146.

137. Hu, S. Z.; Smith, K. M.; Spiro, T. G., Assignment of protoheme Resonance Raman spectrum by heme labeling in myoglobin. *J Am Chem Soc* **1996,** *118* (50), 12638-12646.

138. Ibrahim, M.; Xu, C. L.; Spiro, T. G., Differential sensing of protein influences by NO and CO vibrations in heme adducts. *J Am Chem Soc* **2006,** *128* (51), 16834-16845.

139. Li, X. Y.; Spiro, T. G., Is Bound Co Linear or Bent in Heme-Proteins - Evidence from Resonance Raman and Infrared Spectroscopic Data. *J Am Chem Soc* **1988,** *110* (18), 6024-6033.

140. Spiro, T. G.; Wasbotten, I. H., CO as a vibrational probe of heme protein active

sites. *J Inorg Biochem* **2005,** *99* (1), 34-44.

141. Wang, J. L.; Stuehr, D. J.; Rousseau, D. L., Interactions between substrate analogues and heme ligands in nitric oxide synthase. *Biochemistry-Us* **1997,** *36* (15), 4595-4606.

142. Fan, B. C.; Wang, J. L.; Stuehr, D. J.; Rousseau, D. L., NO synthase isozymes have distinct substrate binding sites. *Biochemistry-Us* **1997,** *36* (42), 12660-12665.

143. Jung, C.; Hoa, G. H. B.; Schroder, K. L.; Simon, M.; Doucet, J. P., Substrate-Analog Induced Changes of the Co-Stretching Mode in the Cytochrome-P450cam-Carbon Monoxide Complex. *Biochemistry-Us* **1992,** *31* (51), 12855-12862.

144. Nagano, S.; Shimada, H.; Tarumi, A.; Hishiki, T.; Kimata-Ariga, Y.; Egawa, T.; Suematsu, M.; Park, S. Y.; Adachi, S.; Shiro, Y.; Ishimura, Y., Infrared spectroscopic and mutational studies on putidaredoxin-induced conformational changes in ferrous CO-P450cam. *Biochemistry-Us* **2003,** *42* (49), 14507-14514.

145. Lee, D. S.; Yamada, A.; Sugimoto, H.; Matsunaga, I.; Ogura, H.; Ichihara, K.; Adachi, S.; Park, S. Y.; Shiro, Y., Substrate recognition and molecular mechanism of fatty acid hydroxylation by cytochrome P450 from Bacillus subtilis - Crystallographic, spectroscopic, and mutational studies. *J Biol Chem* **2003,** *278* (11), 9761-9767.

146. Hill, J.; Nelson, E.; Tilman, D.; Polasky, S.; Tiffany, D., Environmental, economic, and energetic costs and benefits of biodiesel and ethanol biofuels. *P Natl Acad Sci USA* **2006,** *103* (30), 11206-11210.

147. Fujishiro, T.; Shoji, O.; Nagano, S.; Sugimoto, H.; Shiro, Y.; Watanabe, Y., Crystal Structure of H2O2-dependent Cytochrome P450(SP alpha) with Its Bound Fatty Acid Substrate INSIGHT INTO THE REGIOSELECTIVE HYDROXYLATION OF FATTY ACIDS AT THE alpha POSITION. *J Biol Chem* **2011,** *286* (34), 29941-29950.

148. Rude, M. A.; Baron, T. S.; Brubaker, S.; Alibhai, M.; Del Cardayre, S. B.; Schirmer, A., Terminal Olefin (1-Alkene) Biosynthesis by a Novel P450 Fatty Acid Decarboxylase from Jeotgalicoccus Species. *Appl Environ Microb* **2011,** *77* (5), 1718-1727.

149. Belcher, J.; McLean, K. J.; Matthews, S.; Woodward, L. S.; Fisher, K.; Rigby, S. E. J.; Nelson, D. R.; Potts, D.; Baynham, M. T.; Parker, D. A.; Leys, D.; Munro, A. W., Structure and Biochemical Properties of the Alkene Producing Cytochrome P450 OleTJE (CYP152L1) from the Jeotgalicoccus sp 8456 Bacterium. *J Biol Chem* **2014,** *289* (10), 6535-6550.

150. Grant, J. L.; Hsieh, C. H.; Makris, T. M., Decarboxylation of Fatty Acids to Terminal Alkenes by Cytochrome P450 Compound I. *J Am Chem Soc* **2015,** *137* (15), 4940-4943.

151. Wise, C. E.; Grant, J. L.; Amaya, J. A.; Ratigan, S. C.; Hsieh, C. H.; Manley, O. M.; Makris, T. M., Divergent mechanisms of iron-containing enzymes for hydrocarbon biosynthesis. *J Biol Inorg Chem* **2017,** *22* (2-3), 221-235.

152. Li, X. Y.; Czernuszewicz, R. S.; Kincaid, J. R.; Spiro, T. G., Consistent Porphyrin Force-Field .3. Out-of-Plane Modes in the Resonance Raman-Spectra of Planar and Ruffled Nickel Octaethylporphyrin. *J Am Chem Soc* **1989,** *111* (18), 7012-7023.

153. Coyle, C. M.; Vogel, K. M.; Rush, T. S.; Kozlowski, P. M.; Williams, R.; Spiro, T. G.; Dou, Y.; Ikeda-Saito, M.; Olson, J. S.; Zgierski, M. Z., FeNO structure in distal pocket mutants of myoglobin based on resonance Raman spectroscopy (vol 42, pg 4896, 2003). *Biochemistry-Us* **2003,** *42* (34), 10342-10342.

154. Phillips, G. N.; Teodoro, M. L.; Li, T. S.; Smith, B.; Olson, J. S., Bound CO is a molecular probe of electrostatic potential in the distal pocket of myoglobin. *J Phys Chem B* **1999,** *103* (42), 8817-8829.

155. Srajer, V.; Reinisch, L.; Champion, P. M., Protein Fluctuations, Distributed Coupling, and the Binding of Ligands to Heme-Proteins. *J Am Chem Soc* **1988,** *110* (20), 6656-6670.

156. Anderton, C. L.; Hester, R. E.; Moore, J. N., Resonance Raman-Spectroscopy Reveals Novel Ligation Properties of the Porcine Myoglobin Double Mutant H64v/V68h. *Bba-Protein Struct M* **1995,** *1253* (1), 1-4.

157. Kerr, E. A.; Yu, N. T.; Bartnicki, D. E.; Mizukami, H., Resonance Raman Studies of Co and O-2 Binding to Elephant Myoglobin (Distal His(E7)-]Gln). *J Biol Chem* **1985,** *260* (14), 8360-8365.

158. Li, D.; Kabir, M.; Stuehr, D. J.; Rousseau, D. L.; Yeh, S. R., Substrate- and isoform-specific dioxygen complexes of nitric oxide synthase. *J Am Chem Soc* **2007,** *129* (21), 6943-6951.

159. Chang, Y. T.; Veitch, N. C.; Loew, G. H., A theoretical study of benzhydroxamic acid binding modes in horseradish peroxidase. *J Am Chem Soc* **1998,** *120* (21), 5168-5178.

160. Ambros, V., The functions of animal microRNAs. *Nature* **2004,** *431* (7006), 350-355.

161. Goodall, E. F.; Heath, P. R.; Bandmann, O.; Kirby, J.; Shaw, P. J., Neuronal dark matter: the emerging role of microRNAs in neurodegeneration. *Front Cell Neurosci* **2013,** *7*.

162. Barr, I.; Smith, A. T.; Senturia, R.; Chen, Y.; Scheidemantle, B. D.; Burstyn, J. N.; Guo, F., DiGeorge critical region 8 (DGCR8) is a double-cysteine-ligated heme protein. *J Biol Chem* **2011,** *286* (19), 16716-25.

163. Sun, Y. H.; Zeng, W. Q.; Benabbas, A.; Ye, X.; Denisov, I.; Sligar, S. G.; Du, J.; Dawson, J. H.; Champion, P. M., Investigations of Heme Ligation and Ligand Switching in Cytochromes P450 and P420. *Biochemistry-Us* **2013,** *52* (34), 5941-5951.

164. Barr, I.; Smith, A. T.; Chen, Y. Q.; Senturia, R.; Burstyn, J. N.; Guo, F., Ferric, not ferrous, heme activates RNA-binding protein DGCR8 for primary microRNA processing. *P Natl Acad Sci USA* **2012,** *109* (6), 1919-1924.

165. Collman, J. P.; Sorrell, T. N.; Dawson, J. H.; Trudell, J. R.; Bunnenberg, E.; Djerassi, C., Magnetic Circular-Dichroism of Ferrous Carbonyl Adducts of Cytochromes P-450 and P-420 and Their Synthetic Models - Further Evidence for Mercaptide as 5th Ligand to Iron. *P Natl Acad Sci USA* **1976,** *73* (1), 6-10.

166. Sabat, J.; Stuehr, D. J.; Yeh, S. R.; Rousseau, D. L., Characterization of the Proximal Ligand in the P420 Form of Inducible Nitric Oxide Synthase. *J Am Chem Soc* **2009,** *131* (34), 12186-12192.